STUDIES ON OPTICAL FIBRE DIGITAL COMMUNICATION SYSTEMS

A Thesis Submitted
In Partial Fulfilment of the Requirements
for the Degree of
MASTER OF TECHNOLOGY

By

Capt NARENDRA TALWAR

to the
DEPARTMENT OF ELECTRICAL ENGINEERING
INDIAN INSTITUTE OF TECHNOLOGY, KANPUR
OCTOBER, 1979

CERTIFICATE

This is to certify that the work on "STUDIES ON OPTICAL FIBRE DIGITAL COMTUNICATION SYSTEMS" has been carried out under my supervision and guidance and that this has not been submitted elsewhere for a degree.

October, 1979

(P.K. CHATTERJEE)
Assistant Professor
Department of Electrical Engineering
Indian Institute of Technology
KANPUR

TO

MY

PARENTS

ACKNOWLEDGEMENT

I am highly indebted and grateful to Dr. P.K. Chatterjee for generating and stimulating my interest in Optical Fibre Communications. I sincerely thank him for his inspiring guidance and valuable discussions throughout this study.

I am also grateful to Dr. P.R.K. Rao for sparing his time for some useful discussions. Thanks are also due to Dr. Ramesh Garg of ACES, for his prompt help, encouragement and for providing useful material on the subject.

I acknowledge the cooperation extended by my wife during the course of this study.

Careful typing of this work by Mr. J.S. Rawat is highly appreciated.

- Capt. NARENDRA TALWAR

Kanpur
October, 1979

ABSTRACT

Digital communications at optical frequencies using glass fibres as the transmission media offer many advantages over the conventional coaxial communication systems. This new technology is maturing at such a rapid rate that in the next few years it will have wide ranging applications in communications and other related fields.

In this study various features, characteristics and problems typical of optical fibre communications have been reviewed. The requirements to be met by the low noise front-end of the receiver for optical fibre channels have been indicated. The optical fibre channel is dispersive and as such gives rise to inter symbol interference (ISI) at high data rates and longer repeater spacings. To overcome this problem time domain equalization of the front-end output can be resorted to. The performance of a decision feedback equalizer (DFE) in reducing the ISI for a step-index optical fibre channel has been studied. The optical fibre channel considered uses a light emitting diode as the optical source and a PIN photodetector at the receiver. The performance of the DFE designed, has been evaluated by digital computer simulation for various fibre lengths and different signal-to-noise ratios. The results indicated that the equalizer is able to reduce the ISI significantly. Various line codes suitable for optical-fibre communication systems have also been studied.

TABLE OF CONTENTS

		Page
CHAPTER 1	INTRODUCTION	1
	1.1 General	1
	1.2 Advantages of Optical Fibre Communication Systems	2
	1.3 Types of Fibres	3
	1.4 Propagation Through Fibres	8
	1.4.1 Guidance Principle	9
	1.4.2 Rays in Optical Fibres	14
	1.4.3 Effect of Bends and Variation in Diameter	20
	1.5 Optical Fibre Communication Systems	21
	1.6 Applications of Optical Fibres	24
	1.7 Scope of Work	29
CHAPTER 2	THE OPTICAL FIBRE CHANNEL	32
	2.1 Introduction	32
	2.2 Attenuation in Fibres	32
	2.2.1 Absorption Loss	34
	2.2.2 Scattering Loss	34
	2.3 Dispersion in the Fibre	36
	2.3.1 Multimode Delay Spread	38
	2.3.2 Material Dispersion	39
	2.4 Impulse Response of Optical Fibres	40
	2.4.1 Impulse Response of a Step-Index Fibre Excited by a Lambertian Source	41

Page

2.4.2 Frequency Response 48

2.5 Optical Sources 53

2.5.1 Light Emitting Diode (LED) 55
2.5.2 Superluminescent Diode (SLD) 58
2.5.3 Injection Lasers 59
2.5.4 Neodymium - Doped - Yttrium - Alumi - Garnet (Nd:YAG) 60

2.6 Optical Detectors 63

2.6.1 PIN Photodiode Model 66
2.6.2 Avalanche Photodiode Model 69
2.6.3 Noise in Photodiodes 69
2.6.4 Statistical Model of PIN Photodiode 70
2.6.5 Statistical Model of APD 73

2.7 Some Practical Problems in Optical Fibre Communication Systems 75

2.7.1 Splices and Connectors 75
2.7.2 Laying of Optical Fibre Cables 77
2.7.3 Powering of Repeaters 80

CHAPTER 3 RECEIVER DESIGN 89

3.1 Introduction 89

3.2 Receiver Model 89

3.3 Calculation of Noise Power 93

3.4 Effects of Input Pulse Shapes 97

3.5 Effect of Bit Rate 105

3.6 Effect of Fibre Length 107

Page

CHAPTER 4 EQUALIZER FOR OPTICAL FIBRE SYSTEMS 110

4.1 Introduction to Equalizers 111

4.2 Decision Feedback Equalizer Design 112

4.2.1 Evaluation of Noise Auto-correlation Function 120

4.2.2 Evaluation of Tap Gains 122

4.3 Simulation Results 124

CHAPTER 5 PULSE FORMATS FOR OPTICAL FIBRE SYSTEMS 129

5.1 General 129

5.2 Line Encoding 129

5.3 Suitable Codes for Optical Fibre Systems 130

5.3.1 Two-Level AMI 130

5.3.2 Block Codes 133

5.3.3 Correlative Pulse Formats 139

5.4 Comparison of Suitable Codes 143

CHAPTER 6 CONCLUSION 151

REFERENCES 157

APPENDIX 161

CHAPTER 1

INTRODUCTION

1.1 General:

There has been a constant search for higher and higher information carrying capacity transmission media to enable communication engineers to achieve interference free high data rates. Use of glass fibres for long distance communicatio was conceived only about twelve years back. In 1968 fibre losses were of the order of 1000 dB/Km. Within two years a loss of 20 dB/Km in single mode fibres hundreds of meters long was achieved [1] . Since then progress in the field has been rapid and continues vigorously. Fibre transmission loss in wavelength region 0.8-0.9 μm has been reduced to 1-2 dB/Km. The lowest reported loss is 0.47 dB/Km at 1.2 μm wavelength [2] . These wavelength regions/wavelengths are where AlGaAs Light Emitting Diodes (LED's) and Injection Lasers emit. Simultaneously since the advent of laser in 1960 there has been a constant progress to locate suitable and reliable optical sources for the optical fibres. The reliability and mean life of AlGaAs injection laser operating at room temperature has been considerably improved [2] . During this period progress was also made in practical cable and connector designs and associated electronic circuitry. Fibre

optic links offer much higher performance than coaxial cables with very large available bandwidths and many other advantages.

1.2 Advantages of Optical Communication Systems:

An individual optical fibre is of a very small size of the order of 100 μm in diameter and has very low weight which enables us to bunch a number of them together in an optical cable protected by proper sheathing and strengthened by steel wires. The bunching of many fibres together increases the total channel capacity. The fibres themselves are inherently very strong. Compared to metallic cables optical fibre cables have high strength-to-weight ratio, can negotiate tight bends and have low occupancy of duct space. The bending radius of a fibre can be as low as 0.5 cm. Fibres are free from any electromagnetic interferen which makes eavesdroping and jamming a difficult proposition, thus making the system inherently secure. Fibres also have immunity from earth-looping problems.

Even though fibre-optic cables may cost more initially but due to low loss it is possible to achieve large repeater spacings for long distance systems and for short runs they can be eliminated altogether. Coupled with this the small dispersion implies large transmission

bandwidth over long distance, thus making the potential optical fibre systems very economical. Even the cost of the fibre cable is bound to be low in the long run once the systems become commercial and manufacture of fibre starts on large scales due to abundant raw material.

1.3 Types of Fibres:

There are basically three types of fibres which have been practically exploited viz., single mode, step-index and graded-index. Some more types have also been experimented upon. Fig. 1.1 shows the cross-section of the fibre, refractive index profile and symbolic representation of the ray paths inside the fibre for the three most important ones. A few typical dimensions are also shown to provide a physical feel of the size. The central region called core has a refractive index n_1 (typically $n_1 \simeq 1.5$) which is slightly higher than that of the surrounding cladding refractive index n_2; n_o shown is the ambient refractive index (air).

Fig. 1.1(a) shows the refractive index distribution and the ray path of the single mode fibre whose core radius a is very small ($a \simeq 2\ \mu m - 5\ \mu m$) which enables propagation of a single mode only. This is achievable as the core is comparable in size, with the wavelength of the

light being propagated. Coherent sources like lasers can be used as the transmitting device for the single mode fibres.Even if an incoherent source is used with a single mode fibre, since only one mode is propagated, the dispersion is limited to only that. This dispersion is due to the difference in propagation velocities of different colours. This provides the ultimate in transmission bandwidth. This type of fibre has not been very popular due to its high cost as very high precision is required for drawing so narrow a core. Moreover these fibres present much greater problems in joining and splicing than found with the other two types. Fig. 1.1(b) shows the refractive index distribution and the ray path of the step index multimode fibre which can be used with incoherent sources to transmit the signal. For both the above clad fibres the guided wave field is mainly confined to the core region. Some field does extend into the cladding, but it decays almost exponentially with radial distance from the core - cladding interface and becomes negligibly small by the time it reaches the outer surface of the cladding. Therefore, the fibres can be bunched together with very little possibility of having cross talk. The typical fibre diameters are dictated primarily by the strength requirements in single mode fibres

and by electrical transmission requirements in step-index fibres. The relation between core and cladding refractive indices is

$$n_2 = n_1 (1 - \delta) \qquad (1.1)$$

where $\delta \ll 1$, typically

$$\delta = \frac{n_1 - n_2}{n_2} = 0.01$$

Fig. 1.1(c) shows the refractive index distribution and the ray path of an important fibre type in which the core has a graded index which usually decreases radially from maximum value n_1 at the centre of the core according to the law

$$n_r = n_1 (1 - \alpha r^2) \qquad (1.2)$$

where α is a constant and r is the distance from axis. A particular and popular case of graded index is the parabolic gradation of the refractive index as shown by the continuous line in the refractive index profile i.e.,

$$n_r = n_1 [1 - (\delta/a^2) r^2], \; 0 \leqslant r \leqslant a \qquad (1.3)$$

The rays representing different modes which are shown symbolically in the figure illustrate that, because modes corresponding to the rays that enter the fibre at larger angles spend greater time in a region of the core where

refractive index is low, they travel faster than the axial modes, thus the rays focus at periodic positions along the length of the fibre. This compensates for the mode dispersion (to be described later) found in step-index fibre. This type of fibre therefore gives lower mode dispersion than step-index fibres. Graded index fibres normally have a core in which the graded region extends to about half the diameter of the fibre and then remains at a constant level. The energy is thus confined to this 'core'. Although mode dispersion is not reduced to zero as in the case of single mode fibre, values corresponding to a pulse broadening of around 1 ns/Km can usually be obtained in low loss fibres compared to about 50 nsec/Km for step-index fibres.

The graded refractive index profile shown dotted in Fig. 1.1(c) is axially symmetric with maximum near $r=r_m$. The variation across the diameter is only a percent or less. This type of fibre has exhibited very low dispersion (less than 2 ns/Km) at low loss of less than 6 dB/Km.

Figs. 1.1(d),(e) and (f) show refractive index distribution and cross-section of unclad, dielectric tube and single material fibres respectively. In dielectric type the dielectric can be a low loss liquid like

tetrachloroethylene in the centre with a glass tube as the lower index cladding. As the refractive index of a liquid is quite sensitive to temperature, the number of modes could vary appreciably under field environments. Therefore liquid core fibres can be used for long distance transmission in multimode form only. Single material fibres over come the difficulty of fabricating multi-component glasses. The usefully guided modes are carried in the central enlarged member. Single or multimode guidance can be provided with a suitable choice of dimensions for the supporting sheet and the central enlargement [1]. Another type of fibre shown in Fig.1.1(g) is the doubly clad optical fibre. It is reported to have negative waveguide dispersion [24]. It has a 'W' shape refractive index profile and is therefore also referred to as W type fibre.

1.4 Propagation through Fibres:

The concept of propagation of light waves through optical fibres has been dealt with in considerable details by many authors. Detailed mathematical analysis has been done considering optical fibre as a cylindrical waveguide, but, the guiding channel here is not necessarily made to size as in the case of metallic waveguides for obvious reasons, for the propagation of the dominant mode only [3,4].

The analysis is first always based on an ideal waveguide structure and then the practical perturbations are considered which lead to the practical results of intramodal coupling. Because visible light is involved, it is possible to carry out analysis by Ray theory as well as the rigorous approach of electromagnetic theory on wave propagation. Though complete and exhaustive analysis, explaining the details of physical phenomenon involved, is only possible through the latter, Ray optics, however, does provide a simpler picture describing the optical fibre operation. In the following the ray theory is used to explain propagation through fibres [4 and 5].

1.4.1 Guidance Principle.

In classical clad glass fibres, single mode or step - index, the guidance of light along the fibre is by total internal reflection at the cylindrical interface between the core and the cladding. Modern fibre types like the graded - index employ a continuous focusing process to achieve propagation of light which can be considered as a kind of distributed internal reflection. For analysis and understanding the principle involved, it is easier to consider the step-index fibre.

Let us consider a ray entering the fibre as shown in Fig. 1.2(a). From the figure and using the Snell's law, it follows that for $n_1 > n_2$ no real angle θ_2 exists if

$$n_1 \cos \theta_1 > n_2 \tag{1.4}$$

For this inequality to hold, there will not be any refracted ray in the cladding region. For the rays to be confined to the core region the angle θ_1 must not exceed the critical incident angle θ_{1c}, where θ_{1c} is defined as

$$\cos \theta_{1c} = n_2/n_1 \tag{1.5}$$

It is to be noted that total internal reflection is a necessary but not a sufficient condition for propagation of light rays in optical waveguides. At each point of reflection the ray undergoes a phase change. It is these phase shifts which impose an additional constraint. Their evaluation becomes necessary to satisfy the condition that optical paths (phase difference) between two normal planes for parallel rays should differ by an integer multiple of 2π. This condition can be applied to the ray undergoing multiple reflections in an optical waveguide as shown in Fig. 1.2(b). It can be seen from the figure that the wave fronts are also equiphase planes. For the two rays 1 and 2, points A and C

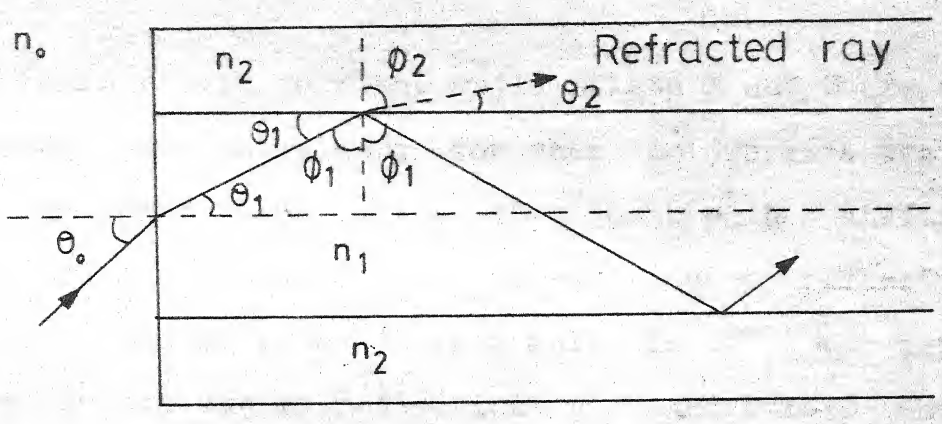

Fig.1·2 (a) Side View of a Step Index Fibre showing a typical Meridional Ray

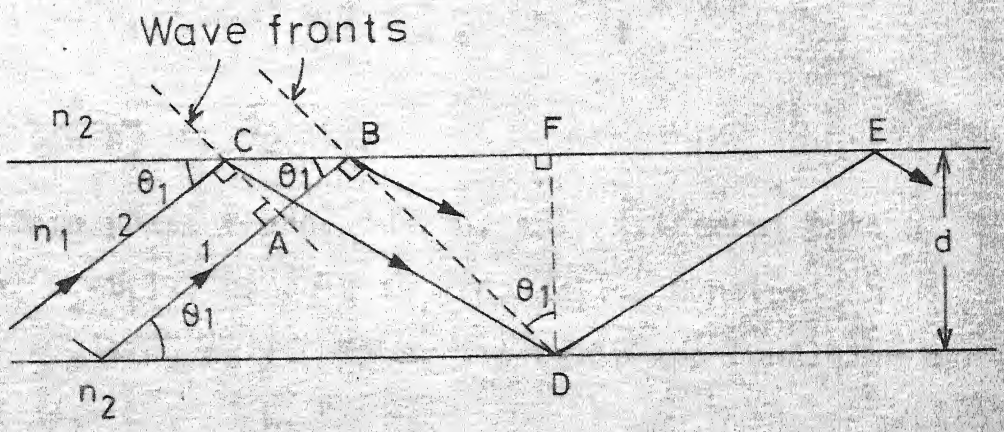

Fig.1·2 (b) Rays undergoing Multiple Reflections

are on an equiphase plane while points B and D are on another equiphase plane. Now when the two rays travel from one equiphase plane to the other their path difference (including the phase shifts in ray 2 due to reflection at C and D) should be an integer multiple of 2π. Let the phase shifts due to reflections at C and D be ϕ (same phase shift at both interfaces as the refractive indices of the two media are the same at both C and D), and to express various distances in terms of d and θ_1, we have

$$\begin{aligned} AB &= BC \cos \theta_1 \\ &= (CF - BF) \cos \theta_1 \\ &= \left(\frac{d}{\tan \theta_1} - d \tan \theta_1\right) \cos \theta_1 \\ &= (\cos^2\theta_1 - \sin^2 \theta_1) \frac{d}{\sin \theta_1} = S_1 \end{aligned}$$

$$\text{and} \quad CD = \frac{d}{\sin \theta_1} = S_2$$

Therefore phase change due to, only different path lengths is $n_1(S_2-S_1)k$, where k is propagation constant in free space ($k = \omega\sqrt{\mu_0 \varepsilon_0}$). Thus, the equiphase condition can be expressed as,

$$n_1 (S_2-S_1) k + 2\phi = 2N\pi \qquad (1.6)$$

Where N is an integer.

This condition implies that rays at all angles satisfying the inequality in Eqn. (1.4) cannot propagate in the optical waveguide. Only rays at discrete values of angle θ_1 satisfying the Eqn. (1.6) can propagate. These discrete values of θ_1 correspond to the various waveguide modes. It then becomes obvious that a calculation of these angles requires the evaluation of reflection phase shift ϕ.

Evaluation of reflection phase shift requires resolving the rays into electric and magnetic fields. Making use of the vector relationship between E and H fields we apply the principle of conservation of energy between the incident, reflected and refracted ray to find the relation betweenincident and reflected power with the usual boundry conditions. This relation is to be found for both perpendicular and parallel polarization. For perpendicular polarization (when E field is perpendicular to plane of incidence) the analysis results in the phase shift angle for total internal reflection to be,

$$\phi = 2 \tan^{-1} \left[\left(\sin^2\phi_1 - \frac{n_2^2}{n_1^2} \right)^{1/2} / \cos\phi_1 \right]$$

Where angle ϕ_1 is as shown in Fig. 1.1(a). For parallel polarization (E field is parallel to the plane of incidence and not that of interface) the phase shift angle

for total internal reflection is found to be,

$$\phi = 2 \tan^{-1} \left[\left(\sin^2\phi_1 - \frac{n_2^2}{n_1^2} \right)^{1/2} / \left(\frac{n_2^2}{n_1^2} \cos\phi_1 \right) \right]$$

The phase shift is different for the two types of polarizations. Thus we see there are discrete values of θ_1 which satisfy the phase condition for total internal reflection and ϕ is different for the two types of polarizations. This means there are two sets of modes which can propagate.

1.4.2 Rays in Optical Fibres:

There are two types of rays that exist in optical fibres meridional rays and skew rays. A meridional ray confines to a single plane called meridional plane. Meridional planes pass through the guide axis. A typical example is shown in Fig. 1.2(a). For skew rays the path does not confine to a single plane and they do not pass through the guide axis.

Let us consider the meridional rays first. Referring to Fig. 1.2(a), a meridional ray incident at an angle θ_o will be guided by the fibre if the corresponding angle θ_1 after refraction at the incident end is less than critical angle θ_{1c} defined earlier by Eqn. (1.5). From Eqn. (1.4) we get,

$$n_1 \sin \theta_1 < (n_1^2 - n_2^2)^{1/2}$$

Using Snell's law we have,

$$n_o \sin \theta_o < (n_1^2 - n_2^2)^{1/2}$$

If n_o, the ambient refractive index of air is unity and θ_m is the maximum value of the angles θ_o, that is possible for ray propagation, then,

$$\sin \theta_m = (n_1^2 - n_2^2)^{1/2} \qquad (1.7)$$

That is a cone of light incident on fibre with conical semi-angle less than θ_m will be accepted and propagated through the fibre. $\sin \theta_m$ is the measure of the light gathering power of the fibre and is known in optics as the numerical aperture. Thus the numerical aperture (NA) of the optical fibre is defined as,

$$\text{NA} = (n_1^2 - n_2^2)^{1/2} \qquad (1.8)$$

This indicates that the maximum light acceptance angle of the fibre is independent of its physical dimensions, and can be made large. Secondly the fibre cross-section can be made small to increase fibre flexibility.

It can be easily shown that the path length of the meridional ray is

$$P(\theta_1) = L \sec \theta_1 \qquad (1.9)$$

Where L is the axial length of the guide. The path length and therefore the transit time of a ray is a function of the angle of the ray. This differential delay between the permitted modes reduces the information capacity of the guide. This will be discussed in more details later. The number of reflections of a meridional ray can be shown to be,

$$n(\theta_1, d) = \frac{L \tan \theta_1}{d} \qquad (1.10)$$

The number of reflections plays an important part as each reflection is associated with some loss. The number of reflections per unit length is:

$$n_m = \frac{\tan \theta_1}{d} \qquad (1.11)$$

Fig. 1.3(a) shows a typical skew ray AXY. Here X and Y are the two reflection points at the core and the cladding interface. XC is normal to the reflecting surface at the point X and ϕ_1 is the angle of reflection the ray makes with the normal XC. YP is perpendicular from Y to the cross-sectional plane containing XC. YP is therefore parallel to the axis and P like Y also lies on the interface. Angle γ is called the azimuthal angle for the ray. Angle θ_1, the angle between the ray and the reflecting surface is called internal axial angle. These angles i.e., θ_1 γ and ϕ_1 are

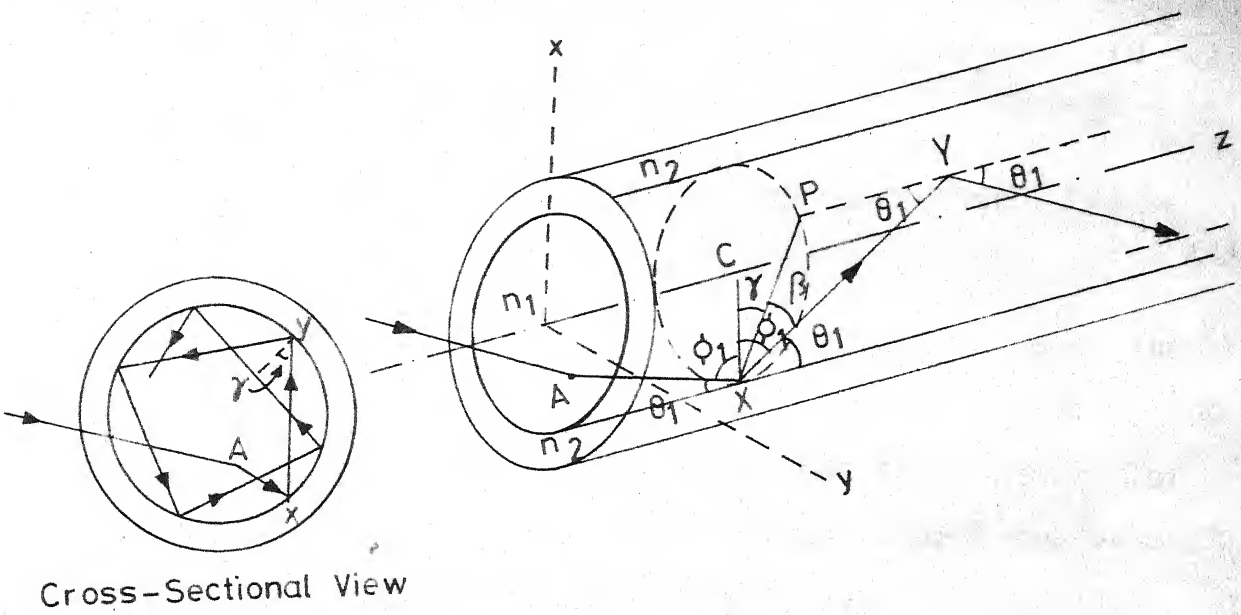

(a) Typical Skew Ray

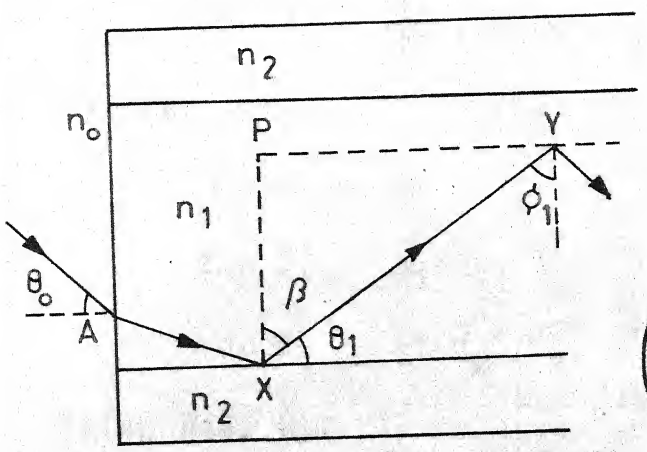

(b)

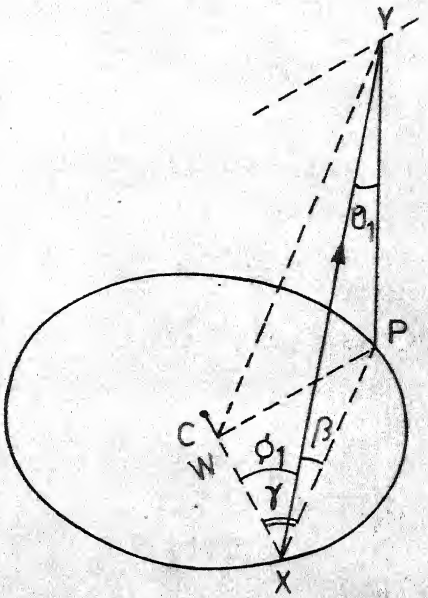

(c)

Fig. 1·3 Skew Ray and Associated Angles

maintained for a particular ray through successive reflections.

Figs. 1.3(b) and (c) give the different views of the relevant angles in detail. We can see that the angles γ and β are in perpendicular planes. Plane YPW is perpendicular to plane WXP as PW is perpendicular to XC, therefore, triangle XWY is a right angled triangle. Therefore,

$$\cos \phi_1 = \frac{XW}{XY} = \frac{XW}{XP} \cdot \frac{XP}{XY}$$

$$= \cos \gamma \quad \cos \beta$$

$$= \cos \gamma \quad \sin \theta_1 \text{ as } \beta = \frac{\pi}{2} - \theta_1$$

$$\sin \theta_1 = \frac{1}{\cos \gamma} \cdot \cos \phi_1 \qquad (1.12)$$

We know for total internal reflection (from Eqn. (1.4)).

$$\cos \theta_1 > n_2/n_1$$

$$\sin \phi_1 > n_2/n_1$$

$$\text{or} \quad \cos \phi_1 < (1-n_2^2/n_1^2)^{1/2} \qquad (1.13)$$

Using Eqn. (1.12), we have

$$n_1 \sin \theta_1 < \frac{1}{\cos \gamma} (n_1^2 - n_2^2)^{1/2}$$

Applying Snell's law

$$n_o \sin \theta_o < \frac{1}{\cos \gamma} (n_1^2 - n_2^2)^{1/2}$$

If n_o is unity and θ_M is the maximum value of the angles θ_o, i.e., the maximum acceptance angle, then

$$\sin \theta_M = \frac{1}{\cos \gamma} \left(n_1^2 - n_2^2\right)^{1/2}$$

$$\text{or} \quad \sin \theta_M = \frac{\sin \theta_m}{\cos \gamma} \tag{1.14}$$

where θ_m is the maximum acceptance angle for meridional rays as discussed earlier (Eqn. (1.7)).

Thus we see that skew rays can be accepted at wider angles than the meridional rays. For $\gamma = 0$, i.e., for the maximum value of cos γ (unity), the ray becomes a meridional ray. As γ varies from 0 to $\pi/2$ the rays tend to travel more along the surface. (At $\gamma = \pi/2$, the ray travels along the surface). For any angle $\theta_o > \theta_m$ there is a range for which the skew rays are accepted. It is interesting to note that for any numerical apperture, θ_M can be equal to 90° for $\gamma = \frac{\pi}{2} - \theta_m$. As an example, let $\theta_m = 30°$. Therefore, NA = 0.5. Then for $\gamma = 90° - \theta_m = 60°$, we get $\theta_o = 90°$. Hence, there will be a cone of light of semi-conical angle of 30°, followed by a dark band and then a ring of light due to skew rays the width of which depends upon angle γ. Thus θ_M depends upon γ and the refractive indices and there exists an angle γ for which ray at any θ_o is accepted. The unit path length for a skew ray is

$$l_s = \sec \theta_1 = l_m \tag{1.15}$$

where, l_m is the unit path length of a meridional ray. The number of reflections (n_s) per unit length for a skew ray work out to be,

$$n_s = \frac{\tan \theta_1'}{d \cos \gamma}$$

$$\text{or} \quad n_s = \frac{n_m}{\cos \gamma} \qquad (1.16)$$

Thus the number of reflections increase in case of the skew rays over the meridional rays. If $\gamma = \pi/2$, the number of reflections is infinite giving a true hellical path along the interface.

1.4.3 Effect of Bends and Variation in Diameter:

Bends in a fibre result in the reduction of the modes being propagated in the straight portion depending on the radius of the bend. We will skip the mathematical analysis leading to this conclusion by just stating that because of a bend the number of the meridional planes, in the bent portion, is smaller than the meridional planes of a straight fibre. The number of such meridional planes is infinite in a straight fibre.

The mathematical analysis of the effects of variation in the diameter of the fibre is also not considered here. If at two points along the length of the fibre, there is a variation in the diameter then that portion can be assumed

to be part of a cone. This reduces the maximum acceptance angle by a ratio r_2/r_1, where r_1 and r_2 are the radii of the fibre at the wider and narrow ends, respectively. This feature can be used to advantage by deliberately making small conical fibre lengths for concentrating light flux density.

1.5 Optical Fibre Communication Systems:

A model of a complete optical fibre communication system is given in Fig. 1.4. Such a system can be divided into two main parts,- one part which deals with the electrical signals, and the other part dealing with the optical energy. The latter part is shown in the dotted line in the figure shown and includes the optical source, the optical fibre and the photodetector.

Like in any communication system the input signal or data first modulates a carrier which is propagated through the channel. Here too we have first an encoder to encode the input data into a suitable code for optical systems. This coded signal then modulates the optical source either directly or indirectly depending upon the type of the source used. The intensity of the light can be modulated either in an analog or digital manner depending upon the modulation format. The optical source converts electrical signals into optical signals. These modulated/coded optical signals

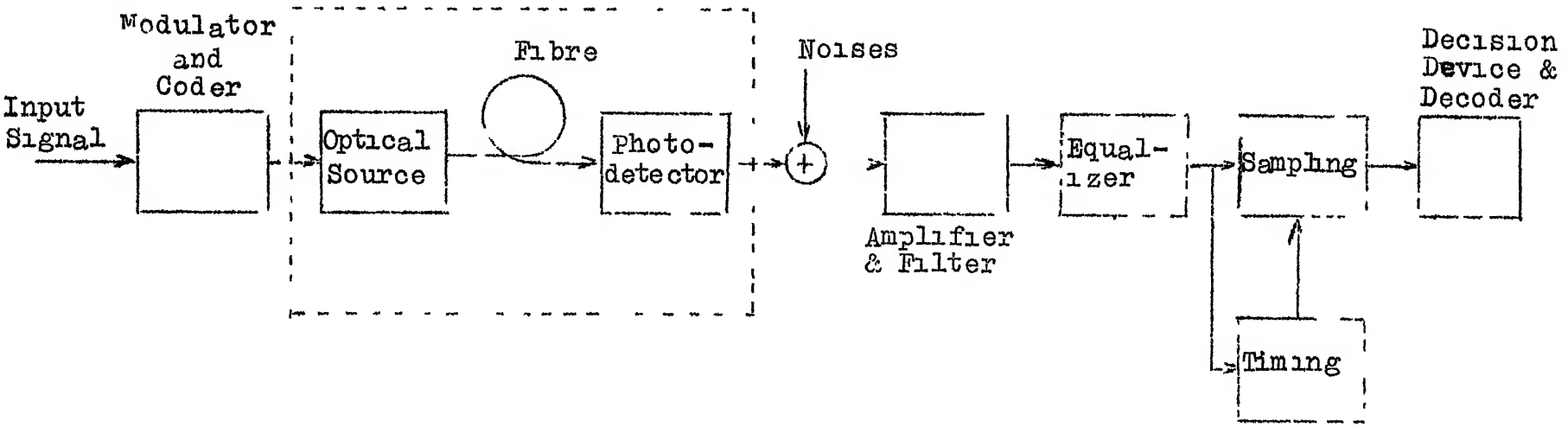

Fig. 1.4 Optical Fibre Communication System

then are propagated in the optical fibre channel. The signal undergoes some losses and distortion depending upon the characteristics of the fibre. The distortion is such that it spreads the signal pulses in time domain. The mechanism of dispersion has been discribed in detail in the next chapter. This spreading results in intersymbol interference in high speed data systems. This attenuated and dispersed optical signal is detected in the receiver by a photodetector. The photodetector changes the optical signal into electrical signal. During the detection process depending upon the type of the photodetector certain noises inherent to the detectors get added to the signal. These noises are of two types viz., thermal and shot noise. Thermal noise is device and circuit dependent where as the shot noise is both device as well as signal dependent. One of these noises dominates depending upon the photodetector used. These noises are added to the photodetector output as shown in the model. The thermal noise is considered to be white Gaussian for the system design. The signal is then filtered to reduce the thermal noise. But as the signal had got dispersed during propagation its shape is required to be restored. The intersymbol interference caused due to the dispersion increases the probability of error. This is reduced by

resorting to equalization. The equalized signal is then sampled at the right instants and the rate at which it is being received. To achieve this some sychronization circuits are used to recover the clock and select the sampling instants. A decision is then made about the sampled signal using a threshold detector, and we get the required signal after it is decoded suitably.

An optical fibre communication system will have minor variations to the one discussed depending upon the application, data rate, fibre length, i.e., repeater spacing, etc. All these aspects have been discussed in more detail in the chapters to follow.

1.6 Applications of Optical Fibres:

The advances made in optical fibre communication systems recently and the number of experimental links that are under trial, and the rate with which new improved components are being marketed by various manufacturers all indicate the bright future and the vast potential of fibre - optics.

As far as communications is concerned, optical fibre cables may be used in a variety of applications where copper-pairs, coaxial cables, and metallic waveguides are now used for transmission of information. The communication

links could be short data links with in a building or long trunk circuits. Data links with in a building may operate at transmission rates of the order of 10 M bits/sec over distances of few meters to few hundred meters. In such applications, therefore, fibres with higher loss (plastic fibres) and greater dispersion could be used along with LED and PIN photodiodes. For intracity and intercity applications where the transmission rate may be about 100 M bits/sec over long distances, low loss and low dispersion fibres would be required. Cable television use of fibre optics is expanding rapidly on worldwide basis. In 1976 Tele Promp Ter Manhattan Cable Television Cable Inc. installed an 800 ft fibre-optic link to carry TV signal from roof antenna to its head-end equipment 34 floors below [6]. Table 1 gives a comparison of some possible digital fibre systems with existing communication systems [7].

Future large scale networks of computers and microcomputers will be heavily dependent upon optical fibres. Already way back in 1976 it was reported that Du Pont was replacing the four-wire cable and conduit connecting two Digital Equipment Corp. PDP-11 mini-computers with two optical fibre channels [6]. Major computer system manufacturers like, DEC, IBM, Burroughs, Hewlett-Packard etc., have

TABLE 1

COMPARISON OF POSSIBLE DIGITAL TRANSMISSION SYSTEMS

System Capacity		Copper cable communication systems		Optical fibre communication systems				
M bit/s	Voice channels	Cable type	Repeater spacing km	Fibre type	Loss dB/km	Repeater spacing km	Light source	Light receiving element
2.048	30	Open wire pairs	2	Step-index	10-4	6-15	LED	PIN PD or APD
8.448	120	0.6 mm-0.9 mm screened pairs	3-4	Step-index	10-4	5-12	LD or LED	APD or PIN PD
34.304	480	2.8 mm coax.	2	Step-index or graded-index	10-4	5-11	LD	APD
140	1920	4.4 mm coax.	2	Graded-index or single mode	10-5	4-8	LD	APD
560	7680	4.4 mm coax. 9.5 mm coax.	1 2	Single mode or graded-index	10-6	2-5	LD	APD

already started using optical fibre short links for intra-package connections and inter-package inter connections [8]. Use of optical fibres for remote computer networks is already under experimentation. The Fibernet experiment [9] using multimode optical fibres has demonstrated the practicability of a 100 M bit/s.km local Computer Networks. This experiment carried about 150 M bits/sec pseudorandom data over a 1/2 km distance through a 19-port star coupler with no errors detected in test sequence of $2x10^{11}$ pulses. For 100 M bits/sec at a distance of 1.1 km, the bit error rate (BER) achieved was $1.1x10^{-9}$.

Light weight, high capacity and freedom from electromagnetic interference make optical fibres attractive for various military uses. Already its use in missile launch control has been reported [8]. Being very light it can be used in place of field cables (single fibre cables) on man pack basis in difficult terrain which will increase mobility. In sensitive areas especially near borders or areas in contact with the enemy, it may be possible for him to infiltrate and eavesdrop using very sensitive equipment capable of picking up EM energy from a wire cable pair running in the vicinity. Optical fibre cables will have freedom from such effects of electronic counter-measure (ECM) techniques. The present day fighter aircrafts have

kilometers of electrical cables in them for use with their sophisticated electronic equipment. If replaced by optical fibres it will reduce the weight taken up by the wiring thus giving the aircraft more speed, higher range, better manoeuvrability or more armament carrying capacity. Also it will make the aircraft free from EMI interference effects. A battle tank is a store house of electrical noise which is picked up by its communication network. Use of optical fibres inside the tank for its intercom system and short links inside other communication equipment, like radio sets, etc., can overcome the present difficulties. Optical fibres have a great use in the naval ships and submarines. The elaborate intercom systems can easily be replaced by these. There is a vast potential in Army Tactical applications too [10].

There are variety of other fields like Business Electronics, Consumer Electronics, Industrial Electronics, specially automative industry (to reduce weight of vehicles to improve efficiency because of shooting petrol prices), and Instrumentation which have a vast potential for fibre-optics. These applications have been comprehensively covered by J.D. Montgomery [8].

The two main aspects which are acting as constraints to still wider applications are the lack of standards and the present high price of components.

1.7 Scope of Work:

To be able to appreciate the special features of an optical fibre communication system and to help design appropriate subsystems, it is imperative to understand the optical fibre channel thoroughly. The optical part of the system consists of the optical source, optical fibre and the photodetector. A fibre has to be characterised for its response so that the communication system can be suitably designed. The characteristics of the optical devices also have an effect on the design of the communication system. All these aspects including some of the problems associated with a practical optical fibre communication system have been reported in Chapter 2.

Some of the characteristics of the propagating medium i.e., the optical fibre, result in pulse spreading. For high speed data signals or for long distance digital data communication this pulse spreading poses a limitation as it results in intersymbol interference (ISI) which increases the error probability. ISI has been combated quite effectively to achieve very low probabilities of error

for moderate data rates in the coaxial systems by using linear and nonlinear equalization techniques. The advantages of achieving higher data rates in optical fibre systems and longer repeater spacings to overcome repeater powering problems, necessitate that ISI be tackled to achieve lower probability of error for more reliable systems. Suitability of the existing equalizer structures have been studied for optical fibre channels. In view of this, a decision feedback equalizer has been designed for a step-index fibre system using a LED as the source and a PIN diode as the photodetector - this being one of the worst combinations in terms of the overall performance of the system. The PIN photodiode and the amplifier following it form the front end of the receiver before the equalizer. In Chapter 3 we have given the structure of the low noise front end of the receiver based on Personick's model [11]. Design of the equalizer and simulation results for a data rate of 10 M bits/sec with different repeater spans upto 10 Km have been reported in Chapter 4.

On the transmitter side choice of a suitable line transmission code to overcome the problems of clock recovery, error monitoring, etc., at the receiver for high

data rate systems becomes important. High data rates also pose problems in the selection of suitable line coding schemes which have less low and high frequency components. In this context various transmission codes have been studied to enable selection of the most suitable one for the application in mind and the system under consideration. This has been reported in Chapter 5.

We then conclude in Chapter 6 with some suggestions for further work possible in this rapidly developing field.

CHAPTER 2

THE OPTICAL FIBRE CHANNEL

2.1 Introduction:

A communication system is always studied and designed for a particular category of channels. This requires that we know the channel well for all its characteristics. We should be able to deduce the effects these characteristics will have on system performance and how will they be tackled in the system design. In view of this, we shall now study the optical fibre channel from a communication engineer's point of view keeping above aspects in mind. In the case of optical fibres the source and the detector being optical devices form part of the optical channel, as shown by the dotted box of Fig. 1.4. In this chapter we study in detail the three constituents of the optical fibre channel, viz., the optical source, the optical fibre and the photodetector. Problems that are typical of the optical fibre channel will also form part of this study.

2.2 Attenuation in Fibres:

Attenuation in fibres has been reduced to such a level these days, that it has already become possible to think of transmission links of more than 10 kms in length over a

fairly wide spectral region. Losses are of two types, - absorption and scattering, and their relative importance depends upon the wavelength region under consideration. Absorption refers to the conversion of light into heat while scattering leads to the conversion of guided into unguided propagation of light and to mode mixing. These losses can originate due to either the material or the waveguide structure. The two types of losses are different for the core and the cladding region, as the power carried in the core and the cladding region is a function of mode number. If the loss coefficients are α_1 and α_2, in the core and cladding respectively, the total loss in the step-index fibre for the mth mode will be [4],

$$\alpha_m = \frac{\alpha_1 P_m^{core} + \alpha_2 P_m^{clad}}{P_m^{total}} \qquad (2.1)$$

where P_m^{core} is the power in the core for mth mode

P_m^{clad} is the power in the cladding for mth mode

and P_m^{total} is the total power in the guide for the mth mode.

The total loss will be obtained by summing over all the modes, weighted by the fractional power in that mode.

2.2.1 Absorption Loss:

Absorption loss can be due to [4]:-

(a) Intrinsic absorption of the basic material.
(b) Impurity absorption
(c) Atomic defect absorption.

Intrinsic absorption is due to charge transfer bands in the ultraviolet region and vibrations in the near infra-red region. For Germanium doped silica the absorption is less than 1 dB/Km in the range 0.7 to 1.5 μm. Impurity absorption is due to the presence of metal ions like of Fe, Cu and Cr in the glass composition. With better purification of glass used for fibre and improved fibre drawing techniques this loss has become negligible. The only important absorbing ion now is OH^- in the range 0.5 - 1.0 μm. High purity of glass is necessary to achieve low losses. Atomic defect absorption can be due to thermal effects during fibrization or by intense radiation of the glass. These losses which can be considerable are important, and glasses less susceptible to these effects have to be chosen e.g., Ge-doped silica.

2.2.2 Scattering loss:

Scattering loss is mainly caused by Rayleigh scattering, Mie scattering, stimulated Raman scattering and stimulated Brillouin scattering [1 and 4] .

Rayleigh scattering is always present, because all transparent materials scatter due to frozen thermal fluctuations of constituent atoms and compositional fluctuations. These cause density and hence index variations within the material. This intrinsic scattering decreases rapidly with increasing wavelength and is below 1 dB/Km for wavelengths above 1 μm. Rayleigh scattered energy appears both in the cladding and the core. In the cladding it can be absorbed and in the core, it appears as backward scattered guided wave, but no serious limitation in transmission bandwidth results [1]. Fluctuation in the concentration of the constituent oxides of the glass material result in Mie scattering.

Stimulated Raman and Brillouin scattering are both nonlinear effects. Below a threshold power density level there is hardly any effect on the transmission. Above this threshold,the principal effect is a frequency shift of the transmitted radiation to low frequencies. Sufficiently large frequency shift would produce amplitude distortion of the receiver. Because of the small core size, confined guidance, (i.e.,power concentration) and the long interaction length, the large fields required to make these effects

significant can be observed at low absolute power levels. For long distance transmission these nonlinear effects constitute an upper limit on the power level that can be transmitted.

In addition to the above causes of scattering loss, there are radiation losses associated with the waveguide structure. The modes which get radiated out are also called leaky modes. This loss is due to finite thickness of the cladding in practice. Losses also occur due to micro-bending and gross bending and these are crucial specially when the fibre is cabled. Attenuation characteristics of a high silica optical waveguide between 0.5 and 1.1 μm are shown in Fig. 2.1. The OH^- absorption bands are clearly visible.

2.3 Dispersion in the Fibre:

The information carrying capacity of optical fibre is limited by signal distortion in the form of pulse spreading. A narrow pulse of optical energy after propagating through the fibre will generally spread out in time with the consequence that long fibres may be limited in bandwidth rather than attenuation. Dispersion (delay-distortion) results mainly due to two factors [12].

(a) Multimode delay-spread,- the variation in the group delay among the propagating modes at a single frequency.

(b) Material dispersion.

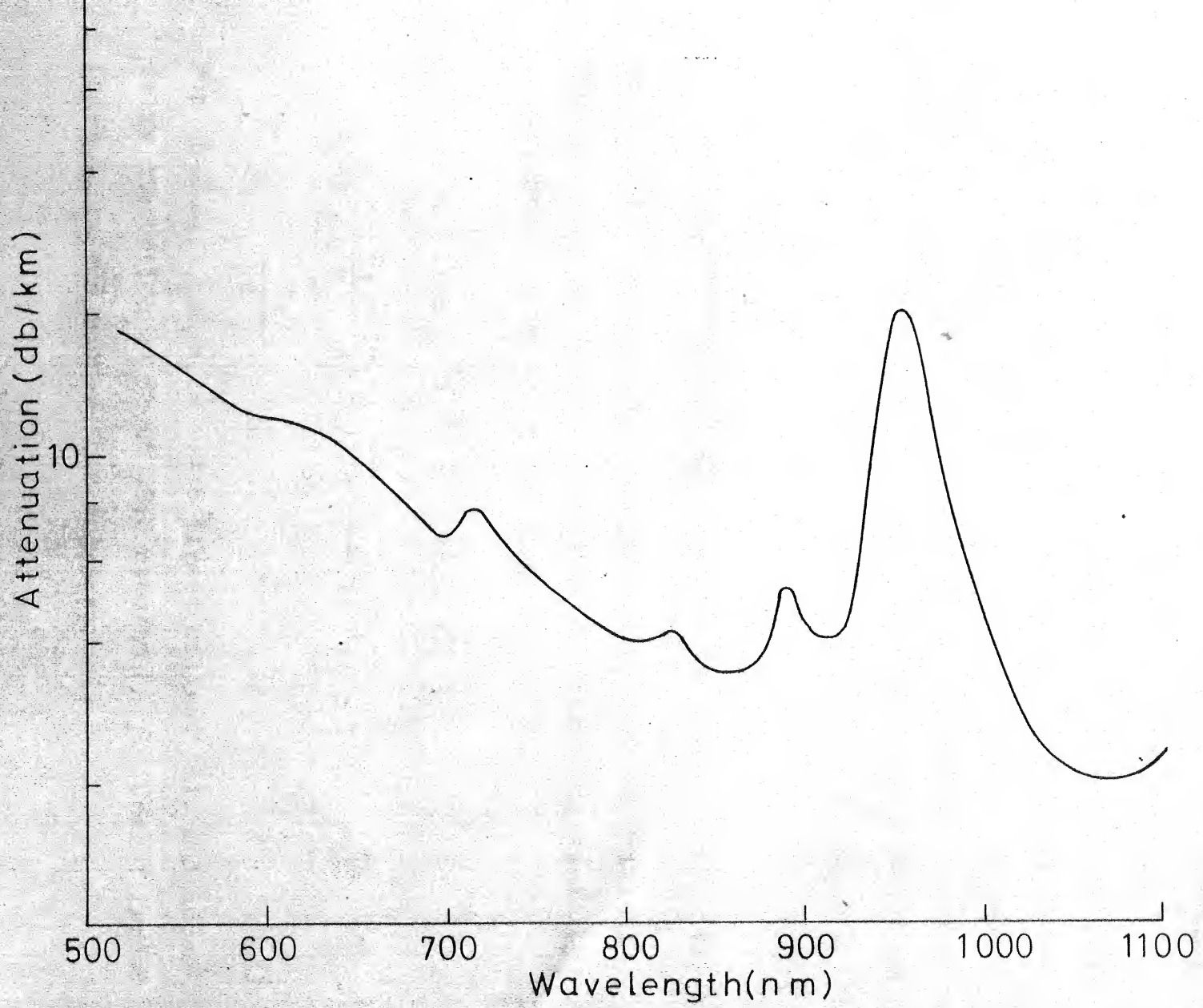

Fig. 2·1 Attenuation Characteristics of an Optical waveguide

2.3.1 Multimode Delay Spread:

As mentioned earlier and shown in Fig. 1.1(b), there is a time delay between the ray travelling along the axis of the optical wave guide and those travelling along the multi-reflection path (in step-index fibres). The slowest ray is the one which travels at the critical angle. This implies there is variation of group velocity with mode. This type of dispersion is also called intermodal dispersion. If t_1 is the time taken by the axial ray, t_{max} is the time taken by critical angle ray to travel the fibre length L then,

$$t_1 = \frac{n_1}{c} \cdot L \qquad (2.2)$$

$$\text{and } t_{max} = \frac{n_1}{c} \frac{L}{\cos \theta_{ic}} \qquad (2.3)$$

where c is the velocity of light and θ_{ic} is the critical angle defined in (1.5). Therefore the maximum time-delay difference between these two rays is.

$$T_d = t_{max} - t_1 = \frac{n_1 L}{c} \left(\frac{1}{\cos \theta_{ic}} - 1\right)$$

$$= \frac{n_1 L}{c} \left(\frac{n_1}{n_2} - 1\right) = \frac{n_1 L}{c} \left(\frac{n_1 - n_2}{n_2}\right)$$

$$= \frac{L\, n_1 \delta}{c} \qquad (2.4)$$

For $\delta = 0.01$ and $n_1 = 1.458$ (fused silica) this multimode delay distortion is about 48.6 nsec/km [1]. Use of graded index fibre can reduce this delay spread.

Delay spread is also affected by mode mixing. During propagation high angled rays can get converted into low angled rays, or vice versa, due to index variations and other geometric perturbations along the length of the fibre. This results in the power in a pulse to transfer among modes and to arrive at the output averaged over all modes, thus reducing the pulse spreading. But, unfortunately, mode mixing also causes loss because power also gets transfered to radiation modes [2]. Thus reduction in pulse spreading has to be traded off with increased attenuation.

2.3.2 Material Dispersion.

This dispersion is due to the variation of the refractive index of glass as a function of the wavelength, which causes variation in group velocity of the mode. Pulses from broad-band sources spread out in time by an amount proportional to the source bandwidth and fibre length. Thus being a chromatic effect, this intramodal dispersion decreases as source monochromaticity increases. Typically a LED source with 50 nm bandwidth will have about 5 nsec/km of pulse spreading caused by material dispersion associated with it [12]. This dispersion is smaller at longer wavelengths (where fibre loss is also lower), going to zero at about 1.3 μm.

2.4 Impulse Response of Optical Fibres:

To investigate, design or simulate any subsystem of the optical fibre system (or for that matter any communication system) we need to characterise the channel. For an experimental link the impulse response of the optical fibre channel used is normally found by measurement of the delay distortion. Delay distortion can be measured either in time domain (impulse-response measurements) or in frequency domain (transfer-function measurements) Barnoski and Personick [12] have outlined a few methods. Many authors have done theoretical analysis and found expressions for impulse response or transfer function for different types of fibres. These theoretical results are based on certain basic assumptions and otherwise ideal conditions. However when an optical fibre of any type is manufactured it may have some perturbations etc. and thus it is always better to obtain its impulse response practically than do any theoretical calculations. But for the purposes of study and theoretical design of a subsystem one may have to use the theoretically suitable and manageable closed form expression for the fibre type under study or use. Some of the methods/theories used are [13]: Wentzel, Kramers and Brillouin (WKB) method using a mode continuum or discrete modes, geometrical optics, perturbation theory and coupled power equations formulation of

equivalent circuit model, geometric optics limit of the coupled power equations, evanescent fields etc. Out of the three theories dealt with in detail for graded index fibres in [13], it was found that there is a good agreement between theoretical calculations based upon WKB method and measurement of the impulse response, and that the perturbation theory gives a qualitative agreement. Gloge [14] has developed and used a power flow equation on the basis of some reasonable assumptions. He obtained an expression for the impulse response of a clad multimode fibre excited by a source with gaussian distributed intensity. The good agreement between his theory and experimental results indicate that power flow equation is a useful description of the power distribution in an optical fibre.

2.4.1 Impulse Response of a Step-index Fibre excited by a Lambertian source:

J.C. Cartledge [15] has used Gloge's power flow equation to derive the impulse response of a step-index fibre excited by a Lambertian source as against a source with gaussian distributed intensity as used by Gloge.

2.4.1.1 Lambertian Source:

The radiation pattern of a flat geometry LED can be approximately characterised by cos θ intensity distribution

which is the distribution for a Lambertian source Fig. 2.2(a). Though more directional beams can be obtained from, an edge - emitting, double-heterojunction, LED e.g., Plessy HR 952 LED [16] has $(\cos \theta)^2$ distribution, but for our purposes we will consider a Lambertian source. The intensity of light at any point along the radiation pattern is given by $I_o \cos \theta$ where I_o is the radiation intensity normal to the source. Consider the source located at the axis of the fibre Fig. 2.2(b). The light flux in the shaded portion of Fig. 2.2(c) is given by

$$dF = \frac{I_o \cos\theta \, dA}{r^2}$$

where dA is the area of the circular band formed by the small element $rd\theta$ when rotated at angle θ,

$$dA = rd\theta \times 2\pi r \sin \theta$$

The amount of light flux F accepted by the fibre is:

$$F = \int_0^{\theta_m} 2\pi I_o \sin \theta \cdot \cos \theta \, d\theta$$

$$= \pi I_o \sin^2 \theta_m \qquad (2.5)$$

Total light flux emitted by the source is,

$$= \int_0^{\pi/2} 2\pi I_o \sin \theta \cos \theta \, d\theta$$

$$= \pi I_o \qquad (2.6)$$

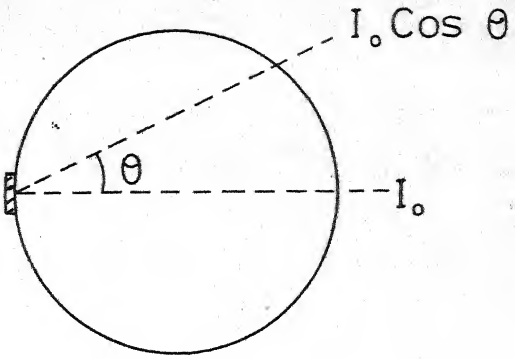

Fig. 2·2 (a)

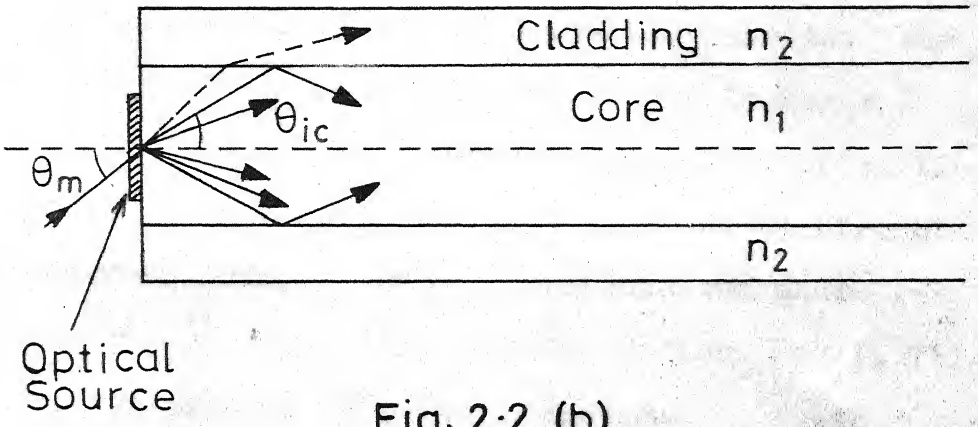

Fig. 2·2 (b)

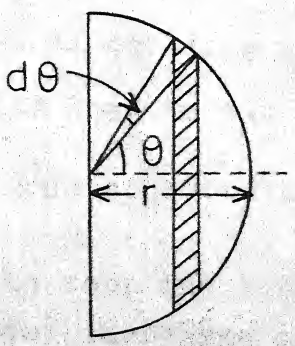

Fig. 2·2 (c)

Fig. 2·2 Radiation Pattern and Light Flux of a Lambertian Source

Therefore the fraction of light collected by the fibre is,

$$f_m = \frac{\pi I_o \sin^2 \theta_m}{\pi I_o} = \sin^2 \theta_m \qquad (2.7)$$

$$= (NA)^2 \quad \text{when } NA < 1$$

$$= 1 \quad \text{if } NA > 1$$

2.4.1.2 Power Flow Equation:

The assumptions made by Gloge [14] in formulating the power flow equation are based on experimental results. For example, the width of the output pulse did not increase linearly with fibre length, but showed a less than proportional increase for long fibres. Measurements of coupling strength showed that a total exchange of power between two modes was likely to occur within less than a meter of fibre [17]. This result made the assumption of a modal continuum rather than thousands of discrete modes fairly acceptable. Hence in this theory, mode coupling took the form of a diffusion process not limited by small coupling amplitudes. Such and other experimental results lead to the assumptions that,

(a) the discrete mode spectrum can be replaced by a continuum;

(b) the loss due to coupling between guided and radiation modes increases as the square of the mode order;

(c) coupling takes place only between adjacent modes and is independent of the mode order.

The power in the fibre is calculated as a function of time, angle θ that optical energy makes with the axis of the fibre which is a continuous variable and the distance Z. Gloge in his previous paper [17] expressed the change (incremental) in power P as a sum of two terms:

$$dP = -A\theta^2 P dZ + \frac{1}{\theta} \frac{\delta}{\delta\theta} (\theta D \frac{\delta P}{\delta\theta}) dZ \qquad (2.8)$$

where the first term comprises attenuation effects in the cladding and the core-cladding interface, out of which term $A\theta^2$ comprises the loss caused at the core-cladding interface. This term is important as power density at the interface increases quadratically with the transverse wave number and thus quadratically with θ. The attenuation coefficient A measured per meter per square radians is evolved from the expression for the total loss $\alpha(\theta)$ in the fibre which is

$$\alpha(\theta) = \alpha_o + A\theta^2 + \ldots \text{ higher order terms.} \qquad (2.9)$$

The contribution of the higher order terms being too little are neglected. α_o comprises loss which is common to all modes. The second term of (2.8) comprises mode coupling effects. This term is typical for radial diffusion in cylindrical configurations and used here due to the assumption of mode diffusion. D the coupling coefficient describes the power transfer that takes place between the

modes that are adjacent in the spectrum and as stated above is assumed to be independent of θ.

If P is a function of time, we can also write

$$dP = \frac{\delta P}{\delta z} dZ + \frac{\delta P}{\delta t} dt \qquad (2.10)$$

The derivative $\frac{dZ}{dt}$ is the velocity of power $P(\theta)$ or the group velocity of the mode with characteristic angle θ, which has been calculated by Gloge with some approximations as

$$\frac{dZ}{dt} = \frac{c}{n(1+\theta^2/2)} \qquad (2.11)$$

where c is the velocity of light and n is the refractive index of the core. Equating (2.8) and (2.10) and using (2.11) gives the power flow equation in the form

$$\frac{\delta \langle p(Z,\theta,t) \rangle}{\delta Z} + \frac{n}{2c}\theta^2 \frac{\delta \langle p(Z,\theta,t) \rangle}{\delta t}$$

$$= -A\,\theta^2 \langle p(Z,\theta,t) \rangle + \frac{D\delta}{\theta\delta\theta}\left[\theta \frac{\delta \langle p(Z,\theta,t) \rangle}{\delta \theta}\right] \qquad (2.12)$$

where $p(Z,\theta,t)$ is the average power distribution as a function of distance Z from the input end, the angle of propagation θ in the fibre and time t.

2.4.1.3 Impulse Response:

Cartledge [15] found the impulse response using the above power flow equation. Using the laplace transform, and

some involved mathematics and again taking termwise inverse Laplace transform with some assumptions and using the condition for Lambertaan source and unit area impulse input as

$$P\ (\ 0,\ \theta,\ s\ ) = \cos\theta$$

the response obtained is

$$h(Z,t) = (2\pi)^{1/2} \exp\ (-at) \sum_{k=0}^{\infty} \sum_{m=0}^{\infty} \alpha_{km}\, D_{-m}(\epsilon) \qquad (2.13)$$

where

$D_{\nu}(x)$ = the parabolic cylinder function

$$a = \frac{2cA}{n}$$

$$\epsilon = (2k+1)\ \left(\frac{D}{tc}\right)^{1/2} z\ , \text{ and}$$

$$\alpha_{kn} = (-1)^m\, 4^{\frac{k+m+1}{t}}\ \frac{(k+m)!}{(2m)!k!}\ \left(\frac{ctD}{n}\right)^{(m+1)/2} \exp\ [-(\epsilon/2)^2\ ]$$

The assumptions are:

(a) $(AD)^{1/2} Z > 0.15$ which means the fibre is sufficiently long

(b) $D < 4A$ which is satisfied by meaningful values of waveguide parameters.

The response involves a double summation and a parabolic cylinder function. Provided $(AD)^{1/2}Z > 1$, Cartledge in his addendum [18] to the above work has stated that, the

impulse response can be accurately approximated by the k=m=0 term of Eqn. (2.13). This results in

$$h(t) = 4\left(\frac{2\pi c\, D/n}{t}\right)^{1/2} \exp\left[-\left(\frac{2cA}{n}\right)t - \left(\frac{DnZ^2}{2c}\right) t^{-1}\right] \qquad (2.14)$$

The impulse response is plotted in Fig. 2.3, 2.4 and 2.5 for various values of A,D and Z. Since the averaging effect of the mode velocities decreases with coupling coefficient D, the asymmetry of the response increases as D decreases i.e. the dispersion defined as full width at half max (FWHM) decreases (Fig. 2.3). Also the number of modes being guided is reduced with decrease in D. As the attenuation coefficient A decreases the FWHM increases since the filtering effect on the higher order modes is reduced (Fig. 2.4). In Fig. 2.6 the dispersion (FWHM) is plotted against the fibre length. The curve exhibits a square root of length dependence.

2.4.2 Frequency Response:

Taking the fourier transform of Eqn. (2.14) we get the frequency response of the step-index optical fibre excited by Lambertian source as [18]

$$H(\omega) = 4\pi(2cD/n)^{1/2} \left(\frac{2cA}{n} - j\omega\right)^{-1/2} \exp\left\{-\left[\frac{2DnZ^2}{c}\left(\frac{2cA}{n} + j\omega\right)\right]^{1/2}\right\} \qquad (2.15)$$

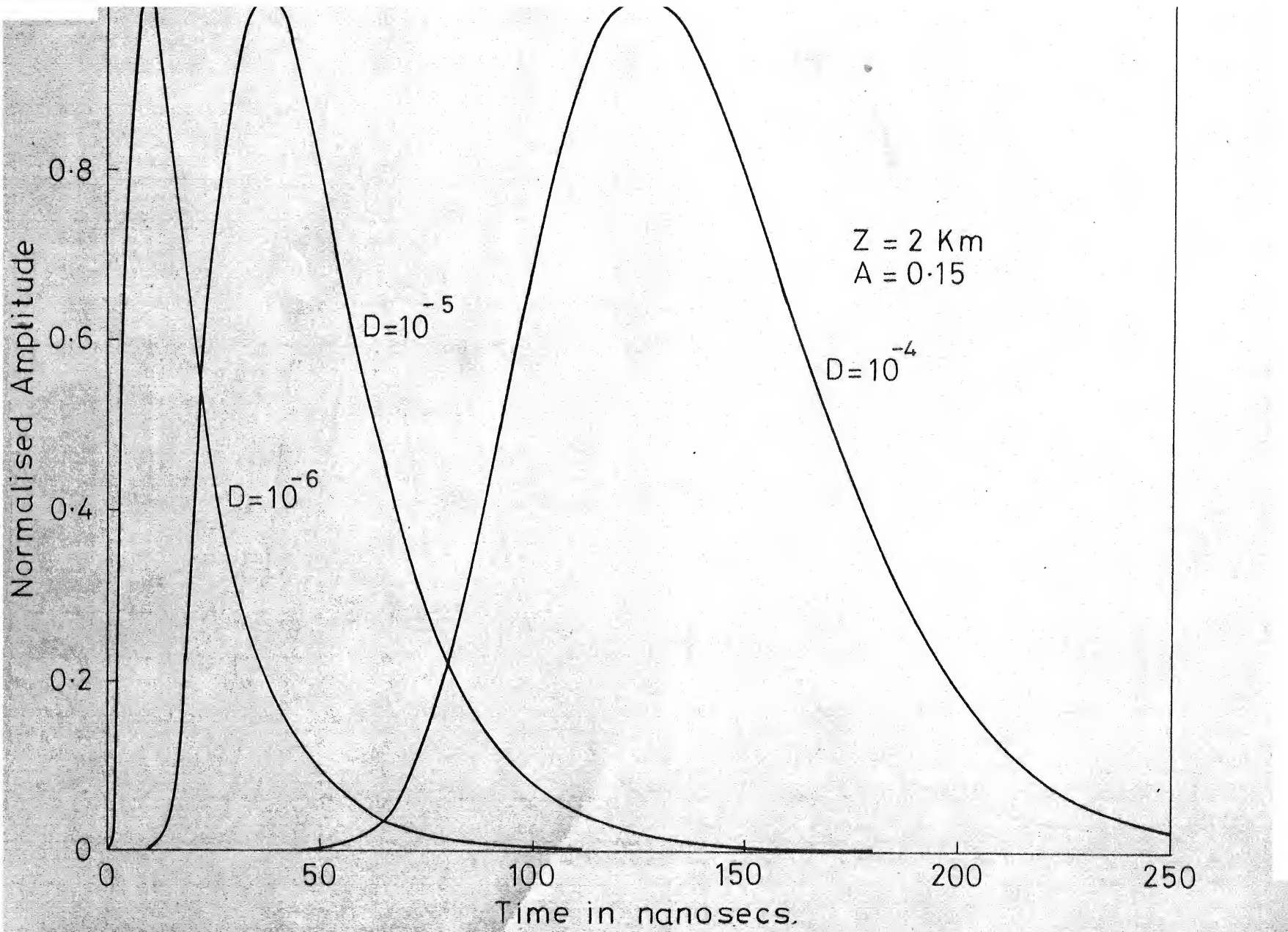

Fig. 2·3 Impulse Responses

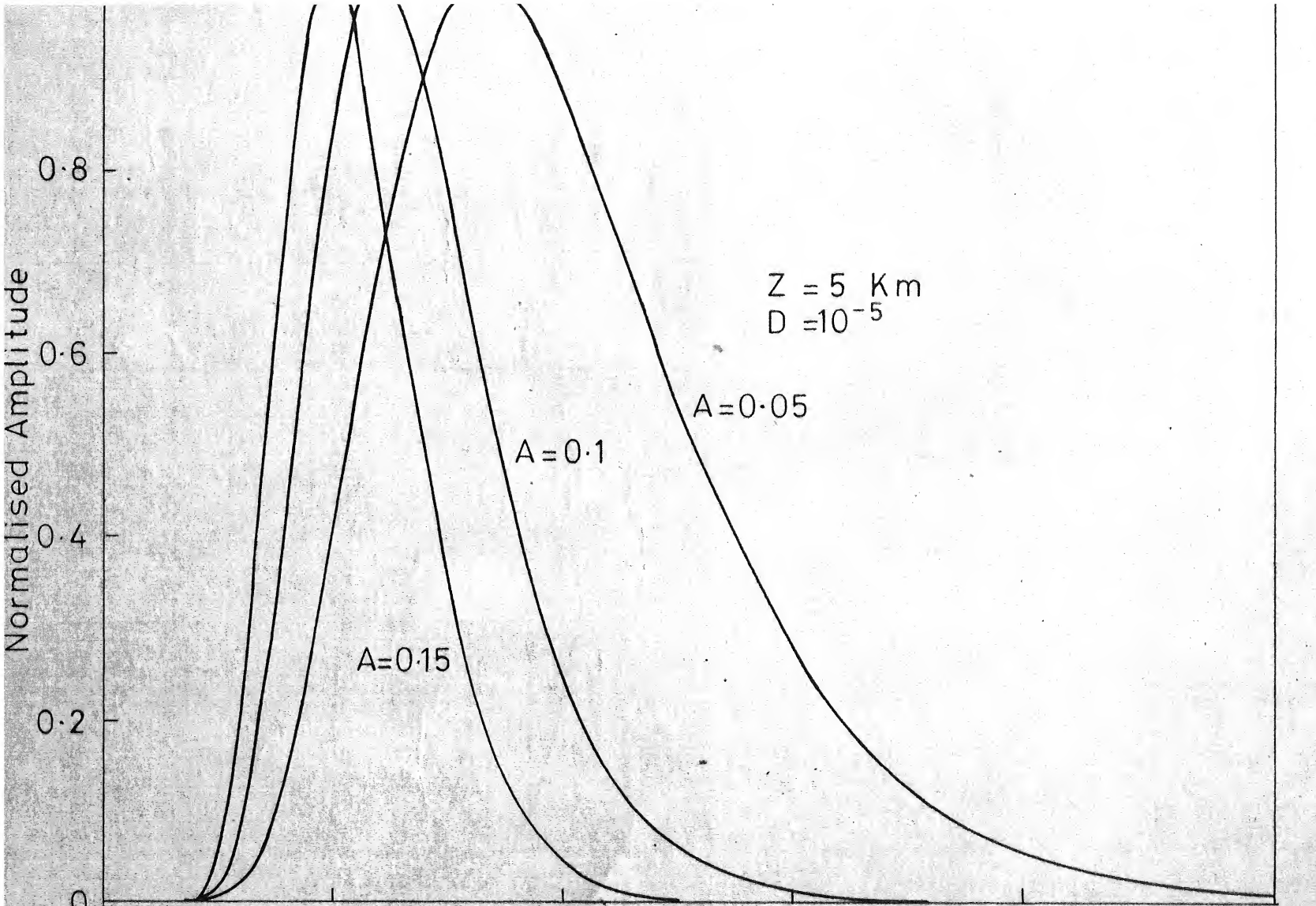

Fig. 2·4 Impulse Responses

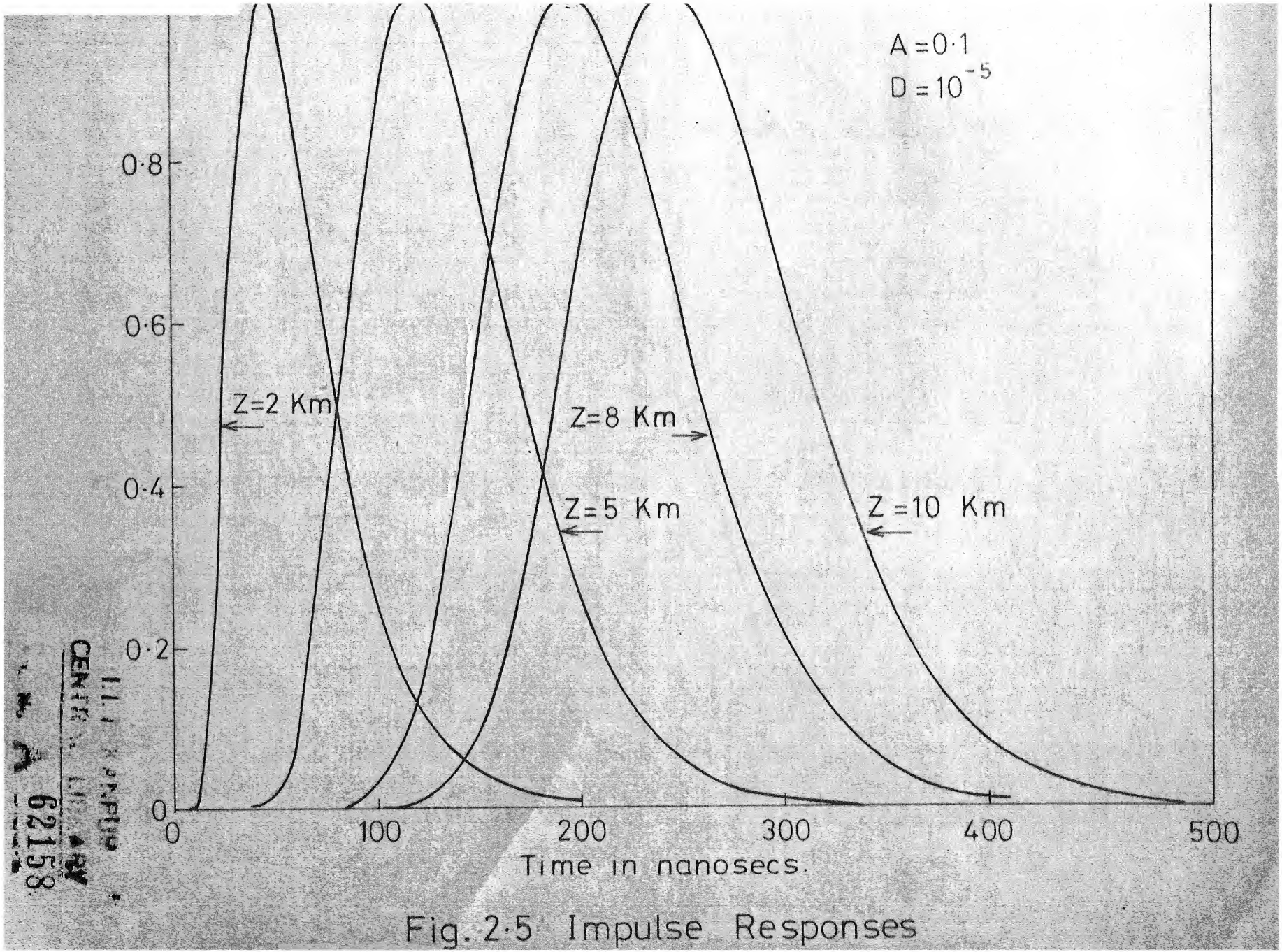

Fig. 2·5 Impulse Responses

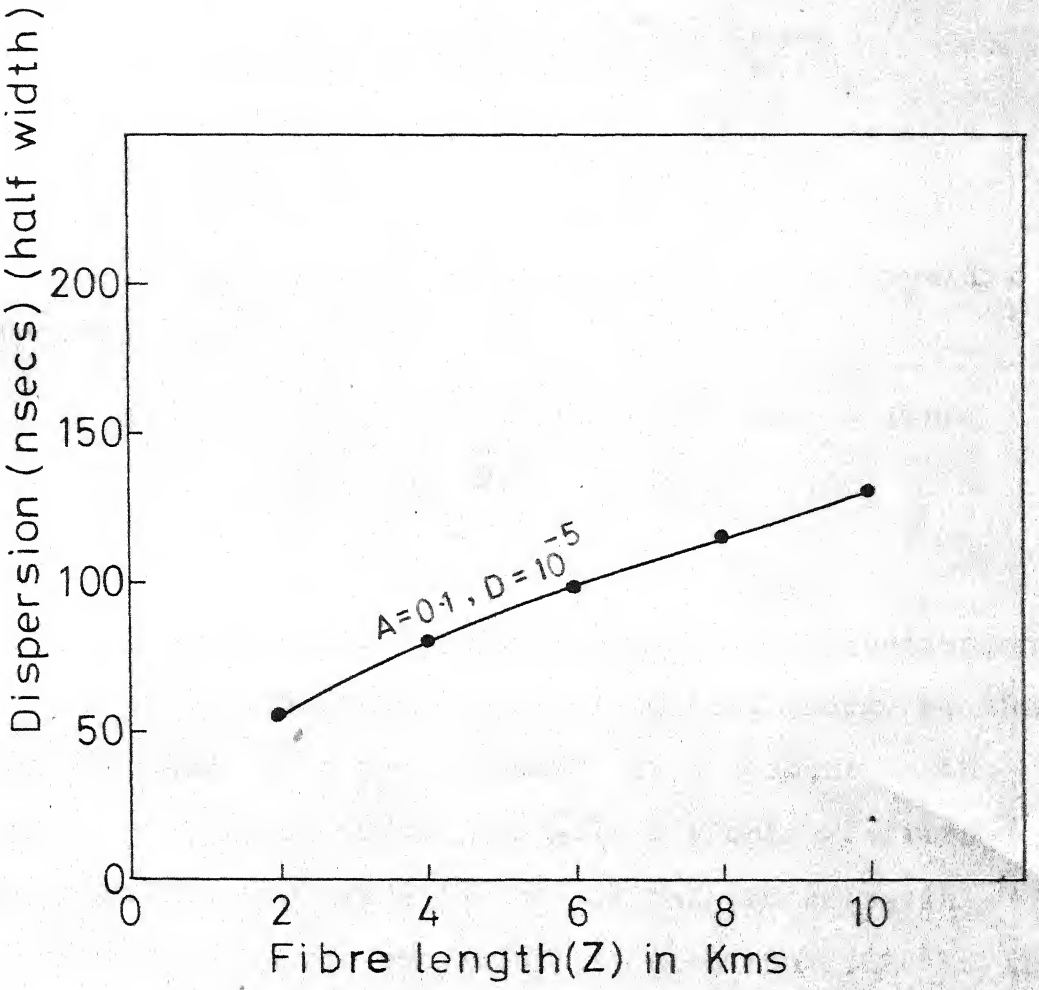

Fig. 2·6 Fibre Length Dependence of Dispersion

Simplifying and separating real and imaginary parts gives,

$$H(f) = 4\pi\left(\frac{c^2 DA}{c^2A^2+\pi^2 f^2 n^2} - J\,\frac{\pi f\, cDn}{c^2A^2+\pi^2 f^2 n^2}\right)^{1/2}.$$

$$\exp\left[-\left(4\,DZ^2A + J\,\frac{4\pi f\, DnZ^2}{c}\right)^{1/2}\right] \qquad (2.16)$$

Modulus of H(f) has been worked out in an Appendix to this chapter.

An amplitude plot for A=0.1, $D=10^{-5}$ and a fibre length Z of 10 km is in Fig. 2.7.

2.5 Optical Sources:

The devices needed in an optical fibre transmission system are for providing a source of optical energy at the transmitting end and a photodetector at the input to the receiver. An optical source suitable for optical-fibre transmission must be reliable, economical and compatible with the fibre. Source compatibility with the fibre is linked with fibre characteristics like its geometry, attenuation and dispersion characteristics, etc. The source and the fibre together have then to suit the system requirements. Presently four types of solid state optical sources are in vogue, viz., the LED, the Super luminescent diode (SLD), the Injection LASER, and the Neodymium-doped Uttrium-Aluminum - Garnet (Nd:YAG) LASER pumped by LED. These emit light within

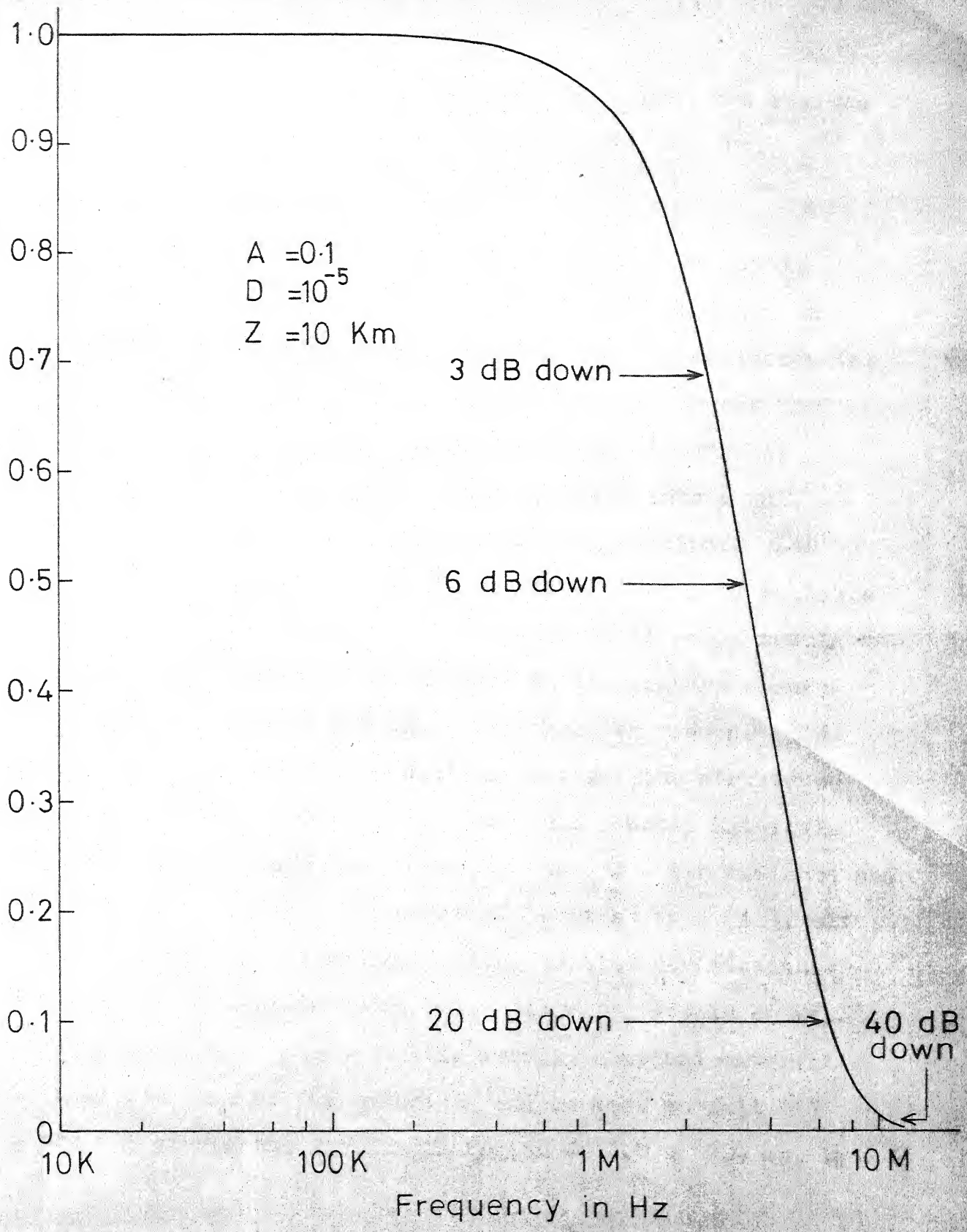

Fig. 2·7 Frequency Response

the 0.8 - 0.9 and 1.0-1.1 μm wavelength ranges, the regions of interest being the low transmission loss regions.

2.5.1 Light Emitting Diode (LED):

The electro-luminescent radiation from an LED is incoherent and arises from the process of recombination of carriers injected across the p-n junction of a semiconductor diode. The usefulness of such an incoherent source for optical communications is its radiance (or brightness) measured in watts of optical power radiated into a unit solid angle per unit area of the emitting surface. LED's have linear output characteristics which makes them suitable for analog applications, They can also be directly modulated. They cost less and are more immune to temperature changes than laser diodes.But the LED's have greater response time giving a lower bandwidth. LED's having various structures and with different combinations of semiconductor materials for p-n junction have been tried to improve their radiance and efficiency. A typical structure of "Burrus" type [1], with higher efficiency and radiance using double-hetrostructure aluminum-gallium-arsenide material (Al_xGa_{1-x} As) is shown in Fig.2.8(a). A property of this ternary compound material is that the peak of the emission can be made to fall any where within the wavelength region of 0.8 to 0.9 μm, by

controlling the mole fraction x, or the aluminum content with no significant change in device efficiency. This allows the system designer to match fibre and source for minimum attenuation. Fig. 2.8(a) also shows a reliable coupling method, where the fibre end is butted against the emitting surface of the LED and secured in place by epoxy resin. In this case the optical power coupled to the fibre is given by [1],

$$P_o = B \cdot A_s \cdot \gamma_s$$

where B is the brightness in watts/Sr/cm^2,

A_s is the Area of emission (active region), and

γ_s is the solid acceptance angle of the fibre (depends upon NA).

$$\gamma_s = 2\pi(\sin\theta_m)^2 = 2\pi(n_1^2 - n_2^2)$$

$$\text{Now } \delta n_1^2 = \frac{n_1 - n_2}{n_1} \cdot n_1^2 = n_1^2 - n_1 n_2$$

For small δ,

$$\delta n_1^2 \simeq n_1^2 - n_2^2$$

Therefore, $\gamma_s = 2\pi n_1^2 \delta$

and $$P_o = 2\pi B A_s \cdot n_1^2 \delta$$

Since P_o is proportional to the solid acceptance angle, one should use fibre with a δ as large as is consistant

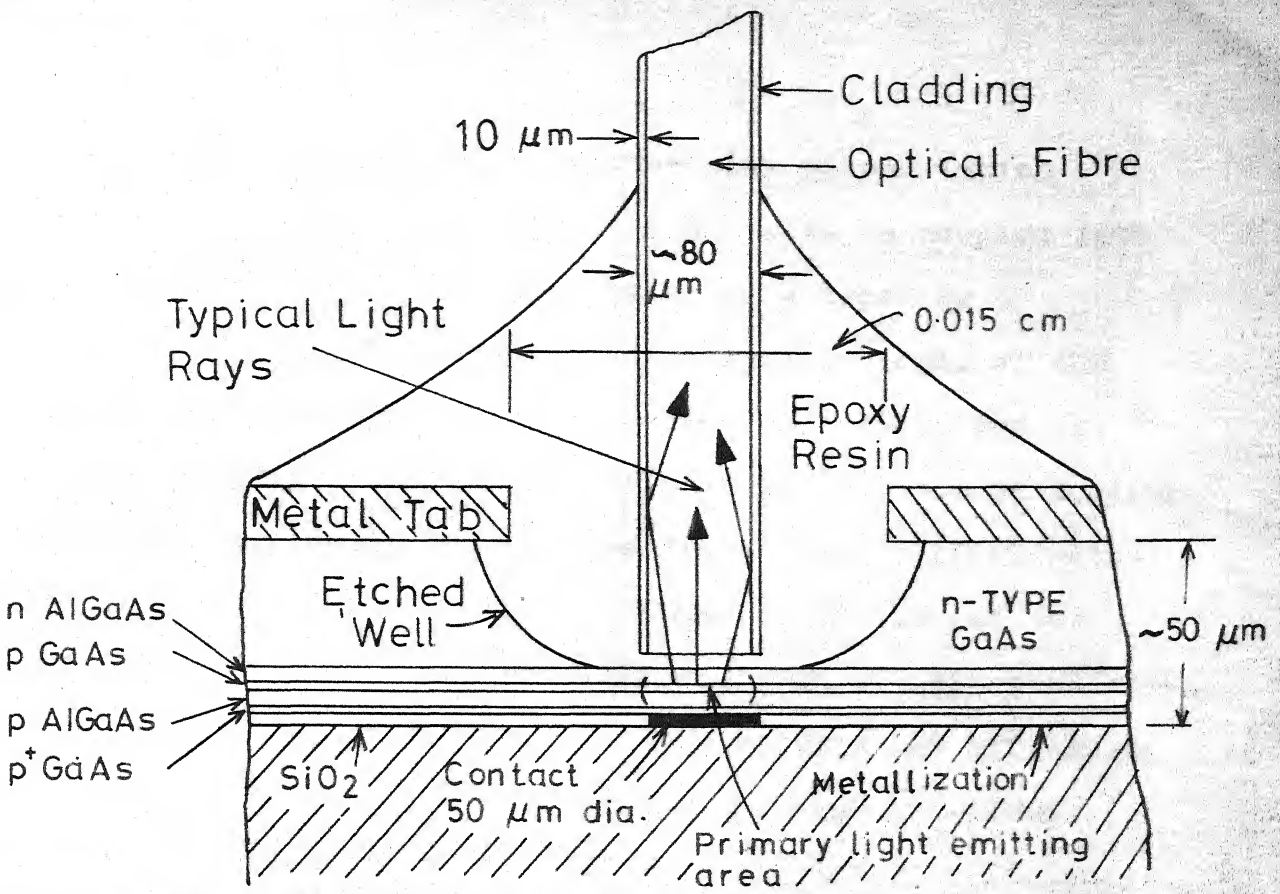

Fig. 2·8 (a) Cross-sectional drawing of a $Al_xGa_{1-x}As$ 'Burrus' type Double-Hetrostructure LED

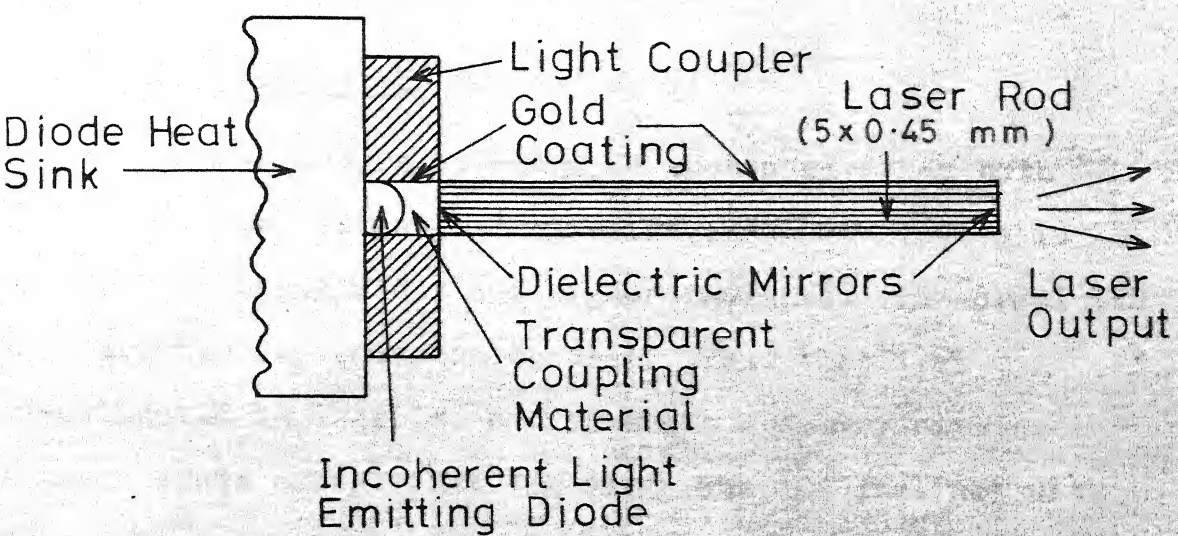

Fig. 2·8 (b) Schematic of the miniature Nd:YAG Laser

with limitations imposed by group-delay spread (which increases with δ). More power could also be coupled into the fibre of larger core area by using a lense or a conical taper which increase the acceptance angle of the fibre. The lense or the conical taper merely serves as a mode converter so that the brightness in the core remains the same. Typically Burrus-type diodes give a power output of 5 to 20 mW. Thus P_o between 5 δmW to 20 δmW can be assumed for system considerations with r.m.s. spectral width of about 350 A°. A tradeoff exists between LED efficiency and achievable modulation bandwidth, so that at highest practical bandwidths of 150-200 MHz, the device efficiency is only 0.5 percent where as it is about 5 percent at 50 MHz optical bandwidth. LED's formed from $GaAs_x Sb_{1-x}$ and GaInAsP have shown encouraging results but are at experimental stage only [19] .

2.5.2 Superluminescent Diodes (SLD's):

When an LED is operated in such a way that both spontaneous and stimulated emission occur it results in narrower spectral width and higher radiance. (In normal LED only spontaneous emission occurs). This was first investigated in GaAs LED's with strip geometry similar to a laser diode except that the strip was 10° inclined with

respect to the normal to the emitting surface to eliminate feedback. Since then modifications to this have been tried using double-hetrostructure (DH) $Al_x Ga_{1-x} As$ material. Peak power outputs of as much as 50 mW (pulsed) have been efficiently coupled into a fibre of NA = 0.63, the spectral widths achieved being 50-80 A° [1].

The SLD in its present form is inefficient compared to laser but the phenomenon of superluminence holds promise for higher radiance and narrower spectral width than LED.

2.5.3 Injection Lasers:

Semiconductor injection laser is exceptionally well suited for optical-fibre transmission being physically small, inherently rugged, highly efficient and can be pumped and modulated directly by means of injection current. Most promising is DH structure design consisting of layers of $Al_x Ga_{1-x}As$ with different values of x grown with liquid-phase-epitaxy and with which low-threshold continuous operation at room temperature has been achieved. As mentioned earlier controlling x can control the wavelength of emission to any desirable value between 0.8 to 0.9 μm. This feature opens up the possibility of frequency multiplexing a number of carriers into a single fibre.

Unlike LED's, high coupling efficiency into multimode fibres can be achieved by merely placing the fibre end next to the output end of the laser, or by using a fibre with a spherical end. On the other hand, single mode coupling is not as easy because the laser mode is elliptical in cross section. Therefore, a section of fibre with suitable taper could be used.

Injection lasers can easily be directly modulated at high speed by variation of the injected current. DH structure lasers can provide 10 mW or more of single or multimode power with sufficiently narrow spectral width to enable neglecting of material dispersion in long distance fibre transmission.

2.5.4 Neodymium - Doped - Yttrium - Aluminum-Garnet(Nd:YAG):

Initial Nd:YAG lasers using elliptical-cylindrical pumping cavity using tungsten halogen lamp as pump, required water cooling etc. They were bulky in size and moreover with an efficiency of 1 percent, were unsuitable for use in fibre systems. Now small size Nd:YAG lasers with low power consumption using end pumping with single LED have been

demonstrated to work at room temperature in a pulsed mode operation. Single-frequency output power of a few milli-watts is expected from these. The Nd:YAG laser is suitable for optical fibres for the following reasons [1]:

(a) Wavelength of emission is 1.064 μm, which coincides with one of the low loss regions of silica fibres.

(b) Because of long wavelength (compared to 0.8-0.9 μm) Rayleigh scattering loss is less ($1/\lambda^4$ dependence).

(c) Narrower spectral emission width and hence less material dispersion.

(d) Relatively easy to obtain single-frequency single-mode output.

(e) LED pumping is expected to yield long life.

However they are not suitable for direct modulation. An external optical modulator is therefore always required. Fig. 2.8(b) shows a schematic of a miniature Nd:YAG laser end pumped by a single LED [1] . Injection lasers these days are being designed at the above frequency range, and the advantage of wavelength of operation of Nd:YAG laser is overshadowed. Table 2 summarises and compares the four optical sources.

OPTICAL SOURCES FOR OPTICAL FIBRE TRANSMISSION SYSTEMS

	Incoherent		Coherent	
Source	Electroluminescent diode (LED)	Superluminescent diode (SLD)	Semiconductor laser	Solid-state ion laser
Material	$Al_xGa_{1-x}As$ double hetrostructure(DH)	$Al_xGa_{1-x}As$ double hetrostructure(DH)	$Al_xGa_{1-x}As$ double hetrostructure (DH)	Nd:YAG
Pump	direct current(dc)	direct current(dc)	direct current (dc)	(AlGaAs)LED
Input electric power	0.2 - 0.5 W	3 - 5 W	0.2 - 0.5 W	1-2 W
Output electric power	5 mW	~50 mW	~ 10mW(single mode) ~ 50mW(multi-mode)	~2mW(Single mode) ~5mW(Multi-mode)
Wavelength of emission	0.75-0.9 μm	0.75-0.9 μm	0.75-0.9 μm	1.06 μm
Spectral width	~350 A°	~50 A°	~ 20 A°	$\leq$1 A°
Coupling efficiency into fibre	$n^2\delta$	$\geq$50%	? 50%	~100%
Modulation	direct	direct	direct	external modulator
Modulation Bandwidth	a few hundred MHz	a few hundred MHz	a few GHz	that of the modulator

2.6 Optical Detectors:

In general optical (photo) detectors convert optical power into electric current by the familiar photo-electric effect. For fibre systems PIN photodiodes and Avalanche photodiodes are the two types of semiconductor optical detectors which have been found to fulfil the following important requirements:

(a) High response at the wavelength of emission of the prospective source (λ= 0.8-0.9 μm for LED and injection laser, and λ= 1.06 μm for Nd:YAG laser).

(b) Sufficient bandwidth or speed of response to accomodate the information rate.

(c) Minimum additional noise introduced by the detector.

(d) Low susceptibility of performance characteristics to changes in ambient conditions.

(e) Compatibility in size, power supply requirements and coupling to the fibre.

PIN photodiode is simpler of the two devices. It is operated in reverse bias as shown in Fig. 2.9(a). Optical power incident on the photodiode as shown gets absorbed and produces electron-hole pairs resulting in mainly displacement current. The number of electron-hole pairs produced depends mainly on the quantum efficiency of the diode. Quantum

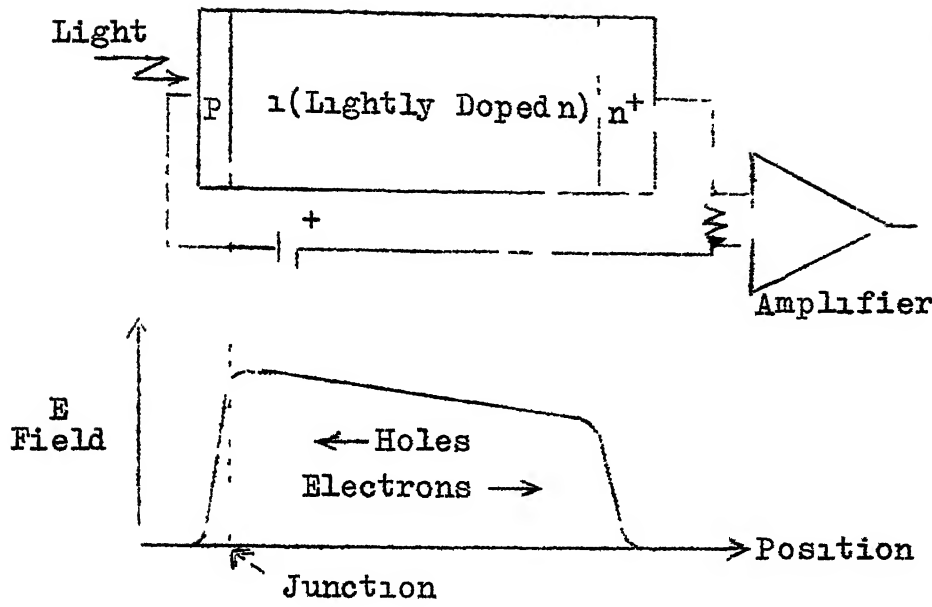

Fig. 2.9(a): PIN Photodetector

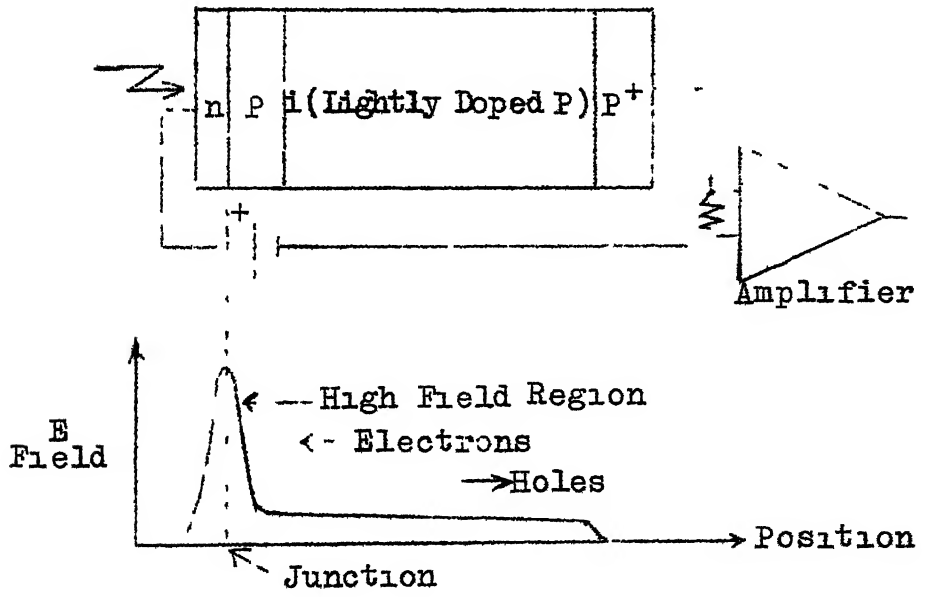

Fig. 2.9(b). APD Photodetector

profile is adjusted to result in a narrow region to the left of the intrinsic (i) region where high electric fields exist. Carriers which drift into this region can be accelerated to velocities which are sufficiently high to generate new electron-hole pairs through the process of collision ionization. These new carriers can in turn generate additional pairs. The result is an effective amplification of the photodiode output current. But, unfortunately, this multiplication is random. The variance of this random process is made as small as possible by proper device design. As stated above the speed of response of a PIN detector is governed by the time it takes for carriers to cross the "i" region. For APD the speed of response is governed by the time it takes for carriers to cross the "i" region plus the time required for multiplication process in the high field region. Detectors of both types have been fabricated with response times less than 1 nanosec. Thus for digital systems operating at speeds below 100 M bits/sec we can idealize the detectors as having an infinite response speed [20]. In practical APD's there is a tradeoff between the gain and the bandwidth (response speed). Mostly made of silicon these detectors have very high quantum efficiencies.

2.6.1 PIN Photodiode Model:

Fig.2.10 shows the PIN photodiode circuit and its

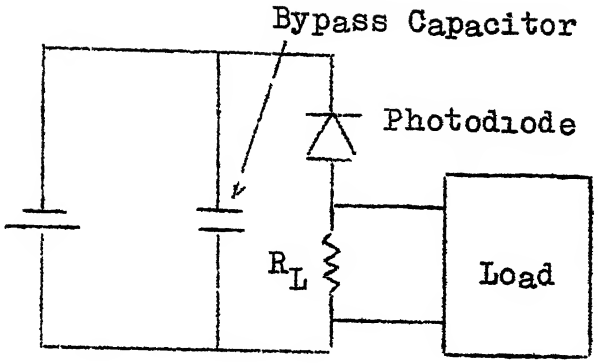

(a) PIN Photodiode Circuit

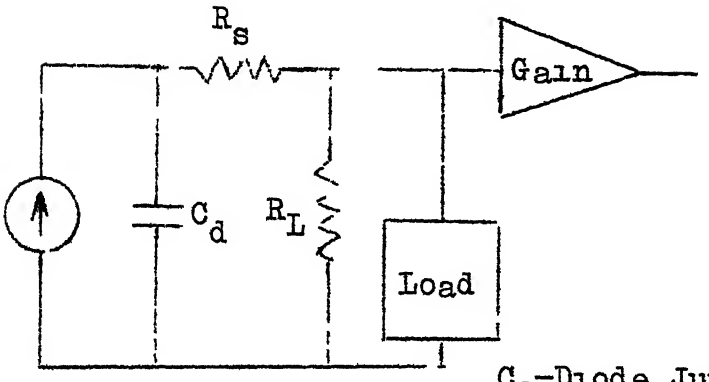

(b) Equivalent Circuit

C_d=Diode Junction Capaci
R_s=Diode Series Resistance
R_L=Physical Load Resistor

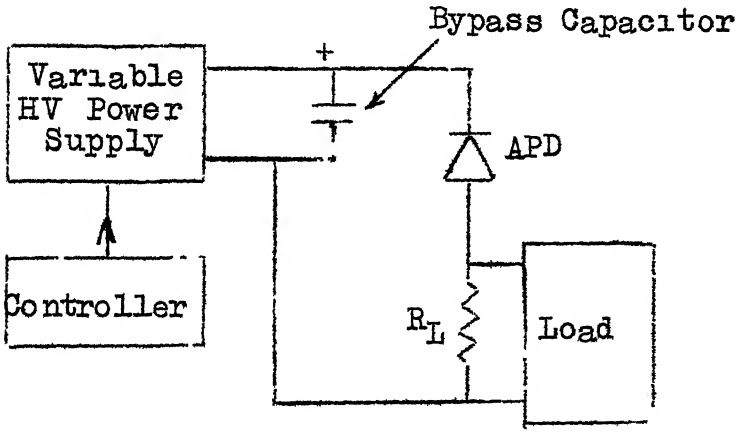

(c) Avalanche Photodiode Circuit

Fig. 2.10: Photodiode Circuits

incremental equivalent circuit[21]. The diode as can be seen is essentially a current source. The small series resistance is negligible in most applications. The load is the amplifier to be used with the photodiode modeled as a resistor in parallel with a capacitor followed by an ideal, infinite impedence amplifier. If A(f) is the amplifier gain and I(f) the detector current at a frequency f, the output voltage is given by:

$$V(f) = I(f)\ Z(f)\ A(f) \tag{2.17}$$

where $$Z(f) = \frac{1}{1/R_T + j\ 2\pi f\ C_T} \tag{2.18}$$

is the impedence of the load, and

$$R_T = 1/(\frac{1}{R_L} + \frac{1}{R_A})$$

and $C_T = C_A + C_d$

If the optical power falling on the detector with responsivity R(amps/watt) is p(t) watts, then the amplifier output voltage is

$$v(t) = p(t)\ R * h_{diode}(t) * h_{amp}(t) \tag{2.19}$$

where * denotes convolution

$h_{diode}(t)$ is the detector impulse response

$h_{amp}(t)$ is the load amplifier impulse response.

It is to be noted that p(t), the received optical power varies in time at a base band rate and not at an optical rate. Further the model assumes that the detector output current is a linearly filtered version of the received optical power.

2.6.2 Avalanche Photodiode Model:

Fig.2.10(c) shows a schematic of an APD biasing circuit. The APD responsivity is a strong function of the bias voltage. Therefore power supply has to be controlled by a temperature compensating circuit to maintain a fixed avalanche gain, because temperature variation varies the detector breakdown voltage. This bias voltage in an APD may be hundreds of volts. This need to provide a controlled high voltage bias is a serious drawback of APD's. The equivalent circuit of an APD is identical to that of a PIN diode as shown in Fig.2.10(b). Since the avalanche gain is bias sensitive, saturation can occur if the applied signal variations are very large, therefore caution must be exercised.

2.6.3 Noise in Photodiodes:

The ultimate performance of a communication system is usually set by noise fluctuations that are present at the input to the receiver. Various sources of noise associated

with the detection and amplification process are depicted in Fig. 2.11. The figure shows noise in an APD. For PIN diode the block containing 'Avalanche gain' need not be considered.

Normally when the photodiode is without the internal avalanche gain, thermal noise arising from the detector load resistance and from active elements of the amplifier circuit dominate. When internal gain is employed, the relative significance of thermal noise reduces.

2.6.4 Statistical Model of PIN Diode:

We have seen that the incident optical power p(t) generates an average current i(t) proportional to p(t) with responsivity as the proportionality constant. The actual process of generation of individual electron-hole pairs, resulting in the displacement currents in pulses (which are summed-up and averaged), is a random process. The difference between the individual actual pulse in any given response, and the average pulse response is the signal dependent noise c(t). For design it is important to know something about the statistics of this noise. We follow the mathematical model evolved by Personick [21].

Assuming that in response to fixed optical power p(t) the carriers are generated at times $\{t_n\}$, and that the

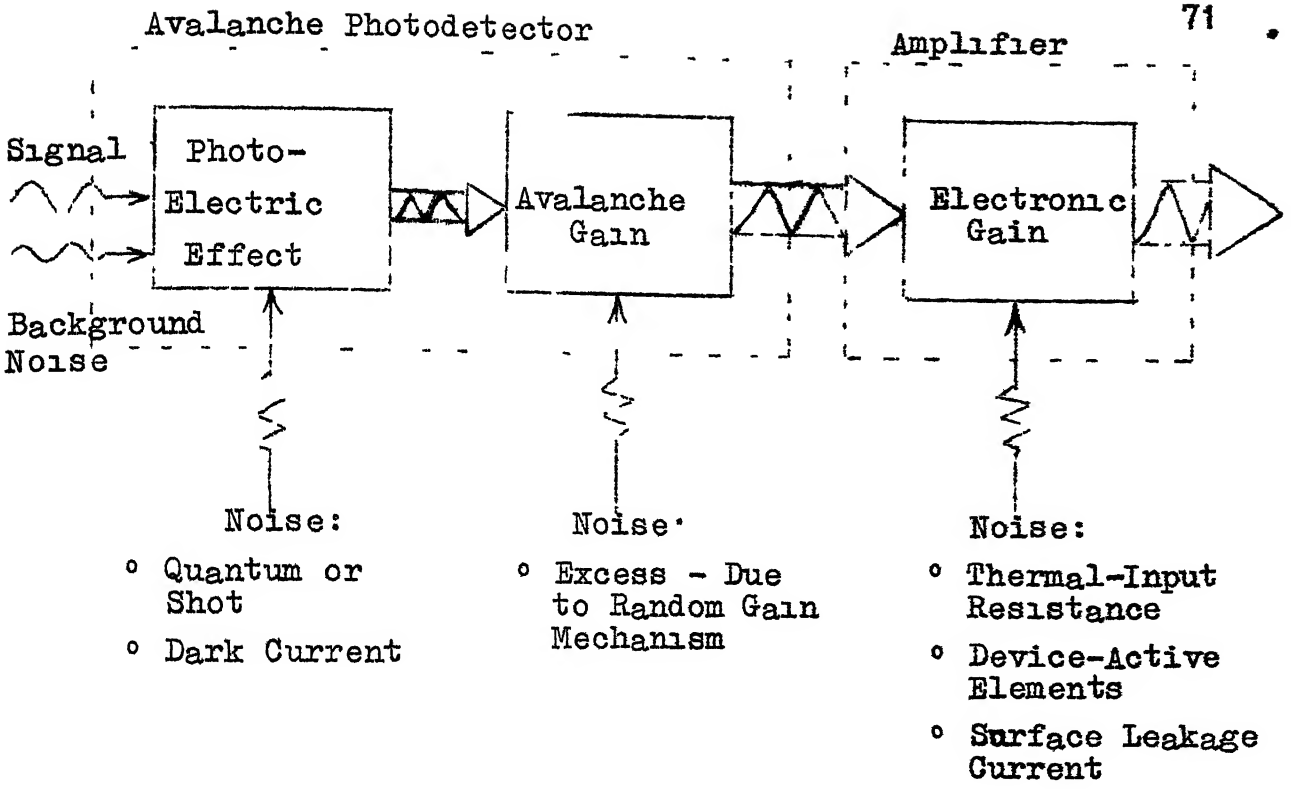

Fig. 2.11: Depiction of Various Noise Sources at the Front-end of an Optical Receiver.

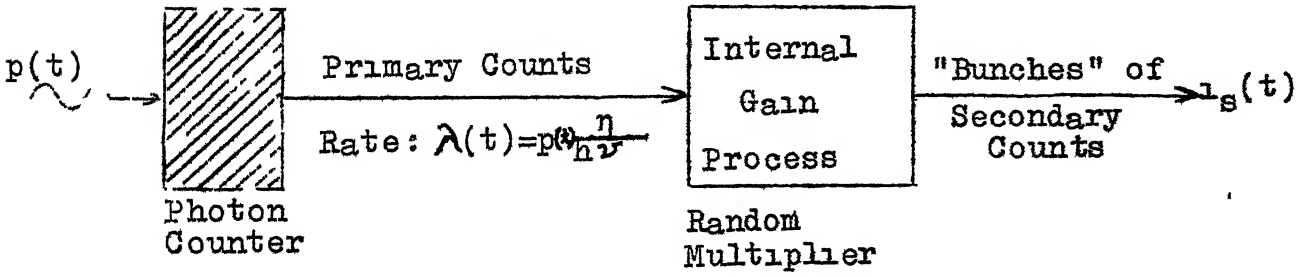

Fig. 2.12: Model of $i_s(t)$ Generation Process

displacement current produced is the same for any electron-hole pair, then the voltage developed across the load is,

$$v_{load}(t) = e \sum_{n=1}^{N} h_{fe}(t-t_n) \qquad (2.20)$$

where e is the charge of an electron, $ch_{fe}(t)$ is the overall impulse response of the diode and the load, to an electron-hole pair generated at time t=0 and N is the total number of such pairs generated. Both N and the set of generation times $\{t_n\}$ are random quantities. If we consider a small interval of time dt such that in it only either 1 or no electron-hole pair is created, then the probability that one pair is created is $\lambda(t)dt$, where $\lambda(t)$ is the average number of electrons generated per second and is given by:

$$\lambda(t) = \frac{p(t)}{h\nu}\eta \qquad (2.21)$$

This pair generation is assumed to be independent from interval to interval. Therefore the total number of pairs created during the time interval $[t, t+T]$ is random with Poisson distribution:

$$\text{Prob}[N = n] = \frac{K^n \exp(-K)}{n!} \qquad (2.22)$$

where K is the mean value of n and given by

$$K = \int_{t}^{t+T} \lambda(t)\,dt = \int_{t}^{t+T} \frac{\eta}{h\nu} p(t)dt \qquad (2.23)$$

Therefore, Eqn. (2.22) can also be written as

$$\text{Prob}\left[N, \{t_n\}\right] = \frac{\exp(-K) \prod_{n=1}^{N} [\lambda(t_n)dt]}{N!} \qquad (2.24)$$

From (2.21) and above, the average voltage across the load can be derived as [21],

$$v_{\text{load av}} = \frac{\eta e}{h\nu} \int_{t}^{t+T} h_{fe}(t-\tau)p(\tau)d\tau \qquad (2.25)$$

From Eqn. (2.20) and Eqn. (2.25) the mean square deviation of the voltage developed across the load from its average value can be found, which constitutes the poisson distributed 'shot'noise. The amplifier output voltage depends upon this voltage plus noise from the diode biasing resistor (Johnson noise) and from the amplifier internal noise sources.

In receivers with PIN photodiode, the thermal noise (due to biasing resistor and the amplifier) deminates the shot noise.

2.6.5 Statistical Model for APD:

The model applicable for a PIN photodiode is also true for an APD upto the generation of primary electrons. To include the avalanche multiplication process and thus generation of secondary electrons the model in Fig.2.12 is suitable [11].

If G is the number of secondary pairs (including the primary pairs) produced through the collision ionization mechanism the voltage developed across the load by the displacement currents flowing in the APD is given by

$$v_{load}(t) = e \sum_{n=1}^{N} G \; h_{fe}(t-t_n) \qquad (2.26)$$

All G are statistically independent and their probability distribution depends upon the type of APD. Thus the current leaving the APD consists of 'bunches' of electrons, the number of electrons in the bunch being a random quantity. In particular it is a function of the ratio of hole collision ionization probability to electron collision ionization probability. That is, as the electron-hole pairs generated drift through the high field region of the detector, one carrier has a stronger probability per unit length of drift to produce a new hole-electron pair. The derivation of the statistics is too complicated and only the useful result relating the mean gain $\langle G \rangle$ and mean square gain $\langle G^2 \rangle$ is given. If k is the ratio of ionization probabilities, then we have [21],

$$\langle G^2 \rangle = F(\langle G \rangle) \cdot \langle G \rangle^2 \qquad (2.27)$$

where $F(\langle G \rangle) = k \langle G \rangle + (2 + \frac{1}{\langle G \rangle})(1-k)$

For an ideal multiplication mechanism obviously we would have $F(\langle G \rangle) = 1$. For good silicon detectors k is between 0.02 and 0.03. For the large class of APD's of interest, it has been found that [11],

$$\langle G^2 \rangle \simeq \langle G \rangle^{2+x} \qquad (2.28)$$

where $\langle G \rangle$ is determined by the applied bias voltage and x, a number usually between 0 and 1, depends upon the diode material. For germanium photodiodes $x \simeq 1$; for good silicon photodiodes $x \simeq 0.5$.

2.7 Some Practical Problems in Optical Fibre Communication Systems:

A practical optical fibre communication system will have several problems which have to be solved satisfactorily for an improved performance of the overall system. Problems which are typical of a fibre system only have been considered here. Some of these are splicing, connections, efficient laying of optical cables and powering of repeaters.

2.7.1 Splices and Connectors:

Splices are required for joining lengths of optical fibres in the field. They must provide low-loss, quick but permanent connections. Connectors are required to couple the

optical cable to the terminal equipment. The basic difference between the two is that connectors are detachable. Numerous fibre to fibre detachable connectors also exist.

Optical energy is required to be coupled from source to fibre, fibre to fibre, or fibre to detector. The factors which effect coupling are core diameter and numerical aperture. Diameter will account for relative ease of coupling Numerical aperture will give the light acceptance angle of the fibre. Therefore it affects the design of the connector so that maximum possible optical energy is coupled to the fibre. An input coupling loss will occur if the angular emission cone of the optical source exceeds that defined by the numerical aperture of the fibre.

Other than detachable connectors source to fibre coupling techniques include close butting, microlensing and use of tapered or bulb-ended fibres [19]. Every type of coupling is associated with some loss. Splices and connectors are therefore required to be designed for low loss.

Since core diameters of optical fibres range from about 20 μm to 60 μm, the fibres must be accurately aligned (within 10% of the diameter) in order to keep the splicing losses small to within 0.5 dB. Splices should also be small,

light weight and rugged. Axial or lateral alignment is most difficult to control. A small end separation or axial misalignment can increase optical loss. Fig.2.13 shows the loss due to end separation and misalignment [6]. An axial off-set d equal to half the fibre core diameter D causes greater than 4 dB loss where as a separation of fibre ends by the same amount gives a loss of 6 dB. Some of the practical splicing techniques that have been explored include the use of V-grooved substrates, circular snug tubes and square loose tubes for single fibres, and multigrooved substrates for mass splicing of multifibre ribbons [2]. Connectors have one additional requirement than splice. It should be able to mate repeatedly without much degradation in coupling efficiency and mechanical strength.

2.7.2 Laying of Optical Fibre Cables:

Optical fibres as drawn are fairly strong. However, abrasion, chemicals and radiations can seriously reduce their strength. To preserve their strength fibres are given a plastic coating soon after they are drawn. Fibres are then bunched together to form cables. Various manufacturers have used different cabling techniques and configurations to produce strong, light weight, small size, handleable, low attenuation cables. Cross-sections of some of the cable configurations is shown in Fig. 2.14.

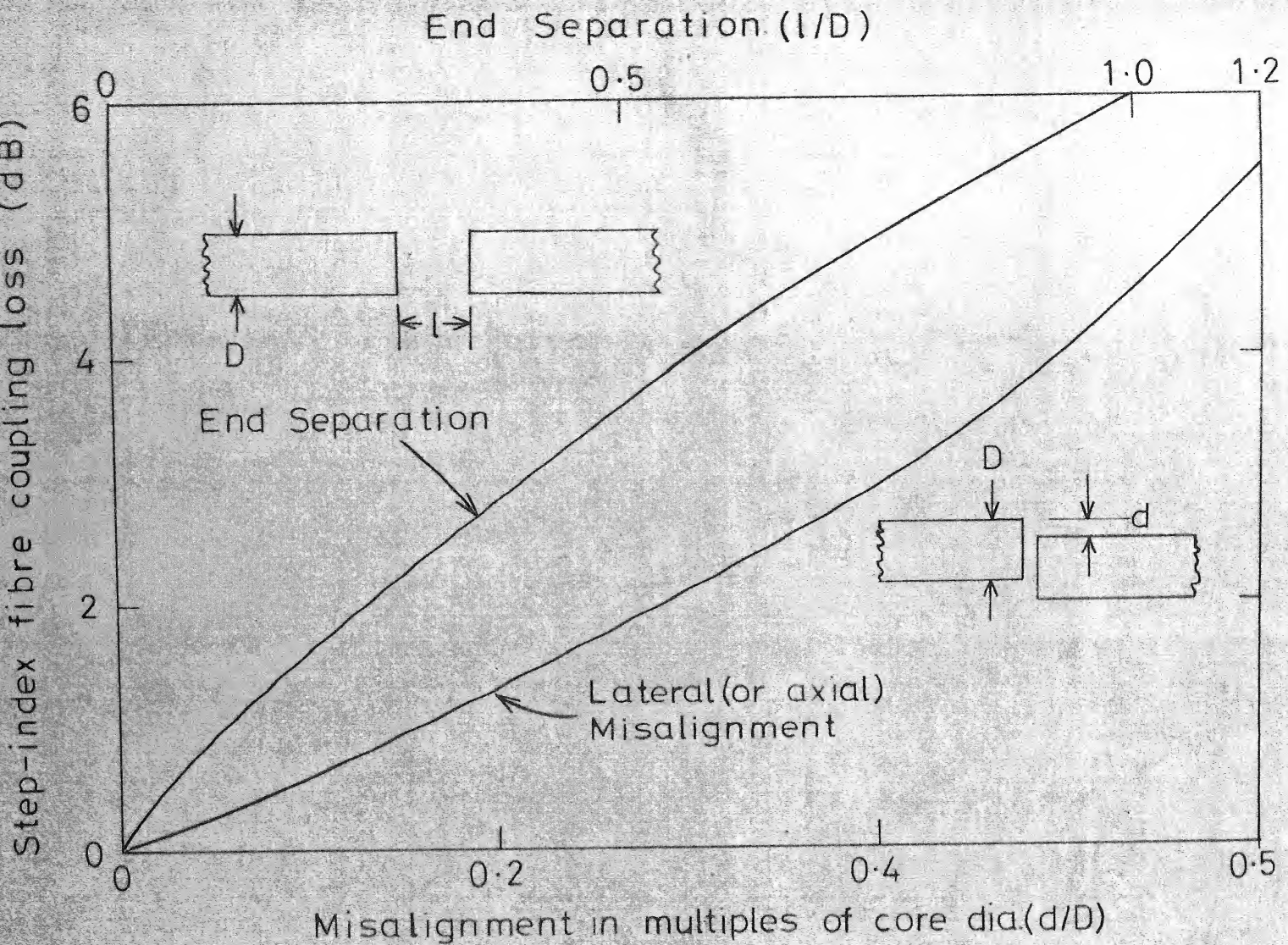

Fig. 2·13 Splice loss due to End Separation and Misalignment

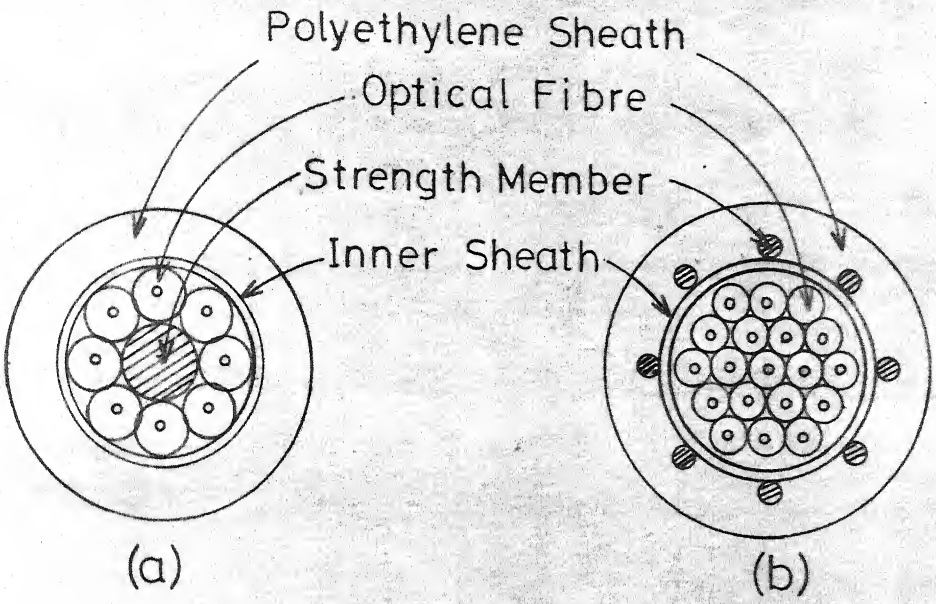

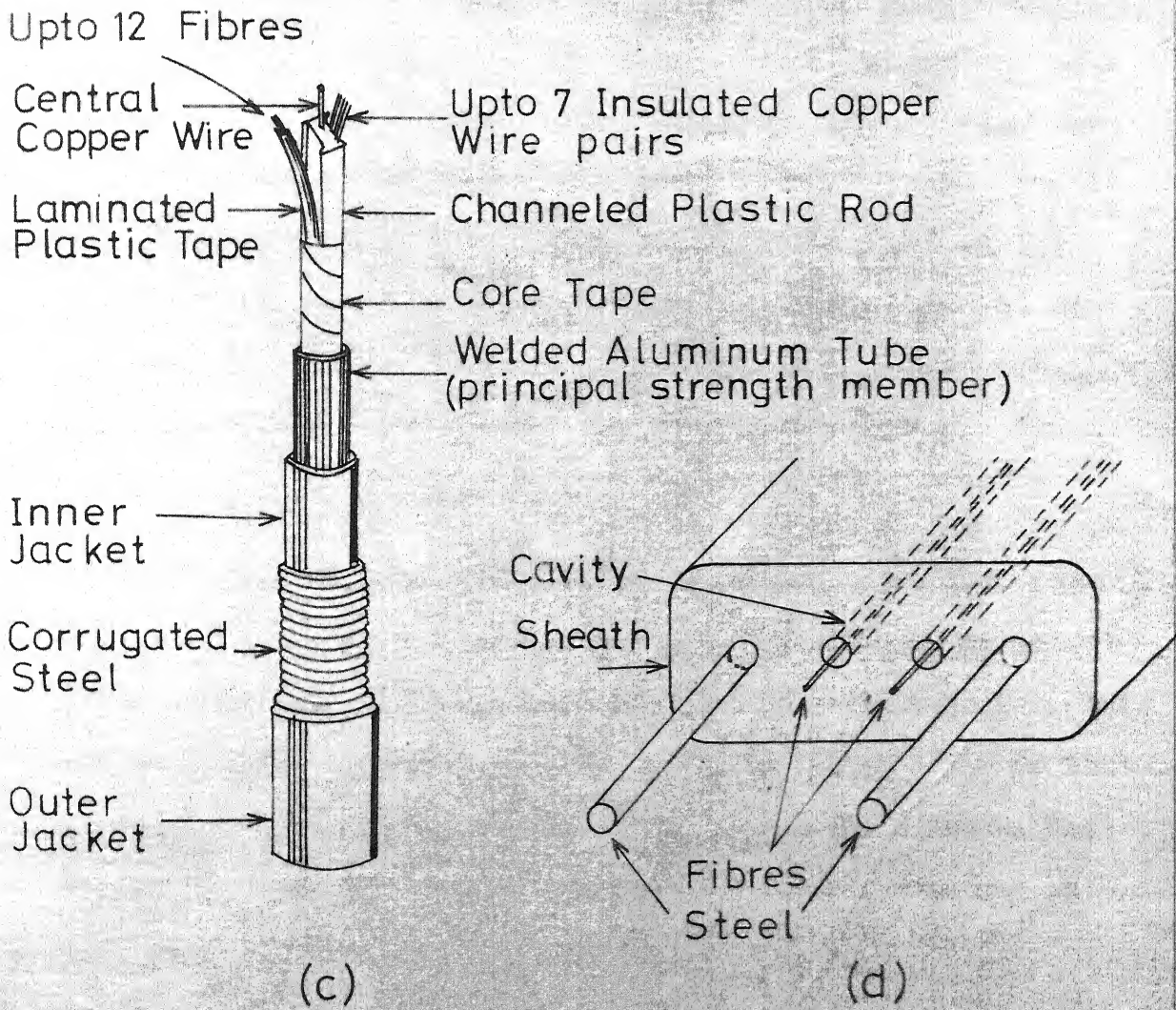

Fig. 2·14 Optical Fibre Cable Configurations

Optical fibre communication cables are usually installed direct by burial in the ground at the depths of two to four feet or they may be pulled into ducts. The two principal differences between optical fibre cables and conventional wire-cables from the installation point of view are, firstly, these are smaller in size, lighter in weight and are produced in longer lengths than conventiona cables, and secondly, a splice introduces much more loss in these than a corresponding splice between conventional wire cables. Many practical trials and installations have been carried out and not much additional difficulties have been experienced as compared to wire cable laying. Infact the larger lengths of the fibre-cables are found to be advantageous [22]. No trials have yet been reported of installation of fibre-cables by ploughing Aerial installati is being considered as a future possibility [10].

2.7.3 Powering of Repeaters:

Powering of repeaters is a very major problem for future long haul systems, since the optical fibre cannot serve as a powering medium as opposed to copper cables. This can be tackled in two entirely different ways. One is that a repeater be locally powered. It is for this reason that efforts are on to achieve as large a repeater spacing as

possible so that one is able to place repeaters at convenient locations along a route where power is available, like some small village or town exchanges enroute. Also to have minimum possible number of repeaters for high data rate links use of equalization in the receiver is being considered. For routes going cross country powering may be feasible by using local batteries. Recent investigations for military uses have shown that 30 day battery operated repeaters are feasible [10].

Another method is to use schemes similar to conventional powering plans used for existing copper cable systems. This entails laying of a pair of copper cable/wires only for powering the repeaters. This may be a costly venture but may be the only alternative. The situation can be made cost effective as compared to conventional systems where each cable carries its own power. In fibre optic systems a number of repeater chains may share a single powering pair. Even if the required quantity of copper in common plans is equal to that required in a seperate powering plan (for each cable pair) common use of the insulator and power regulator and much less number of repeaters may result in overall economy.

A typical powering plan called "series powering", ordinarily used in conventional copper cable systems is shown

in Fig. 2.15(a) [23]. The most important parameter is the powering voltage E_T, the upper limit of which is regulated from the stand point of safety. This is not an efficient plan but for copper cables the plan is defined by the powering phantom circuit which can be occupied by a single repeater chain. Since optical fibre system network structures are not restricted by the structure of phantom circuits there is more freedom available to plan powering networks and an optimum plan can be approached.

For all such plans the main effort is on minimising the powering voltage E_T. E_T has to be minimised under one of the following three conditions, the choice being dependent on feasibility, efficiency and cost effectiveness:-

(a) Constant current receiving - $I_{Rk} = I_R$, $I_R(E_{Rk})_{min} = W_R$ (Minimising E_T with respect to E_{Rk}) and where W_R is received power.

(b) Constant voltage receiving - $E_{Rk} = E_R$, $E_R(I_{Rk})_{min} = W_R$.

(c) Constant power receiving - $I_{Rk}\, E_{Rk} = W_R$.

For the "series powering" plan of Fig. 2.15(a)

$$E_T = (2 I_R R + E_R)\, N = (2 I_R R + (W_R/I_R) N \qquad (2.29)$$

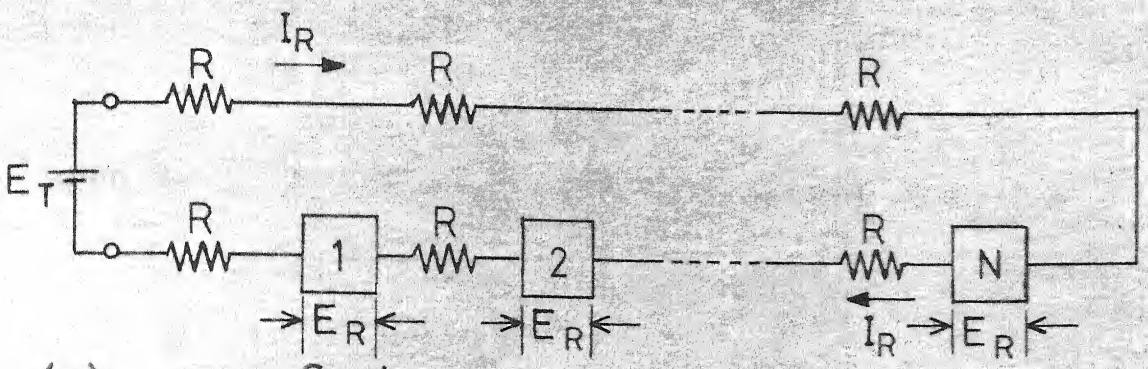

(a) Series powering plan

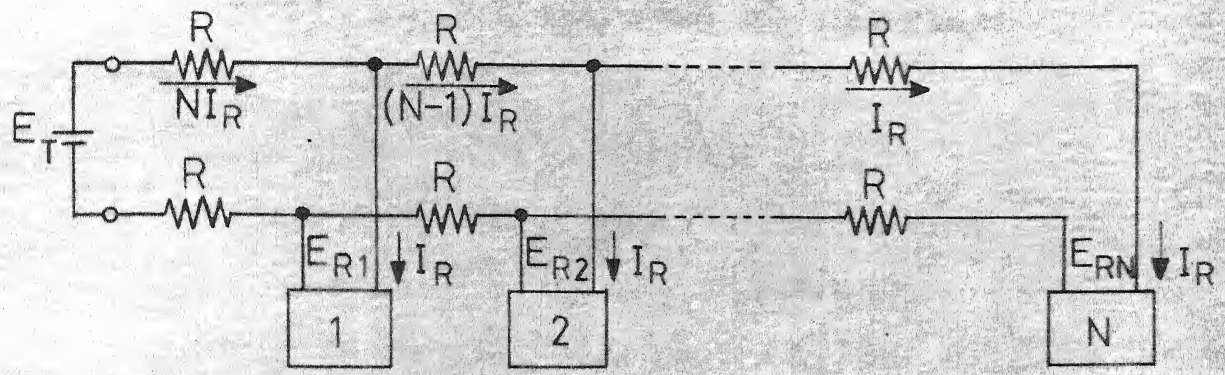

(b) Parallel powering plan-constant current receiving

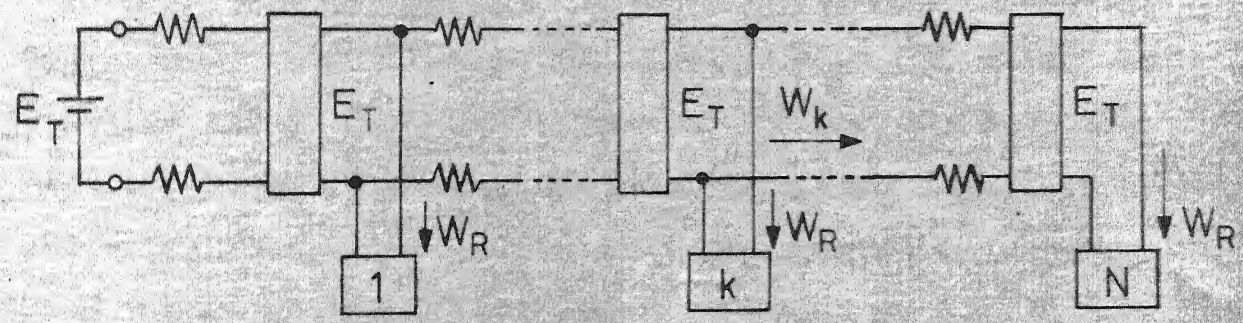

(c) Parallel powering plan - constant voltage retransmission

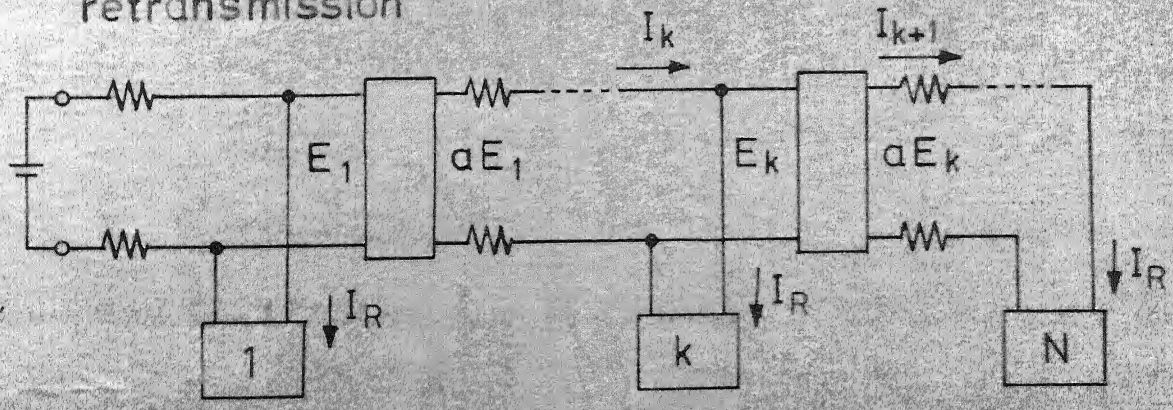

(d) Parallel powering plan - constant ratio transforming

Fig. 2·15 Repeater Powering Plans

where $W_R = I_R E_R$. Minimising E_T with respect to I_R for constant W_R we have,

$$E_{T\ min} = 2\ N \sqrt{2 W_R R} \qquad (2.30)$$

Assuming practical parameters for comparison purposes as:-

power cable impedence R_o = 500 ohms,

power consumption at each repeater station

W_o = 10 watts,

number of repeater stations N = 5,

a plot of E_T and E_R for "series powering plan" is shown in Fig. 2.16(a) as a solid line with the circle on it showing E_{Tmin} value (1000 V), where E_R is about 100V. E_T being very high for any E_R required to power an APD that may have been used in the repeater the plan is inefficient. Fig. 2.15(b) shows "Parallel powering plan-constant current receiving". From the figure it can be seen,

$$E_T = E_R + NI_R \cdot 2R + (N-1)I_R \cdot 2R + (N-2)I_R \cdot 2R + \ldots + I_R \cdot 2R$$

$$= E_R + 2RI_R \left[N \left(\frac{N+1}{2}\right)\right]$$

$$= E_R + N(N+1)R(W_R/E_R) \qquad (2.31)$$

Minimizing E_T with respect to E_R we have,

$$E_{Tmin} = 2\sqrt{N(N+1)RW_R} \qquad (2.32)$$

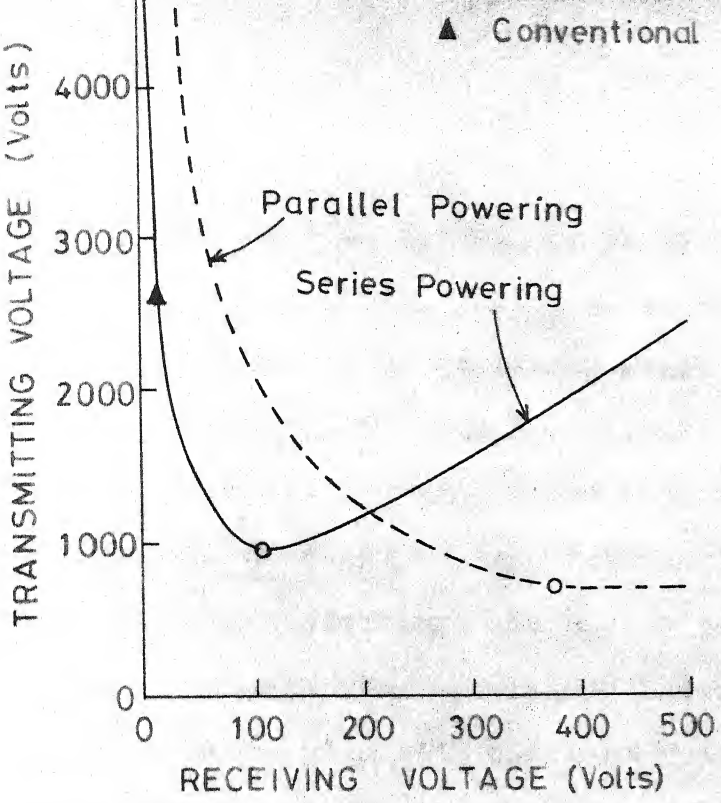

2·16 (a) Plot of Transmitting vs Receiving voltages for Series and Parallel Powering Plan — constant current receiving

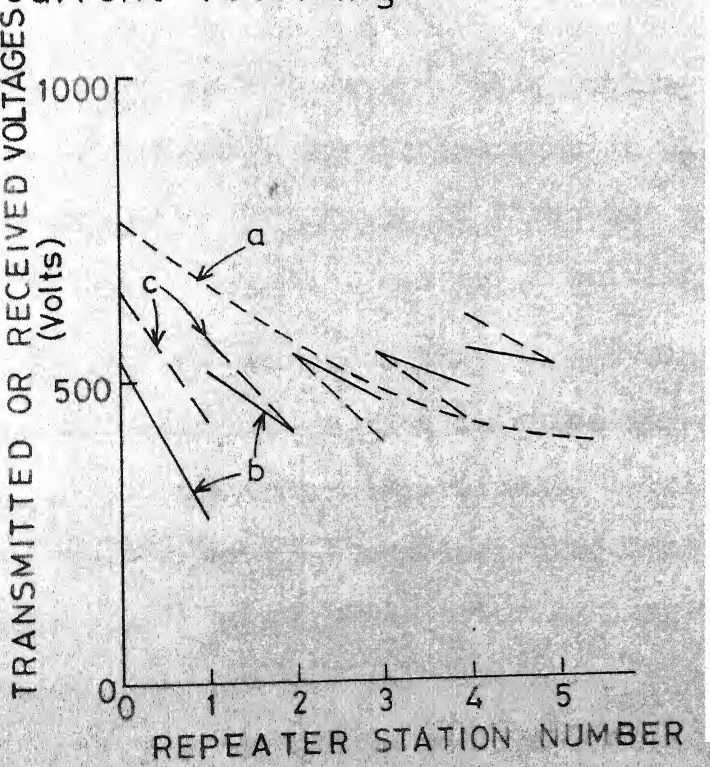

2·16 (b) Comparison of Powering Plans [curve 'a'—Parallel powering plan-constant current receiving (reference), curve 'b' and 'c'—Parallel powering plan-constant voltage transmitting and constant

The dotted line in Fig. 2.16(a) is plotted for the same parameters as given above. ($E_{T_{min}}$=774.6V). Though the corresponding value of E_R is larger still the plan is not efficient. Takasaki [23]has investigated five more powering plans viz., parallel powering plans with constant power receiving, with constant voltage retransmission, and with constant ratio transforming; and series powering plans with three wires and with four wires. He has concluded that "parallel powering plan with constant voltage retransmitting" (Fig. 2.15(c)) is preferable from the stand point of making E_T minimum, however, variation in receiving voltages is relatively large. This problem is overcome in parallel powering plan with constant ratio (voltage) transforming (Fig. 2.15(d) with a little increase in E_T. Fig. 2.16 (b) gives a relative comparison of these two plans with "parallel powering plan - constant current receiving" of Fig. 2.15(b).

It may be concluded that the development of repeaters with small power consumption is quite important in the optical fibre systems. Accordingly, development of optical devices and design of transmission equipment should be carefully based on repeater powering considerations. Just to mention one, optical pulse formats that include more timing component will help realize a timing extractor with small power consumption.

APPENDIX: Modulus of the Channel Frequency Response

From Eqn. (2.16) we have the frequency response

$$H(f) = 4\pi \left(\frac{c^2DA}{c^2A^2+\pi^2f^2n^2} - j\,\frac{\pi fcDn}{c^2A^2+\pi^2f^2n^2}\right)^{1/2}$$

$$\exp\left[-\left(4DZ^2A + j\,\frac{4\pi fDnZ^2}{c}\right)^{1/2}\right]$$

This is of the form

$$H = k(p-jq)^{1/2}\exp\left[-(r+js)^{1/2}\right]$$

Now $(p-jq)^{1/2} = (p^2+q^2)^{1/4}\exp(-j\,\phi/2)$

where $\tan\phi = q/p$

and $(r+js)^{1/2} = (r^2+s^2)^{1/4}(\cos\theta/2 + j.\sin\theta/2)$

where $\tan\theta = s/r$

therefore $\exp\left[-(r+js)^{1/2}\right] = \exp\left\{-\left[(r^2+s^2)^{1/4}\cos\theta/2 + j\,(r^2+s^2)^{1/4}\sin\theta/2\right]\right\}$

Therefore, $H(f) = k(p^2+q^2)^{1/4}\exp\left[-(r^2+s^2)^{1/4}\cos\theta/2\right] \cdot \exp\left[-j(\phi/2+(r^2+s^2)^{1/4}\sin\theta/2)\right]$

Hence, $|H(f)| = k(p^2+q^2)^{1/4}\exp\left[-(r^2+s^2)^{1/4}\cos\theta/2\right]$

where $k=4\pi$, $p=\frac{c^2D^2A^2}{c^2A+\pi^2f^2n^2}$; $q = \frac{\pi fcDn}{c^2A^2+\pi^2f^2n^2}$;

$r = 4DZ^2A$; $s = \frac{4\pi fDnZ^2}{c}$;

$$\cos(\theta/2) = \left[1/2\left(1+\frac{c}{(c^2+d^2)^{1/2}}\right)\right]^{1/2}$$

$|H(f)|$ derived above has been used to plot the frequency response (Fig. 2.7).

CHAPTER 3

RECEIVER DESIGN

3.1 Introduction:

A systematic approach to designing a receiver for a digital optical fibre communication system has been provided by Personick [11]. In particular he has illustrated the proper choice of the front end preamplifier and biasing circuitry for the photodetector. He has also illustrated how the required power to achieve a desired error rate varies with the bit rate, the received optical pulse shape and desired base band output pulse shape. In his analysis he has used avalanche photodiode (APD) as the photodetector in the receiver. Based on his receiver model we shall analyse the front end of the receiver having a PIN photodetector. We shall also find the power requirement (receiver sensitivity) for various lengths of the step-index fibre described in Chapter 2. This gives us the power penalty with increase in fibre length (i.e., repeater spacing). We have also found the power requirements for various input pulse shapes considered by Personick to achieve an output signal which is free from ISI for the channel considered.

3.2 Receiver Model:

The schematic of a typical receiver is shown in Fig. 3.1. The figure shows the equivalent circuit of the

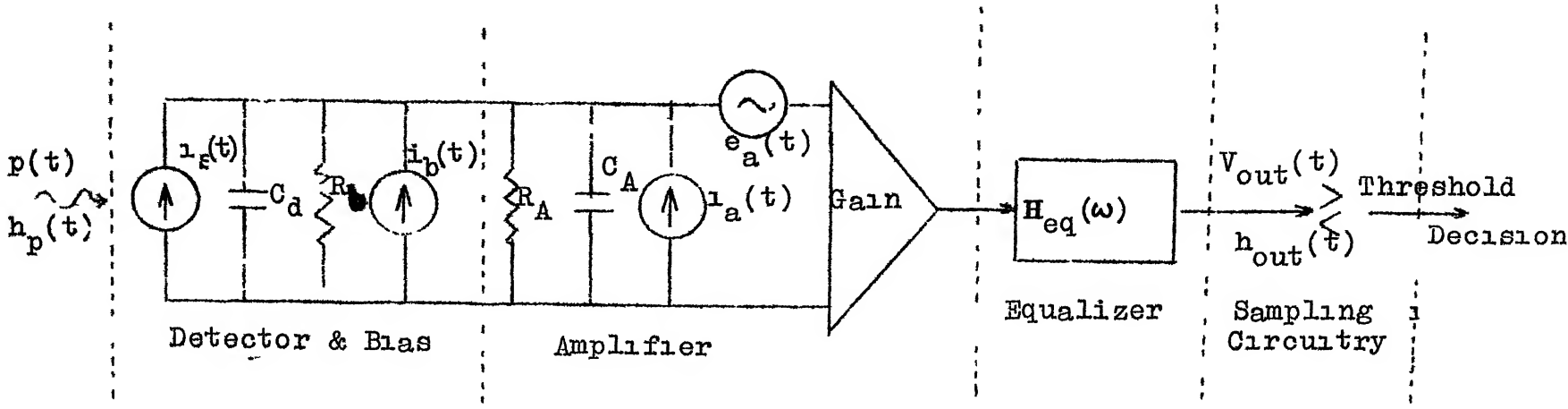

Fig. 3.1: Schematic of a Typical Receiver

photodetector with the bias circuit, the equivalent circuit of the preamplifier, the equalizer and the sampling and decision circuitry. The front end of the receiver consists of the photodetector and a high impedance low noise amplifier. In the first part of the figure the current generator $i_s(t)$ represents the current produced due to the optical power $p(t)$ incident on the detector. C_d is the junction capacitance of the PIN photodiode. R_b is the bias resistor and $i_b(t)$ represents the thermal noise due to R_b. In the second part R_A and C_A are the equivalent shunt resistance and capacitance at the preamplifier input. The amplifier-current noise source $i_a(t)$ and the amplifier-voltage noise source $e_a(t)$ are referred to the input. The noise sources are assumed to be white, gaussian and uncorrelated with the two-sided spectral densities defined as S_I and S_E. The amplifier gain is assumed to be sufficiently high so that the noise introduced by the equalizer is negligible.

The power falling upon the detector is assumed to be of the form of digital pulse stream

$$p(t) = \sum_{k=-\infty}^{\infty} b_k \, h_p(t-kT) \qquad (3.1)$$

where b_k are input symbols and take on one of the two values for each integer values of k, T is the pulse spacing,

$h_p(t)$ is the pulse shape and is positive for all t. Though in general, the pulses do not add linearly in power, but the hypothesis of an incoherent intensity modulated source (LED) exciting a multimode fibre (step-index) enables the guide to be treated as linear in power. Therefore, the assumption of the form of Eqn. (3.1) is reasonable. We shall assume

$$\int_{-\infty}^{\infty} h_p(t-kT) = 1$$

therefore b_k is the energy in pulse k.

From Eqn. (2.21) we have the average detector output current $\langle i_s(t) \rangle$ given as

$$\langle i_s(t) \rangle = \frac{\eta_e \, p(t)}{h \nu} \qquad (3.2)$$

where e is electron charge η , h and ν have been explained in section 2.6. The dark current has been neglected.

Therefore, the average voltage at the equalizer output is

$$\langle v_{out}(t) \rangle = \frac{A \ \eta_e \, p(t)}{h \nu} * h_{fe}(t) * h_{eq}(t) \qquad (3.3)$$

where A is an arbitrary constant and * indicates convolution, h_{fe} is the impulse response of the front end of the receiver i.e.,detector and amplifier and is given by

$$h_{fe} = F[Z(\omega)]$$

where, $Z(\omega) = \dfrac{1}{\frac{1}{R_T} + j\omega(C_d + C_A)}$

R_T is the total detector parallel load resistance,

$$\frac{1}{R_T} = \frac{1}{R_b} + \frac{1}{R_A} \quad \text{and} \quad C_T = C_d + C_A$$

and $h_{eq}(t)$ is the equalizer impulse response.

As output of each block is a linearly filtered version of the input to that block we see that, $\langle v_{out}(t) \rangle$ is of the form

$$\langle v_{out}(t) \rangle = \sum_{k=-\infty}^{\infty} b_k \, h_{out}(t-kT) \qquad (3.4)$$

and $v_{out}(t)$ is of the form

$$v_{out}(t) = \sum_{k=-\infty}^{\infty} b_k \, h_{out}(t-kT) + n(t)$$

where $h_{out}(t)$ is the overall impulse response at the output of the equaliser as mentioned in Fig. 3.1 and $n(t)$ is the deviation (noise) of $v_{out}(t)$ from the average value $\langle v_{out}(t) \rangle$.

3.3 Calculation of Noise Power:

The noise term $n(t)$ above consists of two parts, amplifier thermal noise and the shot noise associated with the detection process. As mentioned earlier that the

detector output consists of electrons which are created at random times and their number is also random but on an average proportional to the incident optical power. The deviations from this average current due to the above randomness results in the shot noise. We now find the variance of the noise n(t) defined as

$$N = \langle n(t)^2 \rangle = \langle v_{out}^2(t) \rangle - \langle v_{out}(t) \rangle^2$$

The noise n(t) depends upon the coefficients $\{b_k\}$ and the time t.

We assume that decisions as to the values $\{b_k\}$ is made by sampling $v_{out}(t)$ at times $t = \{kT\}$ and that the equalised pulses are free from intersymbol interference at these times i.e., we assume

$$h_{out}(0) = 1$$

$$h_{out}(t) = 0 \text{ for } t = kT,\ k \neq 0 \qquad (3.5)$$

Therefore,

$$v_{out}(kT) = b_k + n(kT) \qquad (3.6)$$

In the PIN photodetector considered in the receiver, as there is no avalanche gain, thermal noise part of the noise n(t) dominates the shot noise. We therefore neglect

the shot noise in our further analysis. We can then write the output noise as

$$v_{out}(t) - \langle v_{out}(t) \rangle = n_r(t) + n_i(t) + n_e(t) \qquad (3.7)$$

where $n_r(t)$ is the output noise due to the thermal noise current source i_b representing the resistor R_b, $n_i(t)$ is the output noise due to the amplifier input current noise source $i_a(t)$, and $n_e(t)$ is the output noise due to the amplifier input voltage noise source $e_a(t)$.

We have

$$\begin{aligned} N &= \langle v_{out}^2(t) \rangle - \langle v_{out}(t) \rangle^2 \\ &= \langle (v_{out}(t) - \langle v_{out}(t) \rangle)^2 \rangle \\ &= (\langle n_r^2(t) \rangle + \langle n_i^2(t) \rangle + \langle n_e^2(t) \rangle) \end{aligned} \qquad (3.8)$$

Now as all the three noise parts are white uncorrelated, using the formula for filtered white noise, we have

$$\langle n_r^2(t) \rangle = \frac{2kK}{R_b} \frac{1}{2\pi} \int_{-\infty}^{\infty} \left| Z(\omega)\, H_{eq}(\omega) \right|^2 d\omega$$

where $\frac{2kK}{R_b}$ is the thermal noise due to R_b, k being the Boltzmann's constant and K is the absolute temperature in degrees Kelvin,

$$\langle n_1^2(t) \rangle = S_I \cdot \frac{1}{2\pi} \int_{-\infty}^{\infty} \left| Z(\omega)\, H_{eq}(\omega) \right|^2 \, d\omega$$

and $$\langle n_e^2(t) \rangle = S_E \cdot \frac{1}{2\pi} \int_{-\infty}^{\infty} \left| H_{eq}(\omega) \right|^2 \, d\omega$$

where $H_{eq}(\omega) = F[\, h_{eq}(t)\,]$ = equalizer transfer function.

If $H_p(\omega) = F[\, h_p(t)\,]$ = input power pulse transform and

$H_{out}(\omega) = F[\, h_{out}(t)\,]$ = output pulse transform,

then $$H_{out}(\omega) = H_p(\omega) \cdot Z(\omega) \cdot H_{eq}(\omega) \qquad (3.9)$$

Therefore substituting for each term in Eqn. (3.8) and using the relation in Eqn. (3.9), noise power works out to

$$N = \frac{1}{2\pi} \left(\frac{2 \cdot kK}{R_b} + S_I \right) \cdot \int_{-\infty}^{\infty} \left| \frac{H_{out}(\omega)}{H_p(\omega)} \right|^2 d\omega$$

$$+ \frac{S_E}{2\pi} \int_{-\infty}^{\infty} \left| \frac{H_{out}(\omega)}{H_p(\omega)} \left(\frac{1}{R_T} + j\omega C_T \right) \right|^2 d\omega \qquad (3.10)$$

From Eqn. (3.10) we observe the following:

(a) Regardless of the choice of $H_{out}(\omega)$, the noise is always made smaller when R_b is increased. Therefore, subject to practical constraints and for a fixed amplifier and a fixed desired output pulse shape (which is determined by the equaliser and R_b) it is always better to make R_b, the bias resistor, as large as possible.

(b) For a given S_I and S_E and a given output pulse shape, it is desirable that the amplifier input resistance R_A be as large as possible and that shunt capacitance C_A be as small as possible.

(c) It is desirable that the diode shunt capacitance be as small as possible.

3.4 Effects of Input Pulse Shapes:

Selection of the input pulse shape has considerable bearing on the performance of the system. The choice has to be based on the receiver sensitivity. For the three input pulse shapes considered by Personick [11] we shall find the noise power at the output. The output pulse shape considered is raised cosine in all the three cases so we have an output free from ISI at the sampling instants [kT].

The fibre channel considered is the one discussed in in Chapter 2 with a length Z of 10 Km, attenuation coefficient A = 0.1 and mode coupling coefficient $D = 10^{-5}$. The data rate considered is 10 M bits/sec.

For the system shown in Fig. 3.2 the receiver response consists of the detector amplifier and the equaliser response.

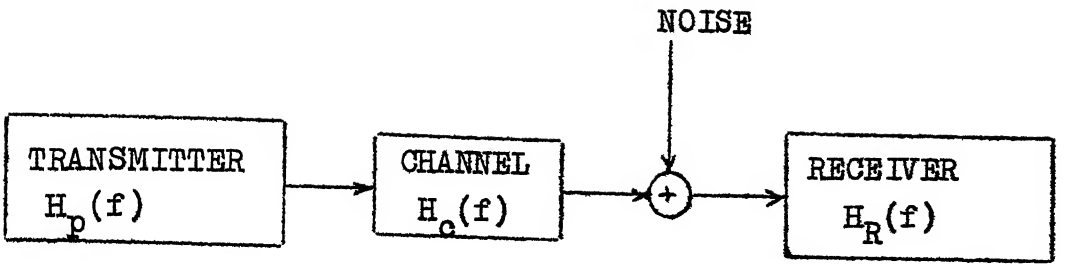

Fig. 3.2 Block Schematic of the System

$$H_{out}(f) = H_p(f) \cdot H_c(f) \cdot H_R(f)$$

$$H_R(f) = \frac{H_{out}(f)}{H_p(f).H_c(f)} \qquad (3.11)$$

For $H_R(f)$ to exist it is necessary that $H_p(f).H_c(f)$ not be zero at any frequency upto the frequency of interest. The three input pulse shapes shown in Fig. 3.3 are:

(a) Rectangular input pulses:

$$h_p(t) = \frac{1}{\alpha T} \text{ , } \frac{\alpha T}{2} < t < \frac{\alpha T}{2}, 0 \text{ otherwise} \qquad (3.12)$$

α is the parameter which gives the width of the pulse in one time slot T (T = 1/Bit rate).

$$H_p(f) = \int_{-\alpha T/2}^{\alpha T/2} \frac{1}{\alpha T} \, e^{-j2\pi ft} \, dt$$

$$= \frac{\sin(\pi f \alpha T)}{\pi f \alpha T} \qquad (3.13)$$

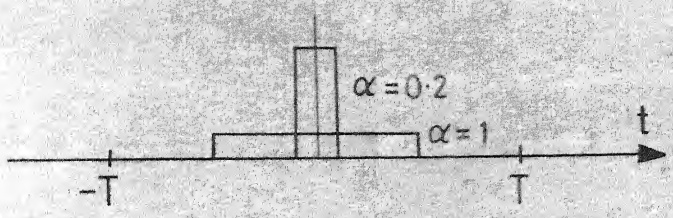

$$h_p(t) = \frac{1}{\alpha T} \text{ for } \frac{-\alpha T}{2} < t < \frac{\alpha T}{2}, 0 \text{ otherwise}$$

(a) Rectangular Pulses

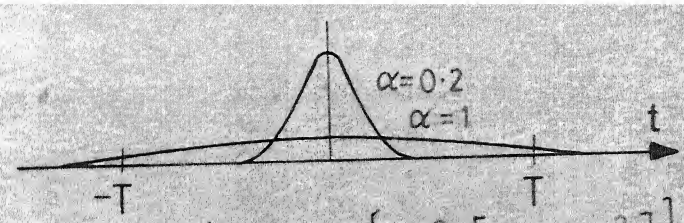

$$h_p(t) = \frac{1}{\sqrt{2\pi}\alpha T} \exp\left\{-t^2/\left[2(\alpha T)^2\right]\right\}$$

(b) Gaussian Pulses

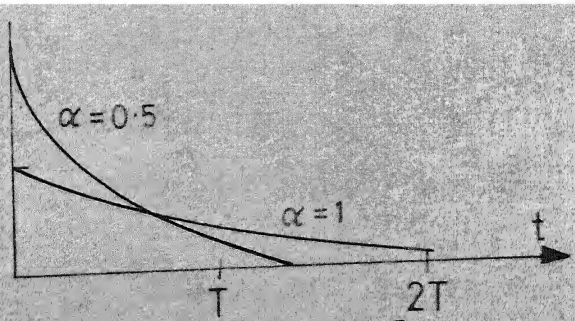

$$h_p(t) = \frac{1}{\alpha T} \exp\left\{-t/\left[\alpha T\right]\right\}$$

(c) Exponential Pulses

Fig. 3·3 Input Pulse Shapes

(b) Gaussian input pulses:

$$h_p(t) = \frac{1}{\sqrt{2\pi}\alpha T} \exp\left\{-t^2/\left[2(\alpha T)^2\right]\right\} \qquad (3.14)$$

$$H_p(f) = \frac{1}{\sqrt{2\pi}\alpha T} \cdot \alpha T\sqrt{2\pi} \cdot \exp\left\{-\frac{(\alpha T)^2(2\pi f)^2}{2}\right\}$$

Therefore $$H_p(f) = \exp\left\{-(2\pi\alpha T f)^2/2\right\} \qquad (3.15)$$

(c) Exponential input pulses:

$$h_p(t) = \frac{1}{\alpha T} \exp(-t/\alpha T) \qquad (3.16)$$

$$H_p(f) = \frac{1}{\alpha T} \cdot \frac{1}{\frac{1}{\alpha T} + j(2\pi f)}$$

$$= \frac{1}{1+j(2\pi f \alpha T)} \qquad (3.17)$$

The raised cosine output pulse response and its transfer function are:

$$h_{out}(t) = \left[\sin\left(\frac{\pi t}{T}\right)\cos\left(\frac{\pi\beta t}{T}\right)\right]\left[\frac{\pi t}{T}\left(1-\left(\frac{2\beta t}{T}\right)^2\right)\right]^{-1} \qquad (3.18)$$

$$H_{out}(f) = T, \qquad \text{for } 0 < |f| < \frac{1-\beta}{2T}$$

$$= T/2\left\{1-\sin\left(\frac{\pi f T}{\beta} - \pi/2\beta\right)\right\}, \quad \text{for } \frac{1-\beta}{2T} < |f| < \frac{1+\beta}{2T}$$

$$= 0 \qquad \text{otherwise.}$$

where β is the role off parameter of the pulse. We consider $\beta = 1$ in our calculations. Therefore

$$H_{out}(f) = T, \qquad \text{for } f = 0$$

$$= \frac{T}{2}\left[1+\cos(\pi fT)\right], \text{ for } 0 < |f| < \frac{1}{T}$$

$$= 0 \quad \text{otherwise} \qquad (3.19)$$

The channel impulse response and transfer function are given in Eqns. (2.14) and (2.16), respectively. The transfer function is reproduced here for ready reference:

$$H_c(f) = 4\pi\left(\frac{c^2.D.A}{c^2A^2+\pi^2f^2n^2} - J\,\frac{\pi f\, c.D.n}{c^2A^2+\pi^2f^2n^2}\right)^{1/2}.$$

$$\exp\left[-\left(4DZ^2A+J\,\frac{4\pi fDnZ^2}{c}\right)^{1/2}\right] \qquad (3.20)$$

where c is the velocity of light in free space and n is the refractive index of the core.

Using Eqn. (3.11) we find the dc response of the receiver which for all the three input pulse shapes is same,

$$H_R(o) = \frac{H_{out}(o)}{H_p(o) \cdot H_c(o)}$$

$H_p(o)$ for all the pulse shapes is unity.

$H_{out}(o) = T/2[\,1+\cos(o)\,] = T$, and

$H_R(o)$ works out to be 386.04933.

As the noise considered is white, to find the noise power at the output we first find the noise equivalent bandwidth of the receiver $H_R(f)$, which is defined as:

$$B_N = \frac{1}{G_o} \int_0^\infty |H_R(f)|^2 \, df$$

where $G_o^{1/2}$ is the centre frequency amplitude ratio or the voltage gain. Here the centre frequency is zero and the voltage gain is $H_R(o)$ (already found above). Then the total noise power at a room temperature of 300°K is given by

$$N_T = G_o \, k \, T \cdot B_N \qquad (3.22)$$

where k the Boltzmann's constant = 1.3805×10^{-23} joules/°K and T the absolute room temperature = 300°K.

First noise equivalent bandwidth and then the noise power have been computed on DEC system 1090 digital computer for all the three pulse shapes for values of α from 0.1 to 1. The values of the total noise power in dBm are given in Table 3. The power penalty for these input pulse shapes is plotted in Fig. 3.4 for various values of α . The results indicate that an ideal rectangular pulse shape requires least power for all values of α . But, this pulse shape is not possible to realize in practice, and the exponential pulse seems to be the next best. In all the cases it

TABLE 3

TOTAL OUTPUT NOISE POWER IN dBm

nput Pulse Shape	Values of α									
	0.1	0.2	0.3	0.4	0.5	0.6	0.7	0.8	0.9	1.0
ectangular	-47.337	-47.183	-46.919	-46.533	-46.004	-45.299	-44.367	-43.110	-41.321	-38.202
aussian	-46.769	-44.740	-40.792	-34.216	-24.391	-10.959				
xponential	-46.822	-45.467	-43.864	-42.303	-40.880	-39.603	-38.460	-37.433	-36.503	-35.656

is indicated that the pulses should be of narrow width. The penalty for increase in the pulse width in case of the exponential input pulse is nearly linear. In case of the Gaussian input pulses the pulses should be extremely narrow.

3.5 Effect of Bit Rate:

To examine the effect of bit rate on the power requirement we perform some normalization on the functions $H_p(\omega)$ and $H_{out}(\omega)$ of Eqn. (3.10) to make them independent of the time slot width T.

$$H'_p(\omega) = H_p\left(\frac{2\pi\omega}{T}\right)$$

and $$H'_{out}(\omega) = \frac{1}{T} H_{out}\left(\frac{2\pi\omega}{T}\right)$$

Rewriting Eqn. (3.10) with $\omega = \frac{2\pi\omega'}{T}$

$$N = \frac{1}{2\pi}\left(\frac{2kK}{R_b} + S_I\right)\frac{2\pi}{T}\int_{-\infty}^{\infty}\left|\frac{H_{out}\left(\frac{2\pi\omega'}{T}\right)}{H_p\left(\frac{2\pi\omega'}{T}\right)}\right|^2 d\omega'$$

$$+ \frac{S_E}{2\pi}\left[\int_{-\infty}^{\infty}\left(\frac{H_{out}\left(\frac{2\pi\omega'}{T}\right)}{H_p\left(\frac{2\pi\omega'}{T}\right)}\right)^2 \frac{2\pi}{T}\frac{1}{R_T^2}\, d\omega'\right.$$

$$\left. + \frac{2\pi}{T} C_T^2 \int_{-\infty}^{\infty}\left(\frac{H_{out}\left(\frac{2\pi\omega'}{T}\right)}{H_p\left(\frac{2\pi\omega'}{T}\right)}\right)^2 \left(\frac{2\pi\omega'}{T}\right)^2 d\omega'\right]$$

Simplyfying and incorporating the above normalization

$$N = \left(\frac{2kK}{R_b} + S_I + \frac{S_E}{R_T^2}\right)T \int_{-\infty}^{\infty} \left| \frac{H'_{out}(f)}{H'_p(f)} \right|^2 df$$

$$+ \frac{S_E}{T}(2\pi C_T)^2 \int_{-\infty}^{\infty} \left| \frac{H'_{out}(f)}{H'_p(f)} \right|^2 f^2 \, df$$

Recalling that the equalised output pulse $h_{out}(t)$ has been normalised to unity at t=0, we obtain*

---

*Using Eqn.(3.5), we can evaluate the arbitrary constant A from Eqn. (3.3) in the following manner.

At $t = 0$ and $k = 0$,

$$\langle v_{out}(o) \rangle = \frac{A\, e\eta\, p(o)}{h\nu} * h_{fe}(o) * h_{eq}(o)$$

From Eqn. (3.4), $\langle v_{out}(o) \rangle = b_o\, h_{out}(o)$

Therefore, $h_{out}(o) = \dfrac{A\, e\eta\, p(o) * h_{fe}(o) * h_{eq}(o)}{h\nu \cdot b_o} = 1$

From Eqn. (3.1), $p(o) = b_o\, h_p(o)$

Therefore, $\dfrac{A\, e\eta}{h\nu}\, h_p(o) * h_{fe}(o) * h_{eq}(o) = 1$

Now, $h_{out}(o) = h_p(o) * h_{fe}(o) * h_{eq}(o) = 1$

Therefore, $A = \dfrac{h\nu}{e\eta}$

$$N = \left(\frac{h\nu}{\eta e}\right)^2 \left[T\left(\frac{2kK}{R_b} + S_I + \frac{S_E}{R_T^2}\right) I_1 + \frac{(2\pi C_T)^2 S_E}{T} I_2\right] \tag{3.23}$$

where

$$I_1 = \int_{-\infty}^{\infty} \left| \frac{H'_{out}(f)}{H'_p(f)} \right|^2 df$$

$$I_2 = \int_{-\infty}^{\infty} \left| \frac{H'_{out}(f)}{H'_p(f)} \right|^2 f^2 df$$

From the Eqn. (3.23) we see that for a fixed input and output pulse shapes and with fixed R_b, R_A, C_T, S_E and S_I, the noise decreases as the bit rate, 1/T, increases until the term involving I_2 dominates. After that, the noise increases with increasing bit rate (due to shunt capacitance C_T).

3.6 Effect of Fibre Length:

We now fix the bit rate to 10 M bits/sec and the pulse width to give a half duty cycle, i.e., $\alpha = 0.5$, and consider the effect of varying the fibre length on output noise power. The excess noise power with increasing length is plotted in Fig. 3.5. We notice that the increase in noise power is uniform and quite large in all the cases. This can be attributed to two factors. Firstly, the increase in the pulse dispersion with increase in the length reduces the channel bandwidth. But, as the desired output pulse

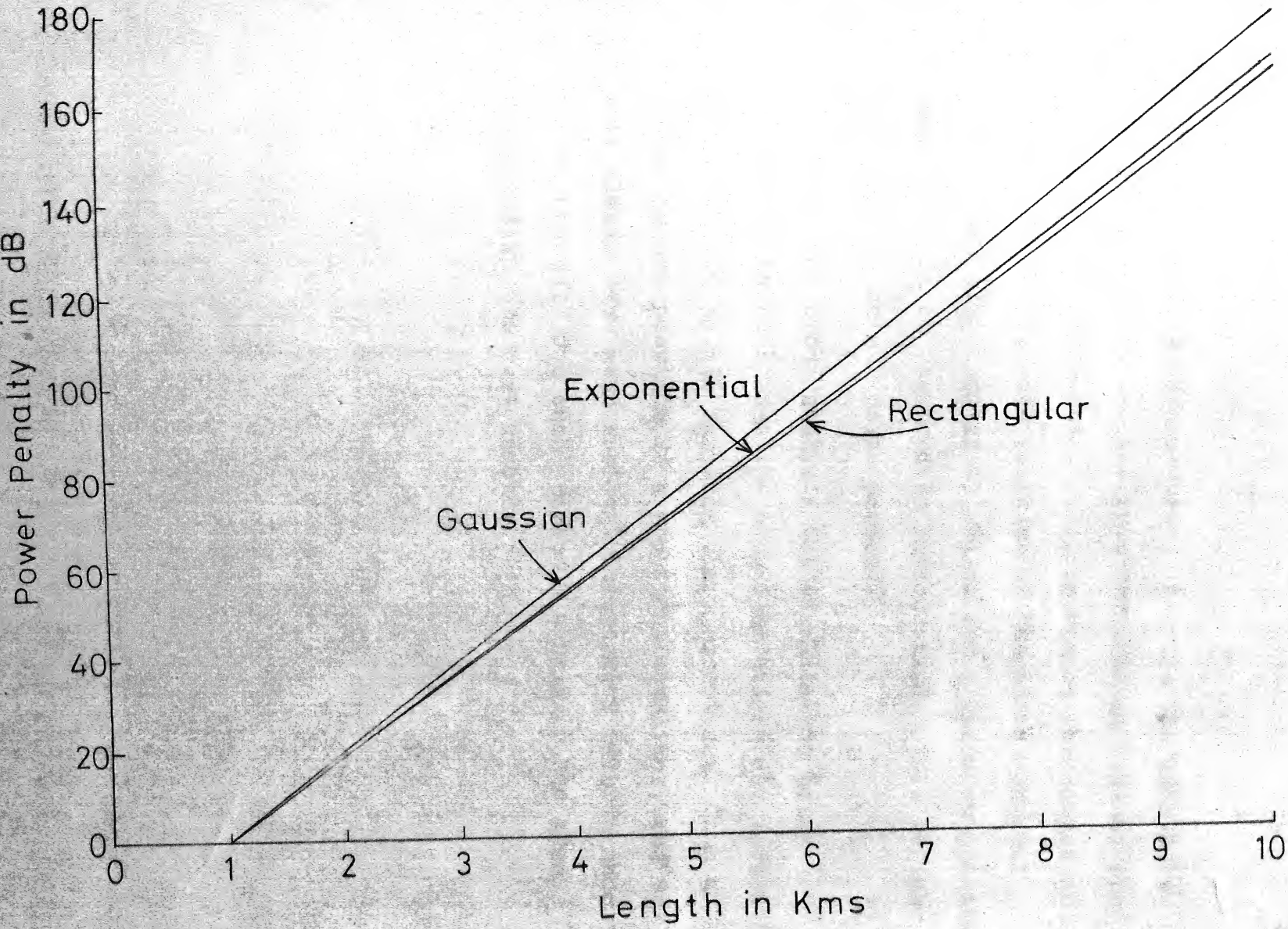

Fig. 3·5 Power Penalty with Increasing Fibre Length

shape is fixed as raised-cosine keeping the data rate constant all the time, the receiver gain as well as the bandwidth thus increases. This increases the output noise power. Secondly, with increase in length the channel attenuation also increases, and so for a fixed output the receiver gain is required to be increased. This further enhances the output noise power.

In the above analysis the equalization being considered is such that the equalized pulses are forced to go to zero at all sampling times except one. Such a scheme is not possible in a practical equalizer, and we will always have some residual intersymbol interference at the output. One such practical equalizer has been described in the next chapter.

CHAPTER 4

EQUALIZER FOR OPTICAL FIBRE SYSTEMS

For moderate to high signalling rates and longer repeater spacings, the degradation in the system performance, as manifested by an increase in the average probability of error, is due to the presence of the two kinds of noises (thermal noise and shot noise) as well as the intersymbol interference (ISI) caused by an over lapping of adjacent transmitted symbols. The intersymbol interference can be reduced by means of equalization at the receiver. For optimum design of the front-end of the receiver and to show the effects of various pulse shapes on the noise power, we assumed (as discussed in Chapter 3) that the receiver output was free from intersymbol interference. It is not possible to design a practical equalizer to achieve this. The ISI has been effectively reduced in coaxial cable systems with the help of linear and nonlinear equalizers. For multimode optical fibre channels also use of linear or nonlinear equalizers has been suggested for the reduction of ISI [25,26 and 27]. It is known that nonlinear equalizers perform better than linear equalizers to achieve low probability of error for dispersive channels [26] . It may be possible to achieve a high data rate without equalization

by the use of single mode fibres in future. But, to make these systems cost effective the repeater spacing, must be as large as possible. A large repeater spacing will give rise to a significant pulse dispersion even with single mode fibres. Thus, the use of equalization can not be ruled out even for such systems [26].

4.1 Introduction to Equalizers:

A statistically optimum equalizer structure from the decision theoretic point of view has been given by Austin [28]. The optimal equalizer comprises a matched filter. a sampler and a tapped delay line (TDL) having an infinite number of taps. Moreover, an infinite number of summers and exponentiators are necessary. Hence, this equalizer structure can not be implemented in practice. He has also shown that suboptimum structures, which are practically implementable, can be obtained by introducing some additional assumptions. Of the two suboptimal structures, one is a linear while the other is a nonlinear equalizer implementation. The linear equalizer comprises a matched filter followed by a TDL. But, it requires a large number of taps for effective reduction of ISI. It also increases the output noise power due to its large bandwidth. The nonlinear equalizer is known as a Decision Feedback Equalizer (DFE).

The DFE has a matched filter (MF) followed by a TDL of moderate length. It makes use of the previous decisions (assumed to be correct) to coherently subtract the intersymbol interference caused by the previously detected symbols. This is done by passing the past decisions through the feedback TDL. The MF and the forward TDL are used to minimize the effects of additive noise and future symbol interference respectively. The two equalization criteria used mostly are the zero-forcing and the minimum mean square error (MMSE) [29]. The zero-forcing criterion minimizes the output peak distortion, if the peak distortion of the unequalised pulse is less than unity. The second criterion minimizes the mean square error (MSE) between the received sequence estimate and the transmitted sequence.

The DFE has been studied in detail by various authors [30,31 and 32]. One of these, given by George, Bowen and Storey, has been used to design an equalizer having fixed tap gains for the fibre channel discussed earlier in Sec. 2.4. Since, the fibres are considered to be only dispersive a fixed tap gain, and not adaptive, equalizer has been considered.

4.2 Decision Feedback Equalizer Design:

The DFE suggested in [30] has a filter matched to the isolated received pulse followed by a tapped delay line

having taps at delays of one baud interval. The past decisions $\{\hat{s}_j\}$ are passed through a feedback tapped delay line. The feedback tap delay line tap gain values are chosen on the assumption that these past decisions are all correct. The output of the feedback TDL is coherently subtracted from the output of the forward TDL to eliminate ISI caused by the previously detected symbols. The forward TDL reduces the ISI caused by the undetected symbols (future symbols). The design analysis given assumes that the signal from the channel is demodulated, filtered and sampled at the symbol baud rate. The equalizer makes the estimate $\tilde{s}_j$ about the transmitted symbol s_j at times $t = jT$. This estimate is given by

$$\tilde{s}_j = \sum_{n=0}^{N} a_n y_{j+n} - \sum_{m=1}^{M} b_m \hat{s}_{j-m} \qquad (4.1)$$

where a_n; $n=0,1,\ldots,N$ are the forward tap gains, and b_m; $m=1,2,\ldots,M$ are the feedback filter tap gains. This estimate is then converted into final decisions $\hat{s}_j$ with a nonlinear memoryless circuit. In the present case of binary digits $\{s_j\}$, this circuit is only a clipping circuit with a fixed threshold. y_{j+n} is the output of the matched filter at time $t=j+nT$.

To find the optimum tap gain values minimum MSE criterion has been used. The resulting design equations [30] are

$$\sum_{i=0}^{N} a_i \left[\Psi_{i,k} + \phi_n(k-i) \right] = x_k ; \quad k=0,1,\ldots,N \qquad (4.2)$$

and $$b_m = \sum_{i=0}^{N} a_i \, x_{m+i} \quad , \; m=1,2,\ldots,M \qquad (4.3)$$

where N = Number of forward TDL taps

M = Number of feedback TDL taps

$$\Psi_{i,k} = \sum_{l=0}^{i} x_l \, x_{l+k-i} \qquad (4.4)$$

$\phi_n(k-i)$ = autocorrelation function of the additive noise n(t) at the delay $\tau = (k-i)T$.

x_k is the kth sample of the overall impulse response at the input of the equalizer. In the present case, since a matched filter has been used, x_k is the kth sample of the autocorrelation function of the channel impulse response at its output.

The fibre impulse response h(t) is given in Eqn.(2.14). To have a significant dispersion a fibre length of 10 Km has been chosen to start with. Typical values of A=0.1 and

$D=10^{-5}$ as mentioned earlier have been chosen so that the response is dependent only on fibre length. For a length of 10 Km the response is taken to be nonzero between 115 nanosecs and 505 nanosecs with a peak value at 245 nanosecs. The normalised amplitude plot of this is given in Fig. 2.5. The discrete response values are obtained at every 10 nanosecs. The other assumptions made are:

(a) The response time of the front-end of the receiver (photodetector and amplifier) is very small compared to the response time of the rest of the receiver, thus, implying that it has a very large bandwidth compared to the channel. Therefore, the matched filter is matched to the channel impulse response only.

(b) The additive noise is white Gaussian.

(c) Data rate for the design purposes is considered to be 10 M bits/sec.

(d) The input to the channel is a sequence $\{s_j\}$ of randomly selected equally likely impulses of amplitude ± 1.

For 10 M bits/sec rate one baud interval, T, is equal to 100 nanosecs. Neglecting the initial delay the impulse response of the channel spreads over four baud intervals. If L is the spread in terms of the number of baud intervals, then LT=400 nanosecs in this case.

The response of the matched filter is h(-t). Therefore the response at the output of the MF is

$$x(t) = h(t) * h(-t) \tag{4.5}$$

where * indicates convolution operation

$$\text{or} \quad x(t) = \int_{-\infty}^{\infty} h(\tau)\, h(t+\tau)\, d\tau$$

As the function h(t) exists from zero to LT,

$$x(kT) = \int_{0}^{LT} h(\tau)\, h(\tau + kT)\, d\tau \tag{4.6}$$

To evaluate it on the digital computer, h(t) has been sampled into 10 samples per baud interval giving a total of 40 samples.

$$\text{Therefore,} \quad x_k = \sum_{i=1}^{40-10k} h_i\, h_{i+10k}, \quad k > 0 \tag{4.7}$$

$$\text{and} \qquad x_{-k} = x_k$$

The amplitudes of h_i are normalised such that

$$\int_{-\infty}^{\infty} h^2(t) = 1 \tag{4.8}$$

This is because Eqn. (4.8) also gives the energy in the signal if the input symbol is an impulse. When evaluating the performance of the DFE for different signal-to-noise ratios (SNR) it would be convenient to keep the signal energy as unity and vary only the noise variance. So this

normalisation is useful and results in

$$x_0 = \int_{-\infty}^{\infty} h^2(t) = 1 \qquad (4.9)$$

For the channel under consideration x_k will have values from x_{-3} to x_3 and will be symmetrical about the peak value x_0 at k=0 as it is the autocorrelation function of the channel impulse response. The values that result are

$$x_0 = 1$$
$$x_1 = x_{-1} = 0.4375216$$
$$x_2 = x_{-2} = 0.0529886$$
$$x_3 = x_{-3} = 0.0021167499$$

$\{x_k\}$ is the input to the equalizer and is of the form shown in Fig. 4.1.

The forward- and feedback- TDL sizes are determined by the input to the euqalizer. There are three (M) feedback taps in our case (Fig. 4.1) as the number of postcursors (past samples) contributing to the ISI is three. The number of precursors (future samples) causing ISI is also equal to three. The choice of the number of forward taps (N+1) is not unique. It has been arbitrarily chosenas 4. As shown later, only the first tap gain (a_0) comes out to be significant, and a_1, a_2 and a_3 are found to be negligible. The equalizer that results is given in Fig. 4.3.

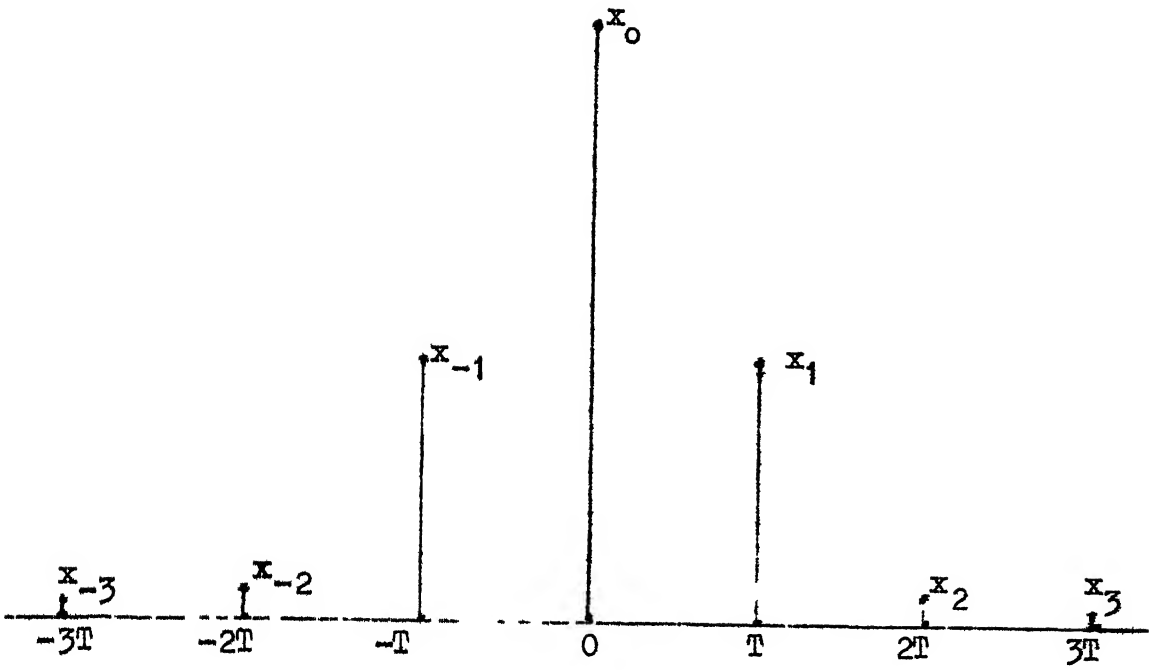

Fig. 4.1: Channel Autocorrelation Function

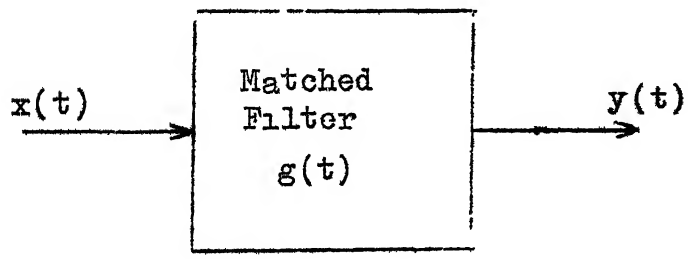

Fig. 4.2: A Linear System

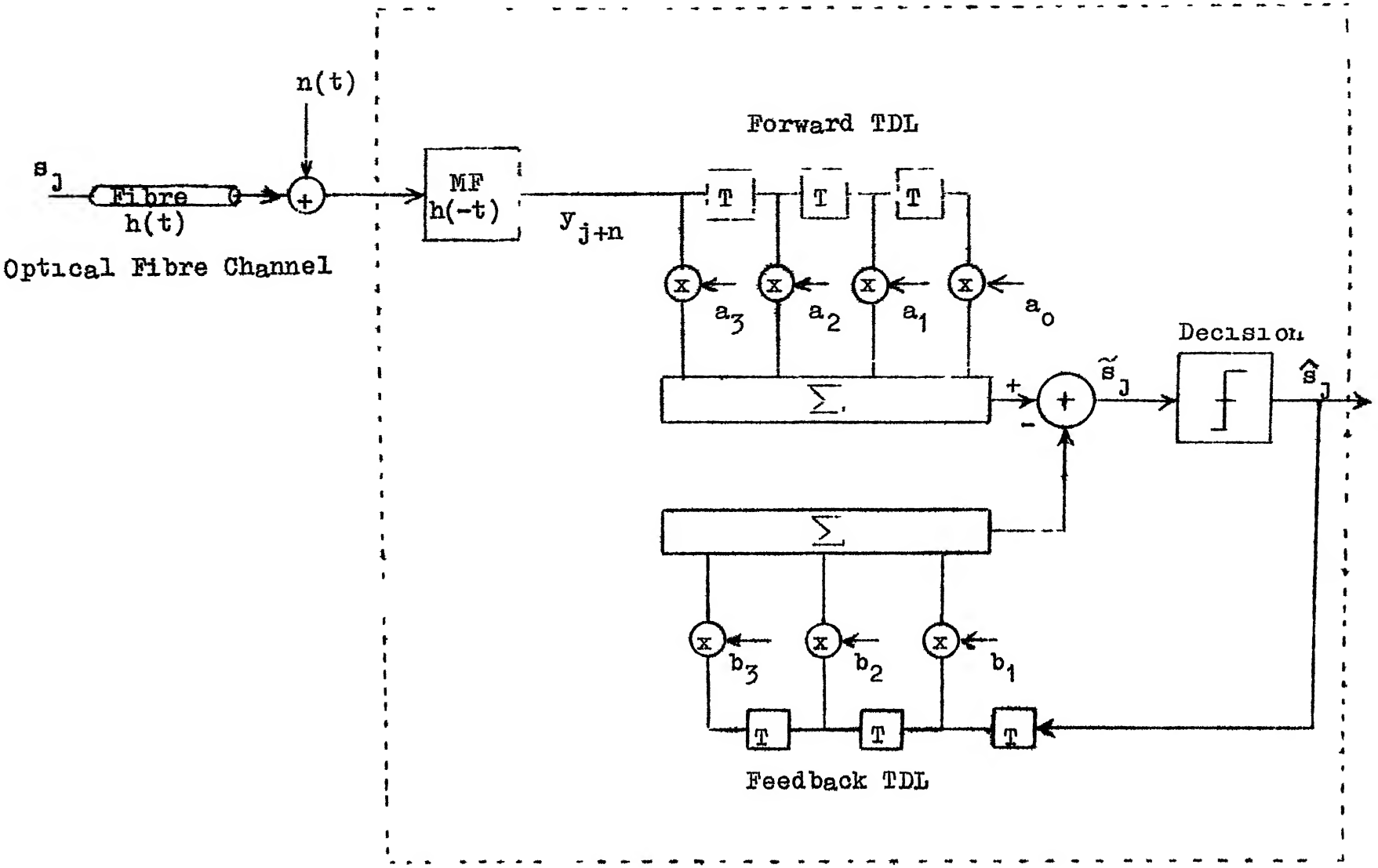

Fig. 4.3: Decision Feedback Equalizer Structure

From the autocorrelation values we can calculate $\Psi_{i,k}$ as shown in Eqn. (4.4)

$$\Psi_{i,k} = \sum_{l=o}^{l} x_l x_{l+k-l}; \quad l=0,1,2 \text{ and } 3 \quad k=0,1,2 \text{ and } 3 \qquad (4.10)$$

4.2.1 Evaluation of Noise Autocorrelation Function:

In general for a linear system (Fig. 4.2) the output autocorrelation function is given by [33].

$$R_{YY}(\tau) = R_{XX}(\tau) * g(-\tau) * g(\tau), \text{ for real } g(t)$$

where $R_{XX}(\tau)$ is the input autocorrelation function. Here the input is a white noise n(t) with power spectral density $\frac{N_o}{2}$ and the filter impulse response is h(-t). Therefore, $R_{XX}(\tau) = \frac{N_o}{2} \delta(\tau)$

then the noise autocorrelation function $\phi_n(\tau)$ at the output of the MF is

$$\phi_n(\tau) = \frac{N_o}{2} [\delta(\tau) * h(-\tau) * h(\tau)]$$

$$= \frac{N_o}{2} \int_{-\infty}^{\infty} h(t)\, h(t+\tau)\, dt$$

As the response h(t) exists between 0 and LT

$$\phi_n(\tau) = \frac{N_o}{2} \int_{o}^{LT} h(t)\, h(t+\tau)\, dt$$

$$\text{or} \qquad \phi_n((k-i)T) = \frac{N_o}{2} \int_0^{LT} h(t)h[\,t+(k-1)T\,]\,dt \qquad (4.11)$$

It can be seen that it is same as x_k except for the multiplying factor $\frac{N_o}{2}$.

To evaluate $\frac{N_o}{2}$, we know that the noise power at the output of the matched filter would be

$$= \frac{N_o}{2} \int_{-\infty}^{\infty} |H(f)|^2 \, df$$

as $h(-t)$ is real and $H^*(f) = F\,[h(-t)\cdot]$

By Parseval's relation

$$\int_{-\infty}^{\infty} |H(f)|^2 \, df = \int_{-\infty}^{\infty} h^2(t)\,dt = \int_0^{LT} h^2(t)\,dt \qquad (4.12)$$

Signal power at the output of the matched filter as stated earlier is

$$\int_0^{LT} h^2(t)\,dt \text{ if the input is an impulse}$$

$$\text{Therefore SNR} = \frac{\text{SIGNAL POWER}}{\text{NOISE POWER}} = \frac{\int_0^{LT} h^2(t)\,dt}{\frac{N_o}{2}\int_{-\infty}^{\infty} |H(f)|^2\,dt}$$

Using Parseval's relation

$$\text{SNR} = \frac{1}{\frac{N_o}{2}}$$

$$\text{Therefore } \frac{N_o}{2} = \frac{\text{NOISE POWER}}{\text{SIGNAL POWER}}$$

But as the signal power considered has been normalised to unity, $\frac{N_o}{2}$ turns out to be the noise variance and equal to the $(SNR)^{-1}$ in each case.

For example,

if SNR = 6 dB, noise variance = 0.251 = $\frac{N_o}{2}$,

and if SNR = 10 dB, noise variance = 0.1 = $\frac{N_o}{2}$

4.2.2 Evaluation of Tap Gains:

Once x_k, $\Psi_{1,k}$ and $\phi_n(k-1)$ are known we form a set of linear equations using Eqn. (4.2). The number of equations will be equal to the number of forward taps. Taking advantage of the fact that

$$x_{-k} = x_k \quad \text{and} \quad \phi_n(-k) = \phi_n(k) \tag{4.13}$$

the set of linear equations (4.14) is obtained (shown on page 123).

These equations have been solved on the digital computer and forward tap gain values obtained for various SNR's (6 dB to 24 dB in steps of 2 dB).

Feedback tap gains are then evaluated using Eqn. (4.3). The evaluation of x_k, $\Psi_{1,k}$, $\phi_n(k-1)$, forward tap gains and feedback tap gains has been done for various SNR values and fibre lengths using one common

But as the signal power considered has been normalised to unity, $\frac{N_o}{2}$ turns out to be the noise variance and equal to the $(SNR)^{-1}$ in each case.

For example,

if SNR = 6 dB, noise variance = 0.251 = $\frac{N_o}{2}$,

and if SNR = 10 dB, noise variance = 0.1 = $\frac{N_o}{2}$

4.2.2 Evaluation of Tap Gains:

Once x_k, $\Psi_{i,k}$ and $\phi_n(k-i)$ are known we form a set of linear equations using Eqn. (4.2). The number of equations will be equal to the number of forward taps. Taking advantage of the fact that

$$x_{-k} = x_k \quad \text{and} \quad \phi_n(-k) = \phi_n(k) \tag{4.13}$$

the set of linear equations (4.14) is obtained (shown on page 123).

These equations have been solved on the digital computer and forward tap gain values obtained for various SNR's (6 dB to 24 dB in steps of 2 dB).

Feedback tap gains are then evaluated using Eqn. (4.3). The evaluation of x_k, $\Psi_{1,k}$, $\phi_n(k-1)$, forward tap gains and feedback tap gains has been done for various SNR values and fibre lengths using one common

$$x_0 = a_0[\Psi_{0,0} + \phi_n(0)] + a_1[\Psi_{1,0}+\phi_n(-1)] + a_2[\Psi_{2,0}+\phi_n(-2)] + a_3[\Psi_{3,0} + \phi_n(-3)]$$

$$x_1 = a_0[\Psi_{0,1} + \phi_n(1)] + a_1[\Psi_{1,1}+\phi_n(0)] + a_2[\Psi_{2,1}+\phi_n(-1)] + a_3[\Psi_{3,1} + \phi_n(-2)]$$

$$x_2 = a_0[\Psi_{0,2} + \phi_n(2)] + a_1[\Psi_{1,2}+\phi_n(1)] + a_2[\Psi_{2,2}+\phi_n(0)] + a_3[\Psi_{3,2} + \phi_n(-1)]$$

$$x_3 = a_0[\Psi_{0,3} + \phi_n(3)] + a_1[\Psi_{1,3}+\phi_n(2)] + a_2[\Psi_{2,3}+\phi_n(1)] + a_3[\Psi_{3,3} + \phi_n(0)]$$

(4.14)

Set of linear equations for forward tap gains

computer program. The program is general enough to compute tap gains for any SNR and fibre length. The tap gain values computed for 10 Km length and various SNR values, and for 8 km and 6 km lengths at an SNR of 16 dB are tabulated in Table 4.1.

4.3 Simulation Results:

To evaluate the performance of DFE it is not easy to get closed form expressions for the probability of error because it is a nonlinear system. The system performance is therefore commonly obtained through digital computer simulation.

A digital optical fibre communication system for the step-index fibre channel described earlier, using the designed DFE receiver was simulated on the digital computer DEC system-1090. In the simulation effects of the photodetector and the preamplifier have been neglected as they were assumed to be broad band. Details of the simulation program are given in Appendix.

The average probability of error at a data rate of 10 M bits/sec for a 10 km fibre length and for SNR values from 6 dB to 20 dB have been plotted in Fig. 4.4. To study the effect of reduction in fibre length the simulation was repeated for equalizer parameters of 8 kms and 6 kms fibre

TABLE 4.1

TAP GAIN VALUES

SNR/LENGTH	FORWARD TAP GAINS			
	a_0	a_1	a_2	a_3
6 dB, SNR, 10 kms	0.79923999	$0.41692232 \times 10^{-8}$	$-0.17700238 \times 10^{-8}$	$0.60804712 \times 10^{-9}$
8 dB, SNR, 10kms	0.86319312	$0.21337771 \times 10^{-9}$	$-0.54532128 \times 10^{-9}$	$0.20397277 \times 10^{-9}$
10 dB, SNR, "	0.90909091	$0.46032699 \times 10^{-8}$	$-0.19231547 \times 10^{-8}$	$0.54245362 \times 10^{-9}$
12 dB, SNR "	0.94064905	$0.49470580 \times 10^{-8}$	$-0.25460981 \times 10^{-8}$	$0.76721220 \times 10^{-9}$
14 dB, SNR "	0.96171349	$0.48026060 \times 10^{-8}$	$-0.19914084 \times 10^{-8}$	$0.55711019 \times 10^{-9}$
16 dB, SNR, "	0.97549663	$0.22790282 \times 10^{-9}$	$-0.59749508 \times 10^{-9}$	$0.22093955 \times 10^{-9}$
18 dB, SNR, "	0.98439834	$0.48869102 \times 10^{-8}$	$-0.20198798 \times 10^{-8}$	$0.56309336 \times 10^{-9}$
20 dB, SNR, "	0.99009901	$0.46782938 \times 10^{-8}$	$-0.14228907 \times 10^{-8}$	$0.34152949 \times 10^{-9}$
22 dB, SNR, "	0.99372999	$0.22759503 \times 10^{-9}$	$-0.59236667 \times 10^{-9}$	$0.19149807 \times 10^{-9}$
24 dB, SNR, "	0.99603471	$0.51601368 \times 10^{-8}$	$-0.26409779 \times 10^{-8}$	$0.78996965 \times 10^{-9}$
16 dB, SNR, 8 kms	0.97549664	$0.20209436 \times 10^{-9}$	$-0.60902863 \times 10^{-9}$	$0.17900272 \times 10^{-9}$
16 DB, SNR, 6 kms	0.97549663	0.0	0.0	0.0

contd...

TABLE 4.1 (contd.)

SNR/LENGTH	FEEDBACK TAP GAINS		
	b_1	b_2	b_3
6 dB,SNR,10 kms	0.34968476	$0.42350618 \times 10^{-1}$	$0.17403446 \times 10^{-2}$
8 dB,SNR, 10 kms	0.37766563	$0.45739406 \times 10^{-1}$	$0.18796025 \times 10^{-2}$
10 dB,SNR, "	0.39774691	$0.48171467 \times 10^{-1}$	$0.19795449 \times 10^{-2}$
12 dB,SNR, "	0.41155428	$0.49843689 \times 10^{-1}$	$0.20482628 \times 10^{-2}$
14 dB,SNR, "	0.42077043	$0.50959864 \times 10^{-1}$	$0.20941306 \times 10^{-2}$
16 dB,SNR, "	0.42680085	$0.51690214 \times 10^{-1}$	$0.21241434 \times 10^{-2}$
18 dB,SNR, "	0.43069553	$0.52161903 \times 10^{-1}$	$0.21435268 \times 10^{-2}$
20 dB,SNR, "	0.43318970	$0.52463973 \times 10^{-1}$	$0.21559400 \times 10^{-2}$
22 dB,SNR, "	0.43477834	$0.52656374 \times 10^{-1}$	$0.21638465 \times 10^{-2}$
24 dB,SNR, "	0.43578670	$0.52778498 \times 10^{-1}$	$0.21688650 \times 10^{-2}$
16 dB,SNR,8 kms	0.34977324	$0.30159879 \times 10^{-1}$	$0.11458148 \times 10^{-2}$
16 dB,SNR,6 kms	0.25706090	$0.14427644 \times 10^{-1}$	$0.42054219 \times 10^{-3}$

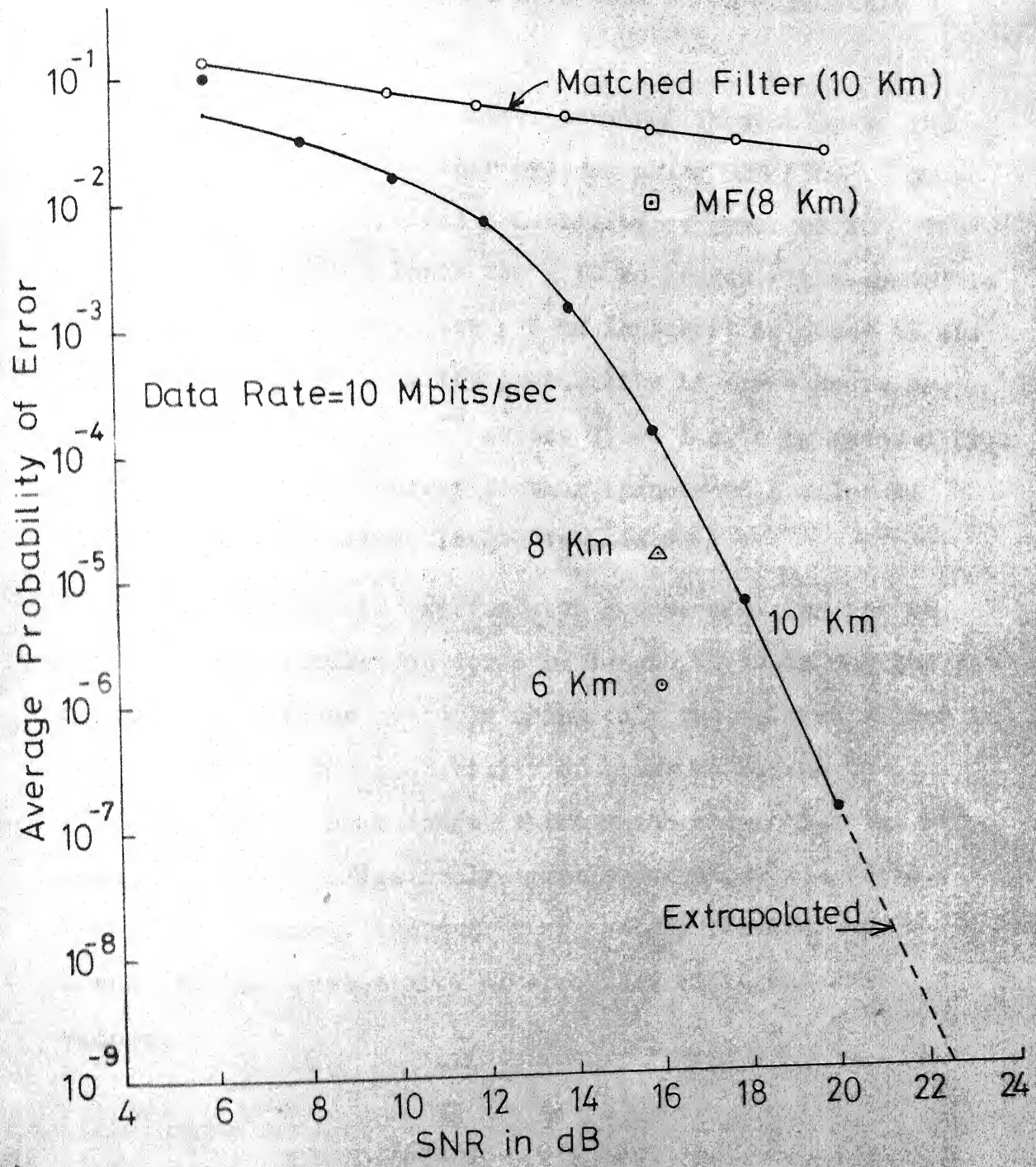

Fig. 4·4 Decision Feedback Equalizer Performance

length at 16 dB SNR. These have been shown separately in Fig. 4.4.

The nature of the curve obtained is similar to the performance curve for other systems using DFE [30]. We notice that for a typical probability of error of 10^{-6} the SNR required at the input for a 10 km length fibre system is about 19 dB, whereas, for a 6 km length it is about 16 dB. For a 16 dB input SNR, the probability of error decreases from 1.6×10^{-4} to 1.8×10^{-5} as the fibre length is reduced from 10 km to 8 km. The error further reduces to a value of 1.27×10^{-6} as the fibre length is made 6 km.

To compare the system with a nonequalizing one we repeated the simulation for 8 km length at 16 dB SNR and for various SNR values at 10 km using only the matched filter in the receiver. The probability of error increases to 1.07×10^{-2} for a 8 km length fibre which shows that the DFE reduced the ISI effectively. Table 4.2 shows the total symbols processed, the number of symbols received in error and the probability of error for different SNR values.

TABLE 4.2

PERFORMANCE OF DFE

SNR/Fibre length	Total Symbols Processed	Number of Received Symbols in Error	Average Probability of Error
6 dB, 10 kms	1000	100	10^{-1}
8 dB, "	1000	48	4.8×10^{-2}
10 dB, "	10000	244	2.44×10^{-2}
12 dB, "	10000	88	8.8×10^{-3}
14 dB, "	10^5	173	1.73×10^{-3}
16 dB, "	4×10^5	64	1.6×10^{-4}
18 dB, "	3.9×10^6	29	7.84×10^{-6}
20 dB, "	2.84×10^7	4	1.408×10^{-7}
*22 dB, "	2.26×10^7	0	
*24 dB "	1.62×10^7	0	
16 dB, 8 kms	1.4×10^6	25	1.786×10^{-5}
16 dB, 6 kms	1.1×10^7	14	1.27×10^{-6}

*Simulation runs stopped at this stage as already considerable CPU time had been used.

CHAPTER 5

PULSE FORMATS FOR OPTICAL FIBRE SYSTEMS

5.1 General:

To achieve high signalling rates and to provide economical wide band optical transmission network we tried to optimize the receiver design. As future systems with low loss fibres are going to have repeater spacings limited by pulse dispersion rather than attenuation, we resorted to equalization to reduce the problem of inter symbol interference. So far we have concentrated our efforts in the optimization of the receiver. But, for the improvement in performance of the overall system it is desirable to consider the transmitter as well. Selection of a suitable transmission code goes a long way to achieve a high data rate system by incorporating several desirable features as described in Sec. 5.2.

5.2 Line Encoding:

The need for encoding arises because the conventional straight binary format has the following limitations:

(a) It cannot provide an error monitoring capability.

(b) It suffers from occasional timing information disappearance.

(c) It can have a large dc content and thus results in base line wander.

Other factors which necessitate encoding and influence the selection are nonlinearity of the available optical sources like laser diodes, tolerance to ISI, bandwidth requirements and optimum transmission power requirements. The base band frequency spectrum must be relatively confined and have a null at zero frequency. This provides lower noise and permits AC coupling in the receiver.

5.3 Suitable Codes for Optical Fibre Systems:

Many of the features and problems stated above are common to digital coaxial or wire-pair cable systems. In these conventional systems the line code normally used is the Alternate Mark Inversion (AMI - originally called "bipolar") code. As the name suggests the polarities of mark are inverted alternately. Fig. 5.1(a) illustrates this coding plan. The advantage of this alternate mark inversion is that it has no d.c. content and any voilation of this rule is indicative of an error. It also contains little low frequency spectral components. This code, being a three-level one, is however not suitable for optical fibre systems using any source other than a LED. But, to utilize its advantages a coding plan called a two-level AMI has been suggested [34].

5.3.1 Two-Level AMI:

This coding plan converts the centre level of AMI to the two other levels. Two of the possible ways are shown

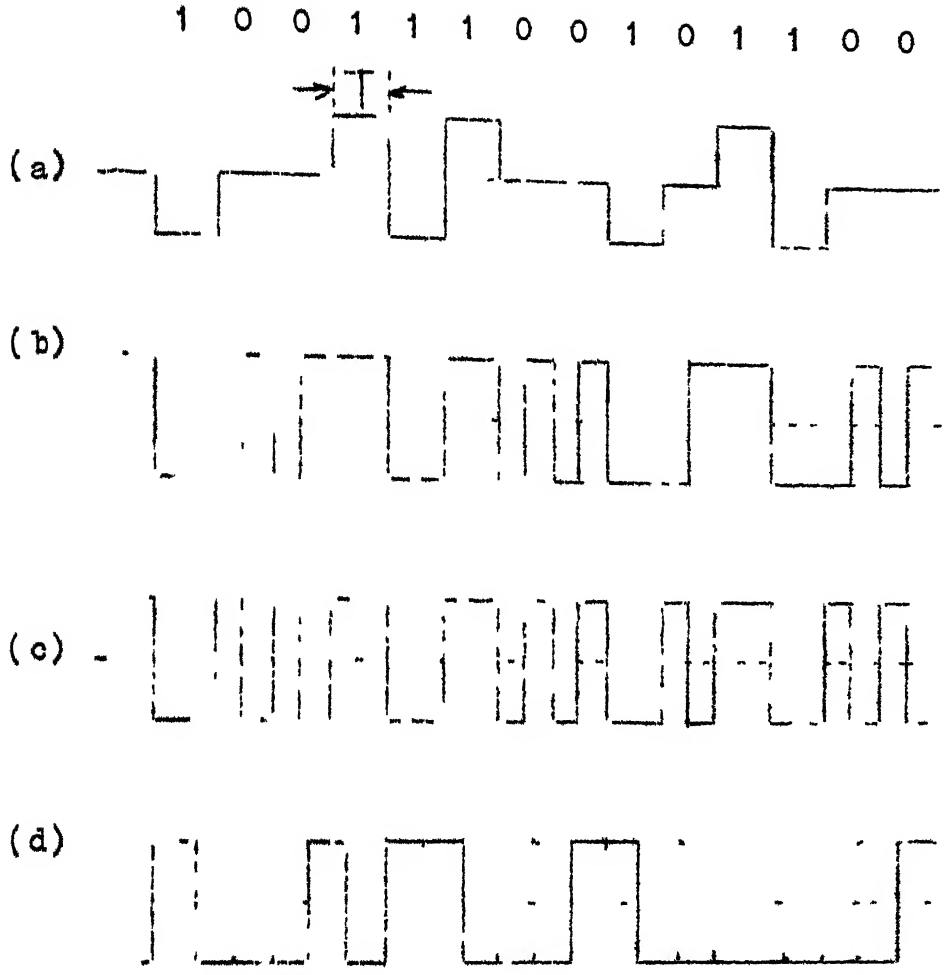

Fig. 5.1. (a) Conventional (three-level) AMI
(b) Two-level AMI Class I
(c) Two-level AMI Class II or 1B2B
(d) 2B3B

in Fig. 5.1(b) and (c). They can be called as two-level AMI class I and two-level AMI class II respectively. These formats have the following features:

(a) They require double the transmission bandwidth required by AMI or straight binary.

(b) For the same data rate and PIN diode as the detector in the system excess optical transmission power is required to achieve the same error rate as for the straight binary plan.

(c) The redundancies incorporated in these codes facilitate error detection.

(d) Clock recovery is easier, and possible with simple timing extractor as abundant timing frequency components exist.

(e) Decision threshold level is insensitive to input level variation, therefore no automatic gain control required in receiver.

(f) Utilisation of optical power is uniform and not pulse pattern dependent.

(g) Code converters are very simple.

All these features help realize a small, stable, reliable and economical repeater and makes AMI format quite attractive except for its increased bandwidth and power requirements [34]. The power penalty for the two-level AMI compared to the straight binary increases for lower fibre

bandwidths where equalization is essential for achieving high data rates. So we look for other pulse formats which have better performance than the two-level AMI.

5.3.2 Block Codes:

The coding scheme implies that a block of m binary digits is converted into a block of n binary digits with the help of some conversion rules and under some constraints to achieve a good coded pulse sequence satisfying the requirements stated above. Such codes are called mBnB pulse formats.

The two-level AMI explained above can itself be termed as a 1B2B code with the conversion rule as shown below.

Straight Binary	Mode 1	Mode 2	
1	1 1 ,	-1 -1	alternately
0	1 -1 ,	-1 1	depending on the last bit of the previous coded set (for class II)

The coding scheme could be made simpler by adopting the rule

1 ⟶ 1 -1

0 ⟶ -1 1

The difference between the two being that the former is converted from AMI and thus retains the pattern of AMI,

whereas the latter is a direct conversion from straight binary and can be considered as a true 1B2B code. It is quite obvious that the 1B2B will have a simpler code converter than two-level AMI.

In general mBnB formats of higher orders are quite suitable for optical transmission. Bandwidth savings can be attained by reducing the conversion ratio n/m. For example 2B3B format shown in Fig. 5.1(d) requires less bandwidth than the two-level AMI as it includes less redundancy. However the converter complexity increases exponentionally as redundancy is reduced [34] . But as we anticipate greater repeater spacing we can afford some complexity in them, their number being less in a long haul system. So one has to strike a balance and select the code accordingly to fulfil the requirements and over come the disadvantages of the straight binary plan. Conventional 2B3B plans try to suppress the dc component in a pulse sequence and as such cannot solve the problems of error monitoring since the redundancy is used up in suppressing the dc component. This can be overcome by using a 2B3B dc constrained code suggested by Takasaki et.al. [34]*.

*It should be noted that "dc component" in optical fibre transmission systems is to be interpreted as a shift from the level located half way between the brightest optical level and the darkness level.

The 2B3B dc constrained format conversion is as per the rule given in Table 5.1.

Table 5.1

Original code	2B3B code Mode 1	mode 2	
0 0	- - +		
0 1	- + -		
1 0	+ - -		
1 1	+ + - ,	- - -	alternately

This conversion rule requires fairly simple code convertors and reconverters. The straight binary symbol '0' is converted to '-' level and symbol '1' is converted to '+' level, then the third symbol is added such that there are a total of two '-' levels except in the case when the original code has the symbol pair '1,1'. In this the modes as shown are used alternatively giving on an average one '+' level and two '-' levels.

This plan produces a dc component in the pulse sequence but it does not suffer from base line wander as the dc level is constrained to a constant level. The dc component does not depend on the pulse pattern.

In general mBnB codes have been used in the conventional transmission systems. The conversion of m bits to n bits has been done keeping in view the need to reduce the dc component. Such suitable low disparity binary codes have been suggested by Griffiths [35]. Disparity d in general for an n digit character code has been defined by Cattermole [36] as

$$d = 2 \sum_{i=1}^{n} a_i - n\,(r-1)$$

where r is the radix of the code and a digit can take a value 0,1,2,...(r-1) and a_i is the value of the ith digit. For a binary code the disparity is then

$$d = 2 \sum_{i=1}^{n} a_i - n$$

which amounts to saying that the disparity of a binary character is the excess of marks over spaces; thus characters 000110 and 100111 have disparity -2 and +2, respectively. The disparity for a code would be the maximum range of disparity. A code with low disparity is also suitable from timing information point of view; because the timing information is defined as the average number of symbol changes per block.

Akin to disparity is the digit sum if rather than 0,1 we consider "-" , "+" levels as expressed earlier and

weight them as -1 and +1, respectively, for all dc suppressed mBnB codes. The frequency spectrum of the code remains unchanged and the disparity in the first case is equal to the digital sum in the second. The running digital sum (RDS) indicates the magnitude of dc wander in a pulse train. It is defined as the sum of the pulse amplitudes in a pulse train after every binary digit since the transmission commenced. For the 2B3B dc constrained format mentioned earlier the '+' and '-' levels in the pulse train would be weighted as '+' = 4/3 and '-' = 2/3, since the dc component is constrained to -1/3 level as shown in Fig. 5.2.

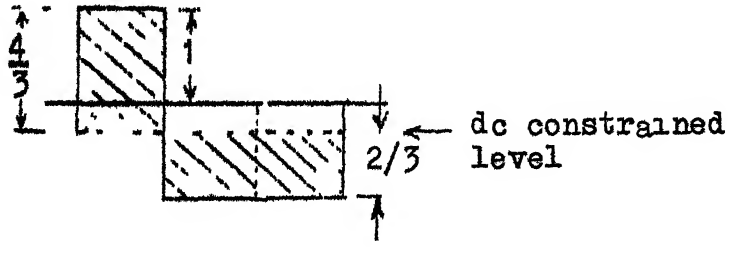

Fig. 5.2 2B3B dc Constrained Format Amplitude Levels

The choice of the coded blocks (words) should keep the RDS as low as possible. If m is odd and n=m+1 the number of zero digit sum words of length n is $\binom{m+1}{(m+1)/2}$ and number of words having positive digit sum is $2^m - \binom{m+1}{(1+m)/2}/2$. The

number of words having negative digit sum is also $2^m - \binom{m+1}{(m+1)/2}/2$. If words of opposite digit sum are paired it forms the alternative forms for transmission. Thus the total words available for low digit sum, infact zero digit sum, on an average in the long run in the present case, will be

$$\binom{m+1}{\frac{m+1}{2}} + 2^m - \binom{m+1}{\frac{m+1}{2}}/2 = 2^m + \binom{m+1}{\frac{m+1}{2}}/2$$

Thus leaving $\binom{m+1}{(m+1)/2}/2$ code words spare of which some may be undesirable from the point of view of transmission. Table 5.2 shows the number of words having particular digit sum for various n=m+1 word lengths

Table 5.2

m+1	Words having digit sum of 0	+2	+4	+6	+8	+10
2	2	1				
4	6	4	1			
6	20	15	6	1		
8	70	56	28	8	1	
10	252	210	120	45	10	1

There will be equal number of words having negative sum as having positive sum. It may be noted that if n is even we

will have even digit sum and if n is odd, odd digit sum and no zero digit sum.

In general n bits of an mBnB code need not be equal to m+1. Specific mBnB codes will be discussed and compared for their RDS and other characteristics in section 5.4.

5.3.3 Correlative Pulse Formats:

These formats entail the application of the known doubinary detection to reduce the bandwidth requirements of two level AMI. Takasaki et.al [34] have shown that doubinary detection of a two-level AMI pulse train results in the original AMI pulse train. In Fig. 5.3 we see that by delaying the pulse train b by half a time slot and adding b with the delayed version c, we obtain an AMI pulse train. This is an application of the correlative signal processing technique.

This process has allowed us to transmit the two level AMI pulse train through the same bandwidth as AMI or straight binary. Thus the technique is suitable for optical fibre communication, since it transmits two level pulse train which is immune to nonlinearity of laser diode and recovers a three level pulse train overcoming the bandwidth disadvantage of the former and is convenient for error detection, dc suppression etc.

Takasaki et.al. [34] have also suggested a modification to conventional correlative level coding plan for use in optical fibre systems. They call the modified plan as Modified duobinary class II shown in Fig. 5.4. The plan transmits a precoded format b. The precoding has been achieved by modulo two addition with the one time-slot delayed version of the input straight binary pulse sequence. The received pulse train is decoded by delaying and subtracting, and we get an AMI (three-level) format d. The setup is shown in Fig. 5.4. This requires less hardware than the two-level AMI with duobinary detection. But the two-level AMI has the advantage of uniform optical power utilization.

5.3.4 Recently Takasaki and Tanaka [37] have suggested the use of adaptive digital transmission to attain drastic economy in fibre optic communications with the present state of the art fibres (multimode fibres). To realize adaptive digital transmission they have investigated combining special line coding plans and phase locked loops with extra-broad pull-in range.

The special plans investigated are·Transition contrained code (TCC), Run length constrained code (RLCC) and Virtual transition constrained code (VTCC). TCC is

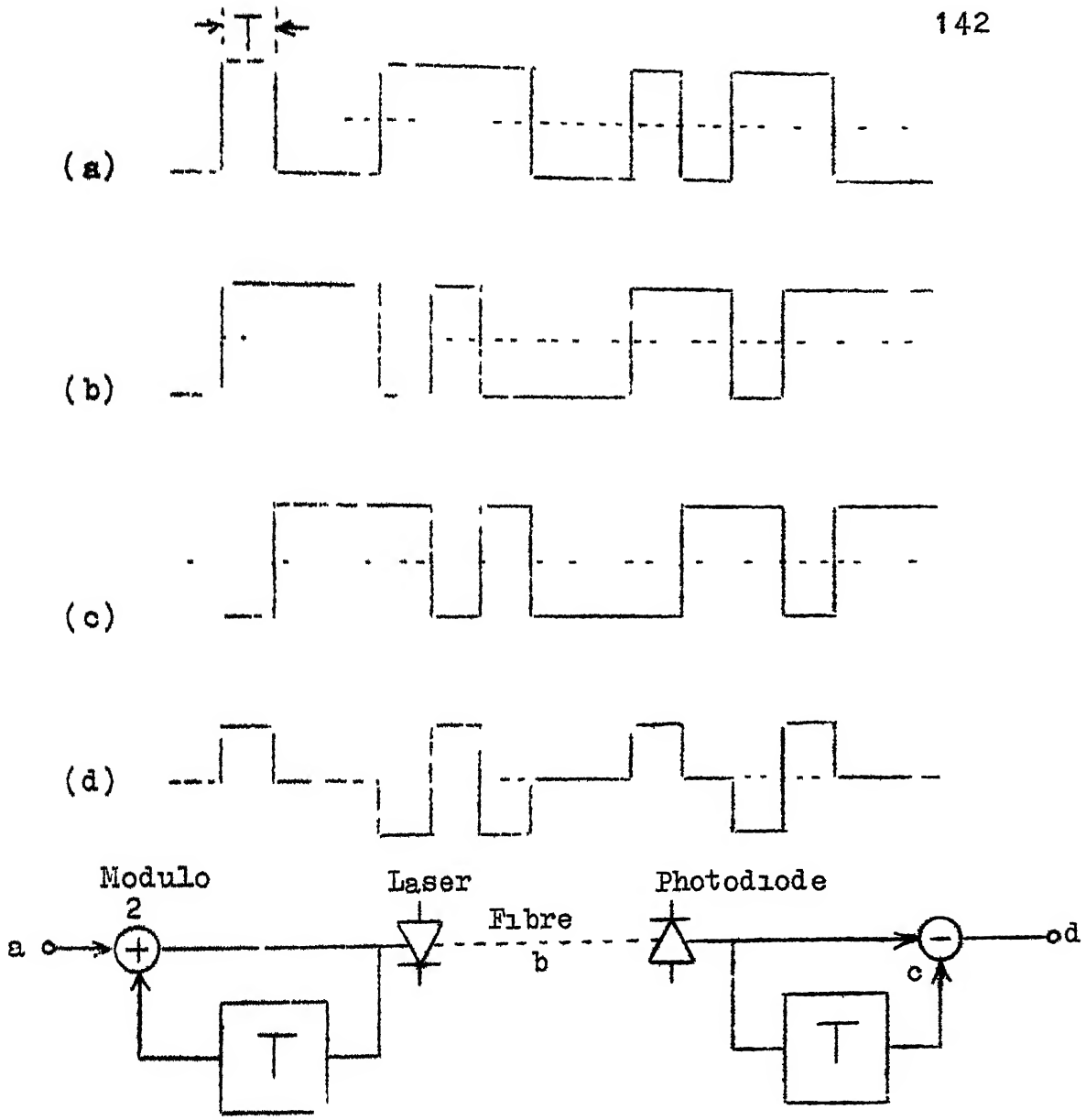

Fig. 5.4: Modified Duobinary Class II
(a) Original straight binary format
(b) Precoded binary format
(c) Precoded format (b) delayed by one time slot
(d) Detected three-level format.

realized by converting '1's of straight binary into a transition at the leading edges of time slots and '0's at the centre. The fact that, pulse frequency can also be known if information on the maximum run length is available, has been used in RLCC. TCC may not always have the ability to suppress spectral components at the end of transmission band. RLCC can overcome this but requires precision tracking of peak amplitudes. VTCC overcomes the problem in RLCC by detecting virtual transitions. This is explained in Fig. 5.5. The original straight binary pulse train (a) is converted into two-level AMI (b) integrating (b) during "on" periods yields (c). Dots on waveform (c) are virtual transitions (VT). Adding VTs to leading edge transitions (circles on (c)) yields information on pulse frequency i.e., (d)+(e) = (f). VTCC seems to be most promising to attain stable adaptive timing required for adaptive digital transmission.

5.4 Comparison of Suitable Codes:

We first compare various optical pulse formats for their running digital sum (RDS). RDS can be found only once the conversion rule is stated. Conversion rules for AMI, two-level AMI, 2B3B and correlative formats have already been given. For the higher order mBnB formats with n as

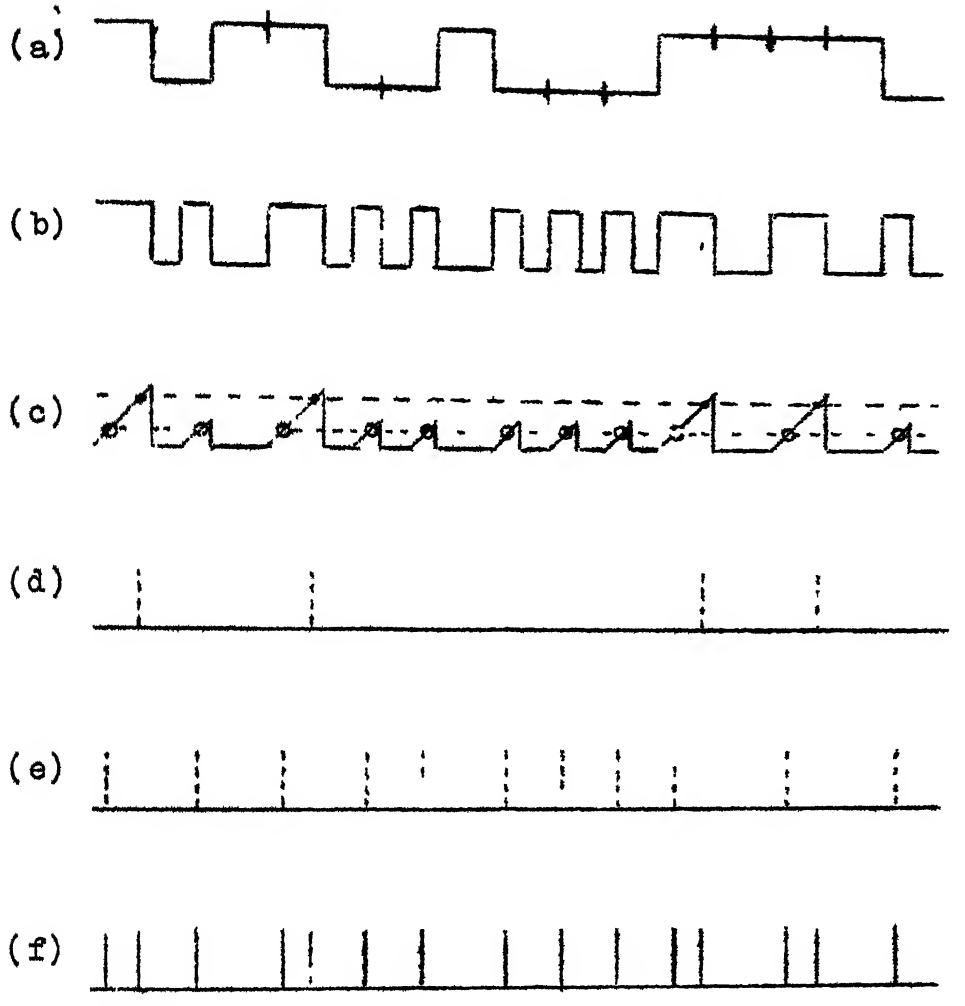

(a) Original Straight Binary Pulse train
(b) Two-level AMI Pulse train
(c) Integrating (b) during "on" periods
(d) Virtual transitions
(e) Leading edge transitions
(f) Information on pulse frequency ((f)=(d)+(e))

Fig. 5.5: Virtual Transition Constrained Code (VTCC)

even and n = m+1 the conversion rule is fairly straight forward keeping in view the requirement of zero digit sum and low RDS. A block of m digits is taken and examined, if it contains one '+' level or one '-' level less overall in the block a '+' level or a '-' level is added respectively to make them equal and thus get 0 digit sum block. Such blocks would be $\binom{m+1}{(m+1)/2}$ in number as explained earlier. For the rest $2^m - \binom{m+1}{(m+1)/2}$, we have $2^n - \binom{m+1}{(m+1)/2}$ available. Out of these we reject blocks with all '-'s or all '+'s. Of the remaining we select suitable complementary pairs and use as a pair in two modes alternately for rest of the blocks to be coded in a predetermined manner. Encoding rule for 3B4B is shown below.

3B4B Code Conversion Rule

Original Code Block	Coded as
*0 0 1	X X X 1
0 1 0	
1 0 0	
*1 1 0	X X X -1
1 0 1	
0 1 1	
0 0 0	-1 1-1-1 or 1-1 1 1
1 1 1	-1-1 1-1 or 1 1-1 1

X implies transmitting the original digits as it is except that for 0 we have '-' level and for 1 '+' level. The conversion conforms to the rule stated above. Rousseau [38] has suggested that we reject blocks which have first n/2 digits identical like (++...+,--...-) and (--..-,++...+) as, though they have zero digit sum, their use in the pulse train will increase RDS. This he qualifies by stating that their succession to each other and some other coded blocks gives the longest sequence of similar digits. If these are replaced by a suitable pair each of complementary blocks from the rest of the unused ones the longest sequence of similar digits can be reduced by one thus reducing RDS. In the above example of 3B4B code the blocks marked * after coding become -1 -1 1 1 and 1 1 -1-1, respectively, and thus fall in this category. On investigat it is found that the two complementary pairs that are left are, -1-1-1 1, 1 1 1 -1 and 1 -1-1-1, -1 1 1 1 which are still worse for they will further increase the sequence length of similar digits in the pulse train. We therefore, have not considered this suggestion in the conversion rules. However in codes where $n > m+1$ e.g., 5B6B this could be adhered to as a wide choice of blocks is available and one should use blocks which keep the RDS minimum. Encoding rule for 5B6B is given below.

Encoding Rule for 5B6B Code

Original code block	Coded as
1 1 0 0 0	X X X X X 1
1 0 1 0 0	
1 0 0 1 0	
1 0 0 0 1	
0 1 1 0 0	
0 1 0 1 0	
0 1 0 0 1	
0 0 1 1 0	
0 0 1 0 1	
0 0 0 1 1	
0 0 1 1 1	X X X X X -1
0 1 0 1 1	
0 1 1 0 1	
0 1 1 1 0	
1 0 0 1 1	
1 0 1 0 1	
1 0 1 1 0	
1 1 0 0 1	
1 1 0 1 0	
1 1 1 0 0	
0 0 0 0 0	-1 1-1 1 1 1 , 1-1 1 -1-1-1 alternately
0 0 0 0 1	1-1-1 1 1 1 , -1 1 1 -1-1-1 "
0 0 0 1 0	-1 1 1-1 1 1 , 1-1-1 1-1-1 "
0 0 1 0 0	1-1 1-1 1 1 , -1 1-1 1-1-1 "
0 1 0 0 0	1 1-1-1 1 1 , -1-1 1 1-1-1 "
1 0 0 0 0	-1 1 1 1-1 1 , 1-1-1 -1 1-1 "
0 1 1 1 1	1-1 1 1-1 1 , -1 1-1 -1 1-1 "
1 0 1 1 1	1 1-1 1-1 1 , -1-1 1 -1 1-1 "
1 1 0 1 1	1 1 1-1-1 1 , -1-1-1 1 1-1 "
1 1 1 0 1	1-1 1 1 1-1 , -1 1-1 -1-1 1 "
1 1 1 1 0	1 1-1 1 1-1 , -1-1 1 -1-1 1 "
1 1 1 1 1	1 1 1-1 1-1 , -1-1-1 1-1 1 "

RDS for these pulse formats has been found and tabulated in Table 5.3. The increase in bandwidth requirement for 3B4B code is 4/3 times the requirement for straight binary i.e., 33% increase. For 5B6B format the increase is 20%. The longest run of similar digits in the case of 3B4B is 4 and in the case of 5B6B is 6. The smaller this value the better it is for clock recovery. Another factor which is worth noting is that in both 3B4B and 5B6B we use only words of zero digit sum and ± 2 digit sum. This makes the hardware much simpler. Of course between the two as stated earlier as we go for higher order mBnB codes the complexity of the coder and decoder increases sharply. mBnB codes with n as odd have the disadvantage that they do not have any zero digit sum words and therefore are not popular.

To find the excess power required for a particular code we use the formula for the optical power required given by Personick [11] when PIN photodiode is used as the detector.

$$P_{required} = \frac{QN^{1/2}}{T}$$

where N has been derived in Chapter 3 and is given by Eqn. (3.23). It is related to Z of Eqn. 30 of [11] as

$$N = \left(\frac{h\nu}{\eta}\right)^2 Z$$

TABLE 5.3

Comparison of Optical Pulse Formats

Sl. No.	Code	Longest Similar Run	RDS Max.& Min.	Bandwidth Required	Power* Penalty	Error Monitoring	Pulse Pattern Affecting RDS
1.	Straight Binary		$\pm \infty$	1	0 dB (reference)	Not Possible	+,+,+,.... -,-,-,....
2.	AMI	-	± 1	1	0 dB	Possible	+,-,0,0,+,0,-,...
3.	Two-level AMI(I)	3	± 3	2	4.124 dB	Possible	++,+-,.... +-,--,....
4.	Two-level AMI(II)	2	± 2	2	4.124dB	Possible	++,-+,-+,.... --,++,-+,....
5a.	2B3B (Conventional) with -1 digit sum	5	+2 -4	1.5	2.358 dB	Not Possible	-++,++-,.... ---,--+,....
5b.	2B3B (Conventional)with +1 digit sum	5	+4 -2	1.5	2.358 dB	"	+++,++-,.... --+,-++,....
6.	2B3B dc constrained	7	$\pm 3\frac{1}{3}$	1.5	2.358 dB	Possible	++-,+--,.... ---,--+,....
7.	3B4B	4	± 4	1.33	1.654 dB	"	+-++,++--,....
8.	5B6B	6	± 5	1.2	1.037 dB	"	+-+---,---+-+,..

*This power penalty is for a data rate of 10 M bits/sec and half duty cycle rectangular pulses.

Q = number of noise standard deviations between signal and threshold at receiver output. Q=6 for an error rate of 10^{-9}.

T = interval between bits = 1/bit rate

For a fixed receiver and same probability of error, N depends only on bit rate and thus the $P_{required}$. $P_{required}$ has been calculated for the receiver parameters considered by Personick [11] for various pulse formats. The power penalty with reference to straight binary for 10 M bits/sec rate and half duty cycle rectangular pulses is tabulated in Table 5.3. The power penalty varies with bit rate at lower rates. At higher bit rates (above about 40 M bits/sec) due to the dominance of the term with 1/T in N, the $P_{required} \propto T^{-3/2}$ (4.5 dB/octave increase in bit rate). The effect of bit rate on excess power required for various pulse formats is plotted in Fig. 5.6.

From the above discussion and the characteristics mentioned in Table 5.3 the most suitable choice for high rate optical fibre communication systems seems to be between 3B4B and 5B6B formats.

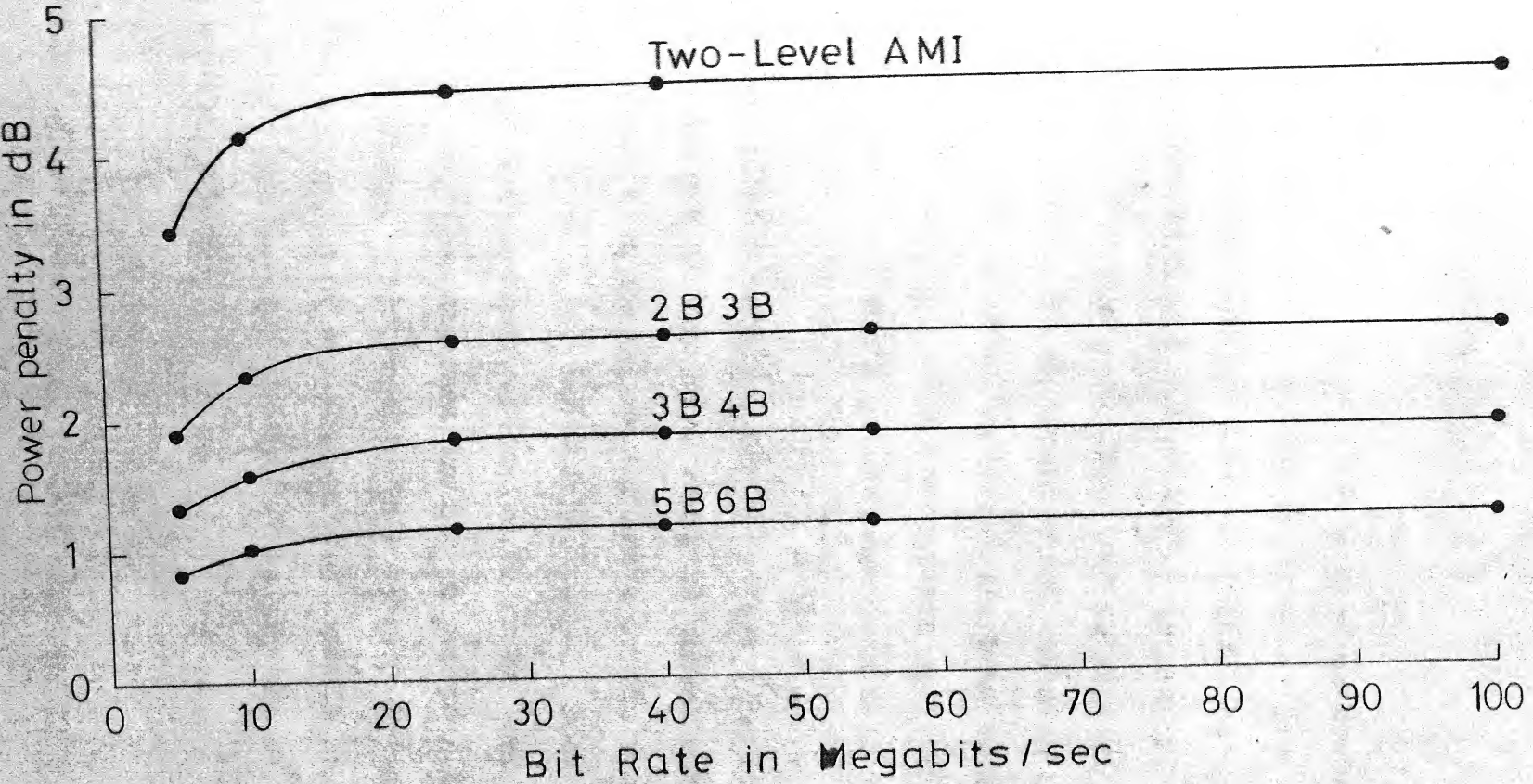

Fig. 5·6 Power penalty for mBnB Codes

CHAPTER 6

CONCLUSION

In this study we have tried to give an overall picture, with emphasis on certain aspects, of the optical fibre digital communication systems. Initially, we reviewed the physical and communication aspects of an optical fibre. The characteristics and parameters of an optical fibre communication system which would be of interest to a communication engineer were then reviewed. For the impulse response of the step-index optical fibre channel, Cartledge's formula [15,18] has been used because it is valid for a Lambertian source, whose light intensity distribution matches fairly closely to that of an LED. With increase in length the response tends to become symmetrical, but, its spread also increases. Inspite of the fact that optical fibres have large bandwidths, to make such communication systems cost effective, there is need to increase the repeater spacings as far as possible for high data rate systems. This results in intersymbol interference due to the spreading of the transmitted symbols in optical fibres. This can be effectively reduced by use of time domain equalization.

The receiver for the optical fibre channel is required to have a low noise front-end amplifier. The front-end of the suboptimum receiver using a PIN photodetector has been derived based on Personick's model [11] . It indicates that a high input impedence amplifier should follow the photodetector. Effects of input pulse shape, bit rate and fibre length on the optical power requirement have also been studied. It has been shown that the rectangular input pulse with a narrow width require the least transmitted optical power.

A design of the decision feed back equalizer has been given for the step-index optical fibre that has been considered in Chapter 2. In this design it is noticed that values of the forward tap gains except for a_0 are negligibly small and so these taps can be removed, thus leaving only one forward tap. Looking at the response just after the matched filter we see there are three precursors (future interfering samples) that cause interference. So the requirement of only one forward tap is not clear. The DFE designed was simulated on DEC system-1090 digital computer to study its performance. The original aim of achieving an average error probability of 10^{-9} could not be attained as it entailed generating and processing 10^{10} symbols in one

simulation run. Moreover, a number of such runs were needed to determine the average error. Since this would have required a very large computing time, we settled for achieving a higher error probability of 10^{-6} only at various values of SNR. Even for this, variation of fibre length and data rate for several values of SNR could not be tried as already quite a bit of computer time had been used. For fibre lengths of 8 Kms and 6 Kms the probability of error was determined only for one value of SNR (16 dB) so that some idea of the effect of the reduction in length can be had. From Table 4.2 it can be seen that for a 20 dB SNR and 10 Km length 28.4 million input symbols were processed and 4 errors were obtained. So proper averaging of the probability of error at this SNR could not be obtained. For higher SNR values of 22 dB and 24 dB simulation could not be completed to achieve lower probability of error as already considerable computer time had been used to achieve a probability of error of about 10^{-6}.

At lower SNR values where there were large number of errors some errors occured in bursts as expected for a DFE. This happens because erroneous output when fed back to the summing point of feedback TDL will not cancell the ISI due to past symbol completely producing another error occasionally

and thus resulting in an error burst. But, this effect was not observed for high SNR cases, because only a few errors occur under such situations making the possibility of an error burst remote.

On the transmitter side various line codes suitable for optical fibre communication systems have been investigated. Amongst the block codes, codes in which m bits are converted to n=(m+1) bits with m as an odd integer are most suitable. They have simpler conversion rule, lower RDO and relatively lower bandwidth requirements as compared to codes with m as an even integer and $n > (m+1)$. Out of these, 3B4B and 5B6B seem to be better suitable as their bandwidth requirements are only a little more than that of straight binary. Moreover, the encoders and decoders for these codes would be less complex as compared to still higher order mBnB codes.

Optical fibres have vast potential for military communications and other military applications besides their commercial applications. Their light weight, small size, freedom from radio frequency and electromagnetic interference is a big advantage for military uses from the point of view of ease of handling and ECM over and above the high capacity.

Many experiments and field trials of optical fibre communication links are under way in several countries of Europe, USA and Japan. A trial system called, The Chicago Lightwave Communications Project installed at Chicago, USA, based on the Atlanta Fibre Systems Experiment conducted in January,1976 [39] , has been carrying a wide range of services on a trial basis since May 11,1977. This is only an example of the efforts being put in this field.

The field of optical fibre communications being vast, attractive and at its infant stage the scope of work is unlimited. Some of the aspects of the present study which could be investigated further are use of other equalization techniques and their comparative study, use of graded-index fibre, using APD in place of PIN detector, etc. Doglliotti and Luvison have suggested tackling equalization as a sequence estimation problem. The optimum estimator structure suggested is derived as a Kalman filter. Amongst the nonlinear equalizers the maximum likelyhood receiver using Viterbi-algorithm detector could be tried. G. Tamburelli of CSELT seems to have done considerable work on nonlinear equalization. For optical fibre systems he has suggested a nonlinear equalizer with a shaping filter [40] called as "digital receiver with distributed and integrated decision feedback and feed forward".

It would be interesting to investigate this structure further.

Graded-index fibres are now being mostly used for practical systems under trial. They also permit higher data rates. It would be of interest to investigate equalizer designs at such higher frequencies and the associated hardware problems.

It is also suggested that study and analysis could be done using the APD as the photodetector in place of the PIN detector as the former has avalanche gain. But, use of APD would bring in the problem of shot noise which must also be considered in the design of the optimum receiver.

REFERENCES

[1] S.E. Miller, E.A.J. Marcatili and Tingye Li, "Research Towards Optical-Fiber Transmission Systems", Proceedings of the IEEE, Vol. 61, No. 12, December, 1973, pp. 1703-1751.

[2] Tingye Li, "Optical Fiber Communication - The State of the Art", IEEE Transactions on Communications, Vol. COM-26, No. 7, July, 1978.

[3] Detlef Gloge, "Propagation Effects in Optical Fibers", IEEE Transactions on Microwave Theory Tech., Vol. MTT-23, Jan., 1975, pp. 106-120.

[4] D.B. Keck, "Optical Fiber Waveguides", in Michael K. Barnoski, Ed., "Fundamentals of Optical Fiber Communications", Academic Press, 1976.

[5] K.C. Gupta, "Class Notes of EE 517 (Opto-Electronics)", Department of Electrical Engineering, I.I.T. Kanpur.

[6] "Fiber-Optic Developments Spark Worldwide Interest", Electronics, August 5, 1976, pp. 81-104.

[7] C.P. Sandbank, "Fiber Optic Communications: A Survey", Electrical Communication, Vol. 50 (1975) No. 1, pp. 20-27.

[8] Jeff D. Montgomery, "Fiber Optic Applications and Markets", IEEE Transactions on Communications, Vol. COM-26, No. 7, July, 1978, pp. 1099-1102.

[9] E.G. Rawson and R.M. Metcalfe, "Fibernet: Multimode Optical Fibers for Local Computer Networks," IEEE Transactions on Communications, Vol. COM-26, No. 7, July, 1978.

[10] Larry U. Dworkin and J. Robert Christian, "Army Fiber Optic Program: An Update", IEEE Transactions on Communications, Vol. COM-26, No. 7, July, 1978, pp. 999-1006.

[11] S.D. Personick, "Receiver Design for Digital Fiber Optic Communication Systems, I and II, Bell System Technical Journal, Vol. 52, No. 6, July-August,1973, pp. 843-886.

[12] M.K. Barnoski and S.D. Personick, "Measurements in Fiber Optics", Proceedings of the IEEE, Vol. 66, No. 4, April,1978, pp. 429-441.

[13] J.J. Ramskov Hansen and E. Nicolaisen, "Propagation in graded-index fibers: Comparison between experiment and three theories", Applied Optics, Vol. 17, No. 17, 1 September,1978, pp. 2831-2835.

[14] D. Gloge, "Impulse Response of Clad Optical Multimode Fibers", Bell System Technical Journal, Vol. 52,No. 6 July-August,1973, pp. 801-816.

[15] J.C. Cartledge, "Impulse Response of a step-index optical fiber excited by a Lambertian source", Applied Optics, Vol. 16, No. 5, May,1977, pp. 1311-1314.

[16] M.K. Barnoski, "Coupling Components for Optical Fiber Waveguides", - Ed., Fundamentals of Optical Fiber Communications, Academic Press,1976.

[17] D. Gloge, "Optical Power Flow in Multimode Fibers", Bell System Technical Journal, Vol. 51, No. 8, October,1972, pp. 1767-1783.

[18] J.C. Cartledge, "Impulse Response of a step-index optical fibre excited by a Lambertian source: addendum", Applied Optics, Vol. 16, No. 12, December,1977, p. 3082.

[19] Jan Conradi, Fedix P. Kapron, and John C. Dyment "Fiber-Optical Transmission between 0.8 and 1.4 μm", IEEE Transactions on Electron Devices, Vol. ED-25, No. 2, February,1978, pp. 180-193.

[20] S.D. Personick, "Receiver Design for Optical Fiber Systems", Proceedings of the IEEE, Vol. 65, No. 12, December,1977, pp. 1670-1678.

[21] S.D. Personick, "Photodetectors for Fiber Systems" in M.K. Barnoski, Ed. "Fundamentals of Optical Fiber Communications", Academic Press,1976.

[22] J.A. Olszewski, G.H. Foot and Yung-Yien Huang, "Development and Installation of an Optical-Fiber Cable for Communications", IEEE Transactions on Communications, Vol. COM-26, July,1978, pp. 991-998.

[23] Y. Takasaki, "Repeater Powering Plans for Fiber Optic Communication Systems", IEEE Transactions on Communications, Vol. COM-26, No. 1, January,1978, pp. 195-199.

[24] S. Kawakami and S. Nishida, "Anomalous Dispersion of New Doubly Clad Optical Fibre", Electronic Letters, Vol. 10, No. 4, 21 February,1974.

[25] S.D. Personick, "Baseband Linearity and Equalization in Fiber Optic Digital Communication Systems", Bell System Technical Journal, Vol. 52, No. 7, September,1973, pp. 1175-1194.

[26] R. Dogliotti and A. Luvison, "Signal Processing in Digital Fiber Communications", Second European Conference on Optical Fiber Communication, Paris, 27-30 September,1976.

[27] D.G. Messerschmitt, "Minimum MSE Equalization of Digital Fiber Optic Systems", IEEE Transactions on Communications, Vol. COM-26, No. 7, July,1978.

[28] M.E. Austin, "Decision-Feedback Equalization for Digital Communication over Dispersive Channels", MIT Research Laboratory of Electronics Technical Report 461 and Lincon Laboratory Technical Report 437, August 11,1967.

[29] R.W. Lucky, J. Salz and E.J. Weldon, Jr., "Principles of Data Communication" McGraw Hill,1968.

[30] D.A. George, R.R. Bowen and J.R. Storey, "An Adaptive Decision Feedback Equalizer", IEEE Transactions on Communication Technology, COM-19, June,1971, pp. 281-293.

[31] P. Monsen, "Feedback Equalization for Fading Dispersive Channels", IEEE Transactions on Information Theory, IT-17, January, 1971, pp. 56-64.

[32] P. Monsen, "Adaptive Equalization of the Slow Fading Channel", IEEE Transactions on Communications, Vol. COM-22, No. 8, August,1974, pp. 1064-1075.

[33] A. Papoulis, "Probability, Random Variables, and Stochastic Processes, Sec. 10.3", McGraw-Hill, Kogakusha, Ltd., 1965.

[34] Y. Takasaki, M. Tanaka, N. Maeda, K. Yamashita and K. Nagano, "Optical Pulse Formats for Fiber Optic Digital Communications", IEEE Transactions on Communications, Vol. COM-24, No. 4, April,1976, pp. 404-413.

[35] J.M. Griffiths, "Binary Code Suitable for Line Transmission", Electronic letters, Vol. 5, No. 4, February,1969, pp. 79.

[36] K.W. Cattermole, "Principles of Pulse Code Modulation", Iliffe Books 1969, Chapter 4.

[37] Y. Takasaki and M. Tanaka, "Fiber Optic Adaptive Digital Transmission", Proceedings 7th National Telecommunications Conference, Dec. 3-6,1978, Birmingham, pp. 5.4.1-5.4.5.

[38] M. Rousseau, "Block Codes for Optical-Fibre Communication", Electronic Letters, Vol. 12, No. 18, 2 September,1976, pp. 478-479.

[39] "Atlanta Fibre System Experiment", Bell System Technical Journal, July-August,1978, Vol. 17, No. 6.

[40] G. Tamburelli, "Nonlinear Equalizer with Shaping Filter", CSELT Rapporti tecnici - Vol. V, No. 4, September,1977, pp. 229-235.

APPENDIX

COMPUTER SIMULATION OF DECISION FEED BACK EQUALIZER

The flow chart shown in Fig. A.1 gives the steps taken in the computer simulation of the DFE. The purpose of this simulation was to study its performance in terms of the probability of error for various SNR's and fibre lengths. As for higher SNR's large computation time was required and it was not possible to get this time in one stretch, the simulation for a SNR had to be divided into many runs. For this purpose, the simulation computer program was divided into three main parts. One part is effective when it is the initial run for a certain SNR/fibre length. The second part is effective when it is a subsequent run and the third part is common to both.

The program for computation of the tap gains is separate(from the simulation program) to avoid revaluation of x_k and channel impulse response samples every time for different SNR's and the same fibre length, as they are independent of SNR. Therefore, in the simulation program pulse spread L, number of forward taps NF, number of feedback taps NB, channel response samples and autocorrelation function samples x_k are read in as data once for a particular fibre length and all SNRs. The value of the SNR, the forward and the feedback tap gains are read in for each SNR.

The data input to the channel is a pseudo-random binary sequence with symbol separation time T normalized to unity. The sequence is obtained by generating uniformly distributed real random numbers using the subprogram RAN and then converting them to +1 for numbers greater than and equal to 0.5 and to -1 otherwise. The signal output at the output of the matched filter is obtained by convolving the signal samples with channel autocorrelation function samples x_k. The zero mean white gaussian noise samples n_k with variance σ^2 are generated by using the Box Muller method.

$$n_k = \sigma[-2.\ln(R_1)]^{1/2} \cos(2\pi R_2)$$

where R_1 and R_2 are uncorrelated uniformly distributed random numbers in the range 0 and 1. For achieving uncorrelated noise samples one baud interval has been divided into ten (M) subsamples. The greater the number of subsamples of noise the better the uncorrelation. But a tradeooff between the computer time and uncorrelation achievable exists. The received signal at the equalizer input is obtained by adding the noise and the signal samples obtained above.

The number of signal samples generated initially in the initial run are one less than required to start the simulation run. Out of the generated signal samples the first MB samples are placed in the feedback tapped delay line

in a correct sequence so that it is assumed that as the simulation starts there is no error in the beginning and correct estimates are available at the feedback TDL. This is to overcome the problem of time that a system will take to stablize and initial errors will have to be neglected in computing the probability of error. After the requisite number of received signal samples at the input of the equalizer are calculated and stored in the respective arrays, we generate a signal sample and a noise sample, add them, and start the processing in the DFE. The output of the forward TDL is obtained and from it the output of the feedback TDL, which is obtained from the already placed symbols, is subtracted. If this output is greater than or equal to 0 we say a +1 is received, otherwise a -1. This estimated symbol is then compared with the appropriate input symbol. The first such symbol would actually be the (MB+1)th symbol as this would be the first symbol having effects of both past and future symbols interference as the first MB symbols generated had been placed in the feedback TDL. Error, if any, increases the error count by one. All registers are then shifted by one symbol and we go back to the same step where we had generated one signal symbol. After a known number of symbols have been processed depending upon the time available for the run, the output of all registers is

stored. This forms the initialization data for the subsequent run. After every run, initial or subsequent, the probability of error is calculated. For a subsequent run after the initialization values have been read in the processing starts from the stage where one signal sample was generated in the initial run.

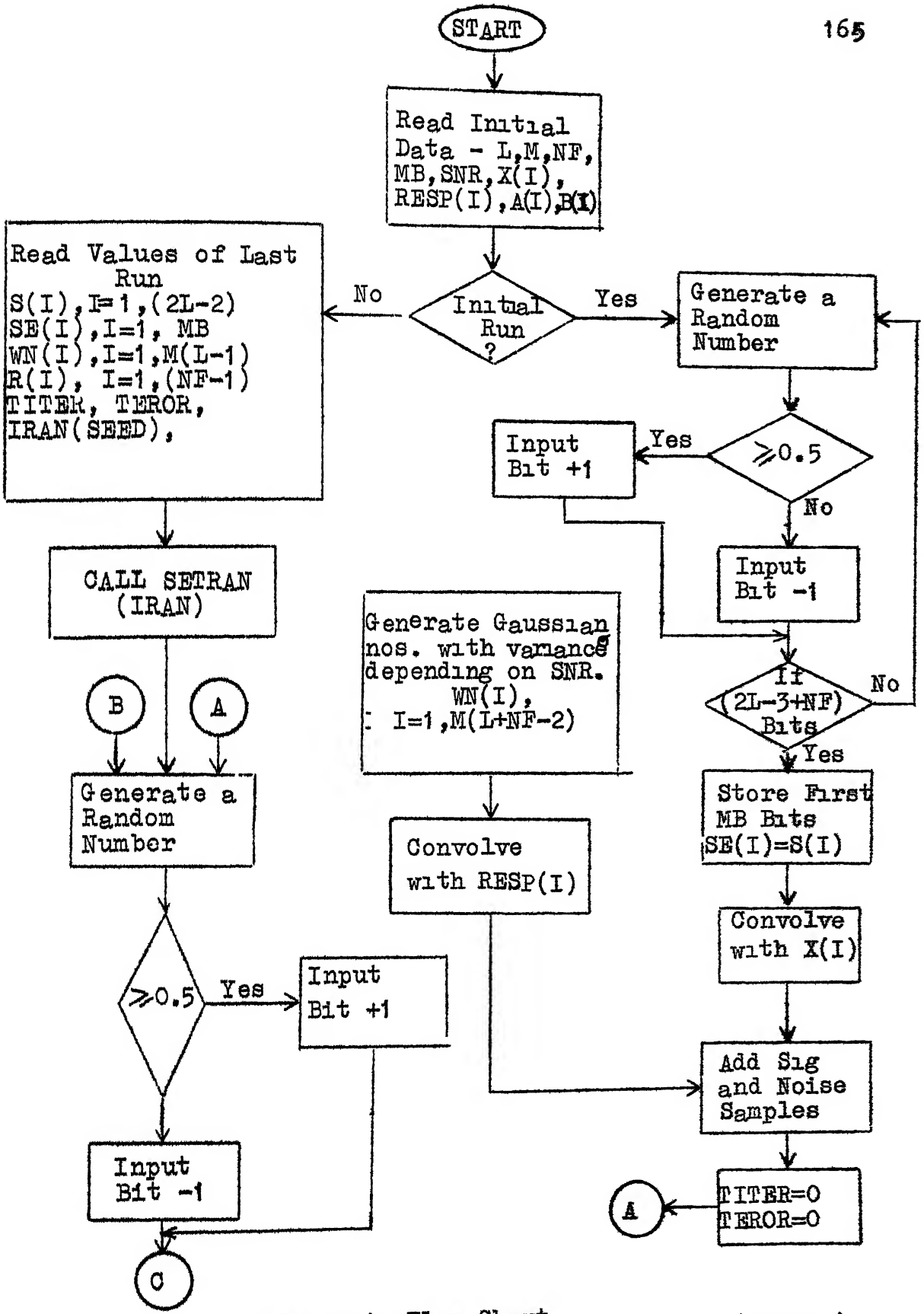

Fig. A.1: Flow Chart (contd.)

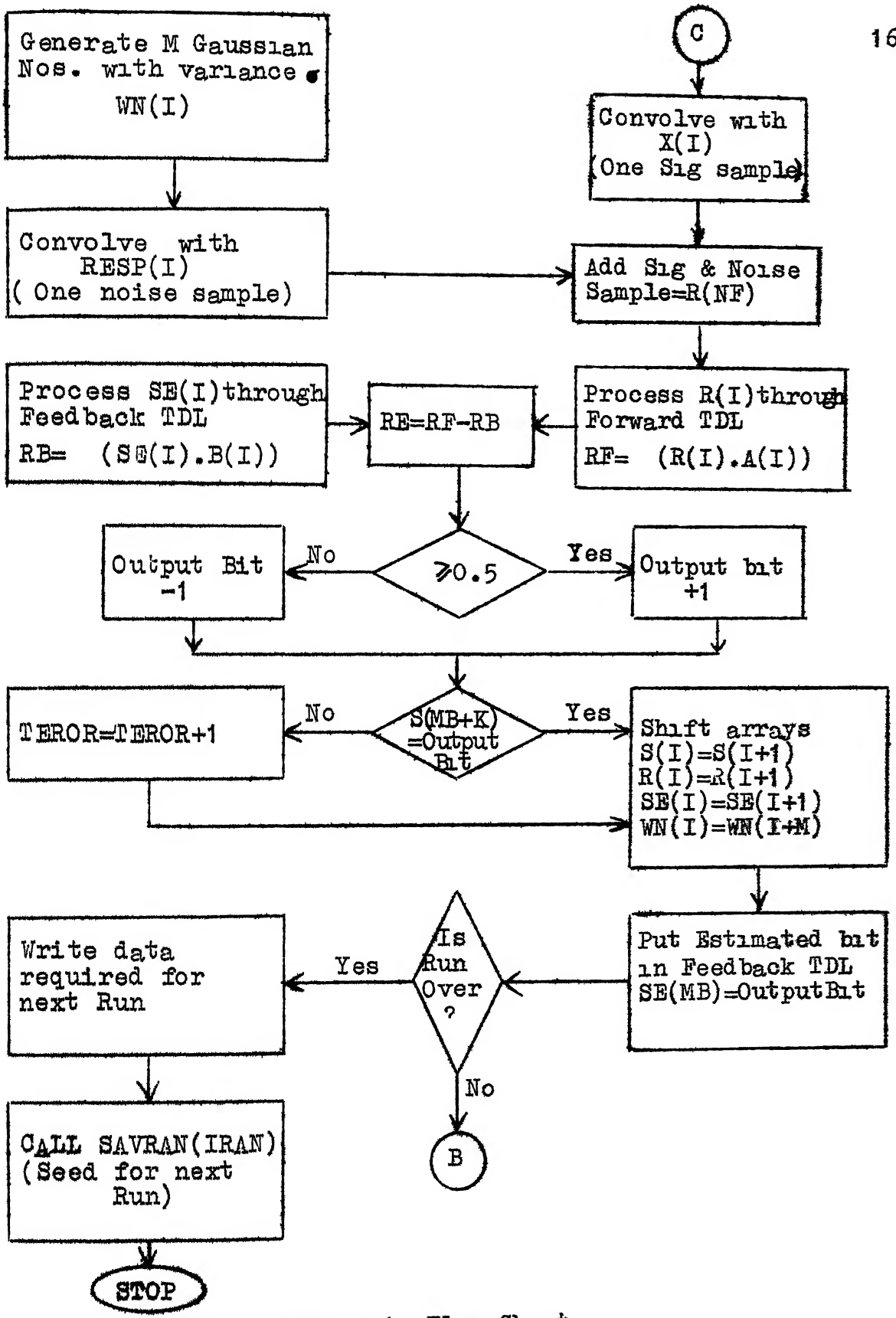

Fig. A.1: Flow Chart